Summer 8-31-2003

Synthesis of nano/micro particles using supercritical method and particle characterization

Abhijit Aniruddha Gokhale
New Jersey Institute of Technology

ABSTRACT

SYNTHESIS OF NANO/MICRO PARTICLES USING SUPERCRITICAL FLUID METHOD AND PARTICLE CHARACTERIZATION

by
Abhijit Aniruddha Gokhale

The thesis work consists of the two parts, jet behavior of solvents (ethanol and acetone) and the particle formation using SAS method. In the first part, the study of the effects of process parameters like temperature, pressure, injection velocity and internal diameter of nozzle on liquid jets are studied. The critical pressure for which liquid jet of solvents changes to gas – like jet, is investigated.

In the second part, the experiments are done to study the process of the particle formation using SAS method. Effects of process parameters like pressure, injection velocity of solution, the inner diameter of nozzle on properties of particles are studied. Few modifications are done in setup to make the experiments easy and effective. Also, a few recommendations are proposed regarding process parameters for future experiments as well as to improve set up.

SYNTHESIS OF NANO/MICRO PARTICLES USING SUPERCRITICAL FLUID METHOD AND PARTICLE CHARACTERIZATION

by
Abhijit Aniruddha Gokhale

A Thesis
Submitted to the Faculty of
New Jersey Institute of Technology
In Partial Fulfillment of the Requirements for the Degree of
Master of Science in Mechanical Engineering

Department of Mechanical Engineering

August 2003

APPROVAL PAGE

SYNTHESIS OF NANO/MICRO PARTICLES USING SUPERCRITICAL FLUID METHOD AND PARTICLE CHARACTERIZATION

Abhijit Aniruddha Gokhale

Dr. Boris Khusid — 08/05/2003
Associate Professor of Mechanical Engineering, NJIT

Dr. Ernest Geskin — 08/05/2003
Professor of Mechanical Engineering, NJIT

Dr. Chao Zhu — 08/05/2003
Associate Professor of Mechanical Engineering, NJIT

BIOGRAPHICAL SKETCH

Author: Abhijit Aniruddha Gokhale

Degree: Master of Science

Date: August 05, 2003

Undergraduate and Graduate Education:

- Master of Science in Mechanical Engineering,
  New Jersey Institute of Technology, Newark, NJ, 2003

- Bachelor of Engineering in Mechanical Engineering,
  Maharashtra Institute of Technology, Pune, India, 2000

Major: Mechanical Engineering

This thesis is dedicated to my parents.

ACKNOWLEDGEMENT

I take this opportunity to express my deep gratitude towards my Adviser, Dr. Boris Khusid, for giving the prospects to work in the most advanced and exciting field with his excellent guidance, friendship and always being there whenever required throughout the research.

Also, the special thanks to Dr. Rajesh Dave for his financial and morale support without which it was highly impossible to achieve desired goals. I am thankful to Dr. Jiyanjun Luo and Yeuyang Shen for the timely help they offered throughout the duration.

I would also like to give thanks to the New Jersey Commission on Science and Technology for funding this research.

TABLE OF CONTENTS

TABLE OF CONTENTS
(Continued)

Chapter **Page**

LIST OF FIGURES

Figure **Page**

Figure **LIST OF FIGURES** **Page**
(Continued)

Figure **LIST OF FIGURES** **Page**
(Continued)

Figure **LIST OF FIGURES** **Page**
(Continued)

Figure **LIST OF FIGURES** **Page**
(Continued)

SYMBOLS

Thermal Conductivity	:	$\wedge$
Pressure	:	P
Temperature	:	T
Critical Pressure	:	P_c
Critical Temperature	:	T_c
Volume	:	V
Critical Volume	:	V_c
Helmholtz free energy	:	A
Reynolds Number	:	Re
Injected Solution Velocity	:	V_{sol}
Injected CO_2 Flow Rate	:	V_{CO2}
Diameter of particles	:	D
Maximum Diameter of Particle	:	D_{max}
Density of CO_2	:	ρ_{CO2}
Density of solution	:	ρ_{sol}
Inner Diameter of Nozzle	:	D_{nozzle}
Jet Length	:	L
Heat Capacity	:	Cp

CHAPTER 1

INTRODUCTION

1.1 Motivation

There is an increasing demand for *ideal* particles from pharmaceutical, nutraceutical, cosmetic and specialty chemistry industries for various purposes. Conventional particle formation processes have certain disadvantages like having less control on the particle size distribution, particle morphology, purity and rusticity [1]. The new methods of using supercritical fluid technologies for particle formation show great promise in the area of pharmaceutical materials and drug delivery systems.

For drug delivery systems, particles formation methods should have the following features:

- Operates with relatively small quantities of organic solvent(s),
- Molecular control of process,
- Single step and scalable process for solvent-free final product,
- Ability to control desired particle properties,
- Suitable for wide range of chemical types of therapeutic agents,
- Capability for preparing multi-component systems,
- GMP compliant process [2].

Supercritical Fluids methods prove to be very useful in manipulating these properties of manufactured particles.

1.2 Objectives

Although numerous papers which were published in the last decade, contributed to the design of SAS apparatuses and the product development, SAS processes are still optimized empirically since very little has been achieved in mastering quantitatively the dynamics of phenomena underlying this process. A detailed analysis of the jet flow is the first step in the development of a comprehensive model capable of facilitating the design and optimization of the SAS technology. The objective of this thesis is to study the behavior of liquid jets in binary system and the effects of operating parameters on the jets as well as the particle formation using SAS method.

CHAPTER 2

REVIEW OF SUPERCRITICAL FLUIDS TECHNOLOGIES AND APPLICATIONS

2.1 Supercritical Fluids – Properties and Applications

Concepts of Supercritical Fluids:

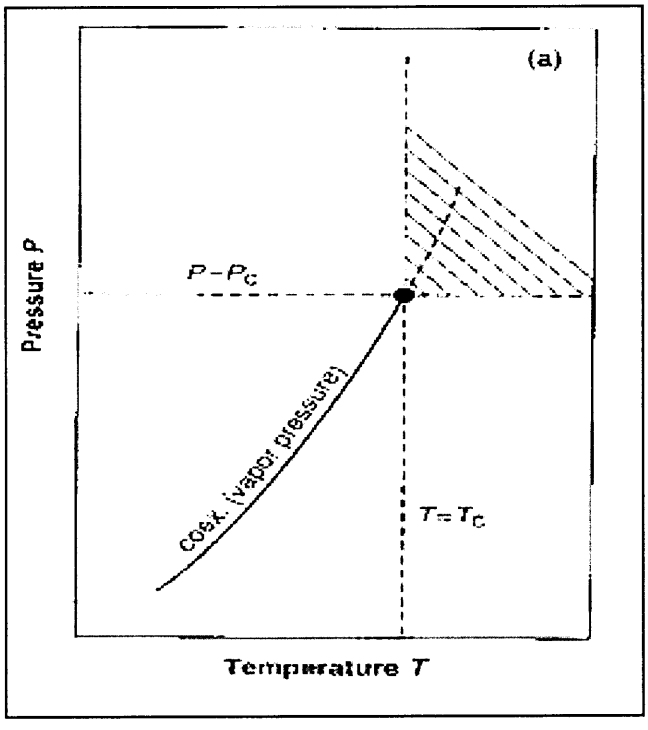

Figure 2.1 Graph of pressure – temperature. Hatch lines show supercritical region.

Supercritical fluids (SF) are substances at temperatures and pressures above their critical points [2]. SFs have density values that enable appreciable solvation power, whilst the viscosity of solutes in SF is lower than in liquids and the diffusivity of solutes is higher, which facilitates mass transfer. Also, and significantly for particle formation is that SFs are highly compressible, particularly near the critical point, and their density and thus the solvation power can be carefully controlled by small changes in temperature and/or

pressure. In Figure 2.1, the region in pressure (P) – temperature (T) phase space is defined where the fluid is supercritical according to the above definition, namely the first quadrant. In P - T diagram, the vapor pressure curve indicates the conditions under which the vapor and liquid coexist and the critical point corresponds to the point where the distinction between vapor and liquid disappears [3]. In the Figure 2.1 the critical isotherm is indicated $T = T_c$ and critical isobar is indicated $P = P_c$. If the liquid is heated at constant pressure exceeding the critical pressure, it expands and reaches a vapor-like state without undergoing a phase transition. This phenomenon is called as "the continuity of state".

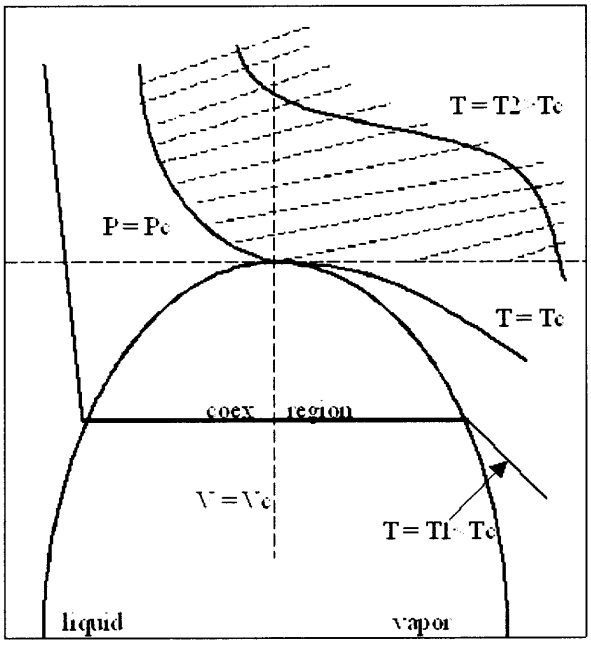

Figure 2.2 Represents pressure – volume diagram of fluid. The hatched lines show supercritical region.

Figure 2.2 represents the pressure – volume diagram of the same fluid. The region corresponds to the supercritical states in Figure 2.1. The single vapor pressure curve corresponds to a coexistence curve with two branches, one for the vapor and another for the liquid; the branches meet in the critical point where the difference between the

two phases disappears. The critical isochore, $V = Vc$, is indicated. Coexisting vapor and liquid states have the same pressure but different molar volume, so that the isothermal compressibility is infinite throughout the two-phase region. The critical point is the last point in two-phase region, and the only point in the one – phase region, where the compressibility is infinite. All supercritical isotherm have finite slope everywhere, but the slope may be very small (the compressibility very high) in the vicinity of the critical isochore. The critical isotherm is the first isotherm to reach zero slope which is the indication of infinite isothermal compressibility and incipient instability.

Thus, a fluid is critical when the difference between coexisting liquid and vapor phases disappears. At this point the isothermal compressibility of the one phase fluid becomes infinite. In the supercritical region, a state of liquid-like density can transform into one of vapor like-density by tuning the pressure or the temperature, without the appearance of an interface. The further from the critical point, the easier it is to gently manipulate the density by tuning pressure or temperature. In the supercritical fluids, a range of intermediate-density states can be reached which are not available at sub critical temperatures and pressures [3].

Properties Intermediate Between Those of Vapor and Liquid :

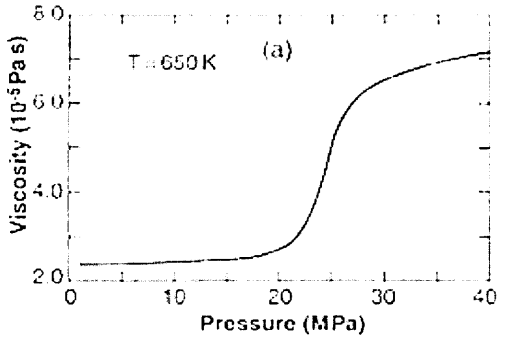

Figure 2.3 A graph of viscosity vs pressure is shown.

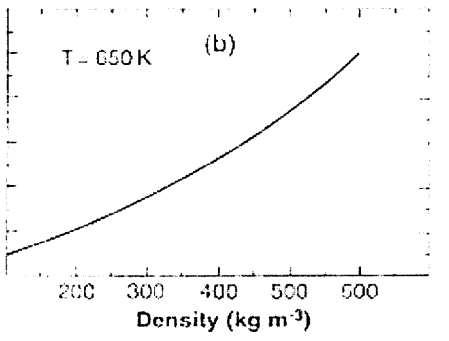

Figure 2.4 A graph of viscosity vs density is shown.

Since the supercritical fluid has densities intermediate between those of vapor and liquid, its properties are also intermediate between these phases. Consider water as an example (Fig 2.3). Its viscosity along an isotherm 3 K above T_c ascends pressure abruptly from vapor-like to liquid-like values.

In Figure 2.4, the viscosity is shown as a function of density along the same isotherm. Now the behavior is very simple and regular (the very weak critical divergence of the viscosity is not visible on this scale). The difference between Figures 2.3 and 2.4 is due to the diverging compressibility.

In Figure 2.5, the dielectric constant of water is plotted along the 25 MPa isobar as a function of temperature. It drops from a value of 80 near the freezing point to about 20 near 600 K. In the supercritical range, however, the dielectric constant undergoes another steep drop as the critical isochore is crossed. The critical-point value of the dielectric constant is about 4 and on the 25 MPa isobars it falls below 2 beyond 700 K [3].

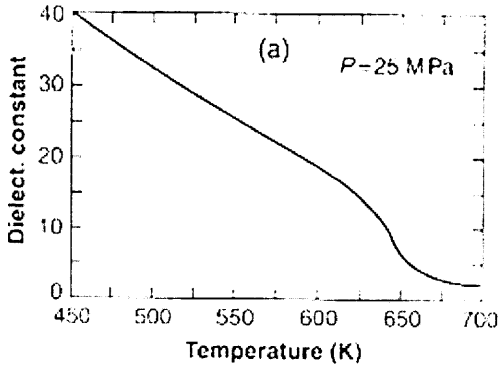

Figure 2.5 A graph showing dielectric constant vs temperature for a supercritical fluid.

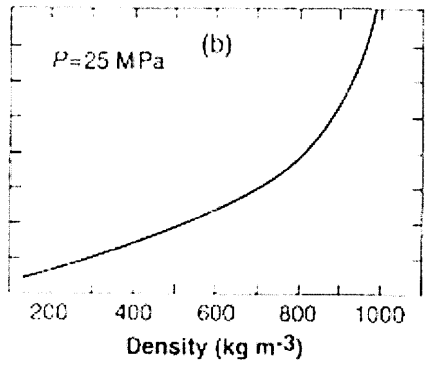

Figure 2.6 A graph showing dielectric constant vs density for a supercritical fluid.

In those conditions, water is a low-dielectric fluid being a poor solvent for electrolytes and a good solvent for organics. In Figure 2.6, the dielectric constant is plotted versus density along the same 25 MPa isobar. The steep drop seen near the critical point in the temperature dependence in Figure 2.5, which is due to the diverging expansion coefficient, is replaced by a smooth and gradual decrease in the density representation in Figure 2.6.

Properties Not Intermediate Between Those of Vapor and Liquid :

The properties such as isothermal compressibility, expansion coefficient and heat capacity, which display an extremum near the critical density, cannot be intermediate between those of vapor and liquid. As example, in Figures 2.7 and 2.8 the isobaric heat capacity of supercritical water is shown along an isobar. The sharp spike in Figure 2.7, with temperature as the abscissa, is the equivalent of the broad maximum in Figure 2.8, with the density as abscissa.

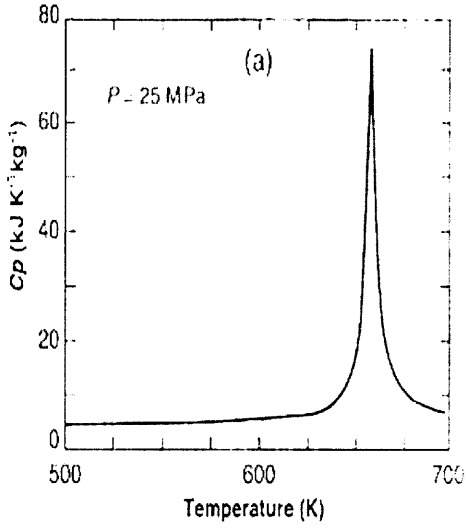

Figure 2.7 Isobaric heat capacity is of supercritical water is shown against temperature.

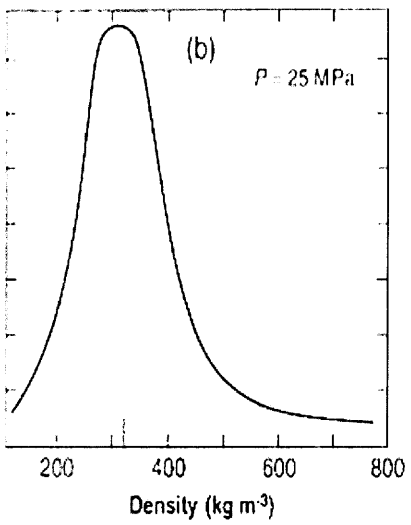

Figure 2.8 Isobaric heat capacity is of supercritical water is shown against density.

The diverging expansion coefficient is the reason that a small change in temperature causes a huge density change. Even for properties that reach very large values, the behavior is easier to understand and characterize as a function of a density, rather than a field variable. The thermal conductivity $\wedge$ of pure fluids diverges at the critical point about half as strongly as the isobaric heat capacity, and therefore the thermal diffusivity, $\wedge / \rho C_p$, goes to zero as shown in Figure 2.9 and Figure 2.10.

The coefficient of self-diffusion does not have an anomaly near the critical point. However, the mutual diffusion coefficient is the more important characteristics. The binary diffusion coefficient approaches zero at the mixture critical point. In dilute mixtures, the decrease of binary diffusion coefficient is not seen until the critical line is approached very closely [3].

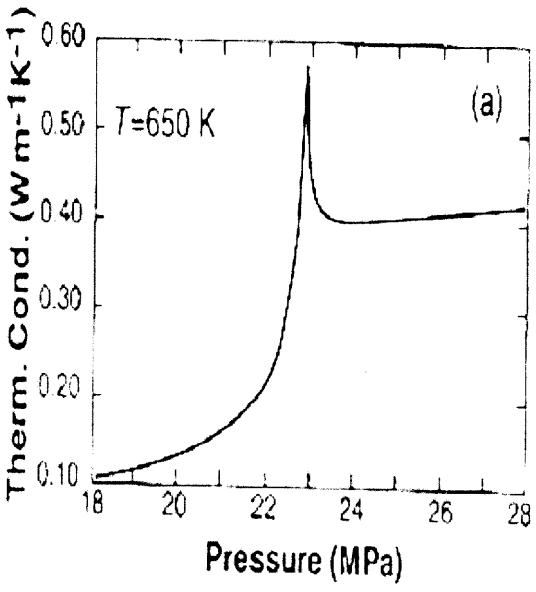

Figure 2.9 Thermal conductivity is shown against pressure for supercritical fluid.

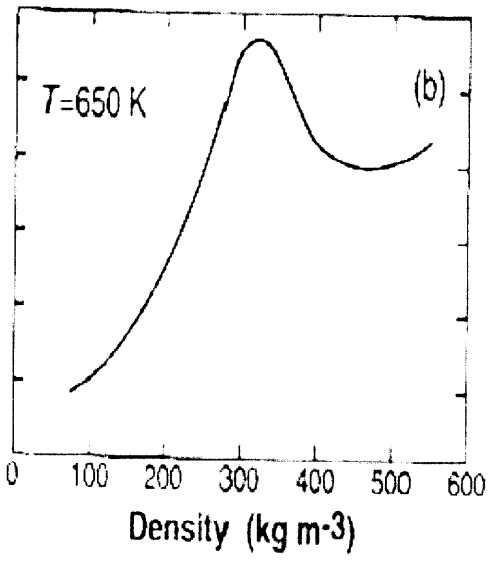

Figure 2.10 Thermal conductivity is shown against temperature for supercritical fluid.

For many practical purposes, such as supercritical expansion and chromatography, the mixture is dilute, and it can be assumed that the coefficient of binary diffusion is intermediate between that in the vapor and that in the liquid. Since the diffusion coefficient decreases roughly inversely proportional to the density, diffusion in supercritical solvents is much more rapid than in liquid solvents, thus increasing the speed of diffusion-controlled chemical processes [3].

Supercritical Fluid Phase Behavior: Binary fluid mixture phase diagrams are represented as two-dimensional projections of the three-dimensional P-T-x diagram onto the P-T plane, or as two-dimensional sections of the P-T-x diagram, with variables T-x at constant P, P-x at constant T, or P-T at constant x. Here x is the mole fraction of the second component (solute).

Type I binary fluid phase diagram :

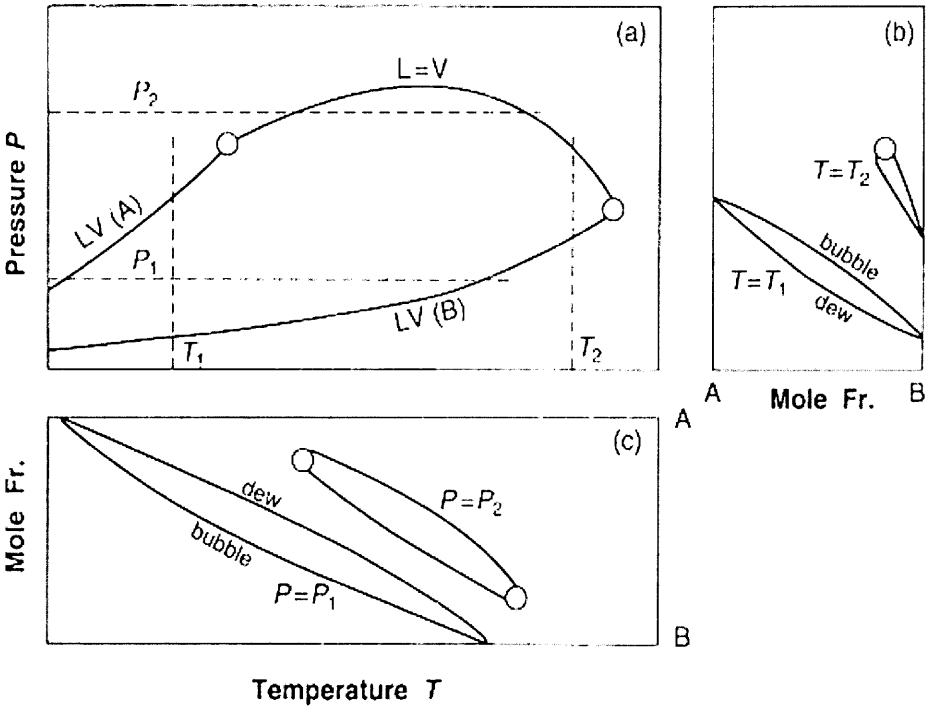

Figure 2.11 The figure explains different types of binary fluid phase diagrams.

The first diagram in Figure 2.11 shows a critical line connecting the two pure-fluid critical points and no additional phase separation in the liquid phase. The corresponding P-x and T-x diagrams are shown as sections for constant chosen pressures, or temperatures, respectively. In the P-x and T-x diagrams, line parallel to the composition axis connects true coexisting phases on the dew-bubble curves. The liquid phase is richer in less volatile solute than the vapor phase. The constant x isothermal compressibility K_{Tx} is finite in the two-phase mixture because the pressure

rises as the two-phase mixture is compressed. It fallows that K_{Tx} is finite as well at the mixture critical point. For a mixture to display Type-I phase behavior, the two components must not differ greatly in critical temperature, and the interactions between unlike pairs must be stronger (more attractive) than the average of like-pair interactions. As example, CO_2 with methanol, and with alkanes up to butane [3].

Type III Binary Fluid Phase Diagram :

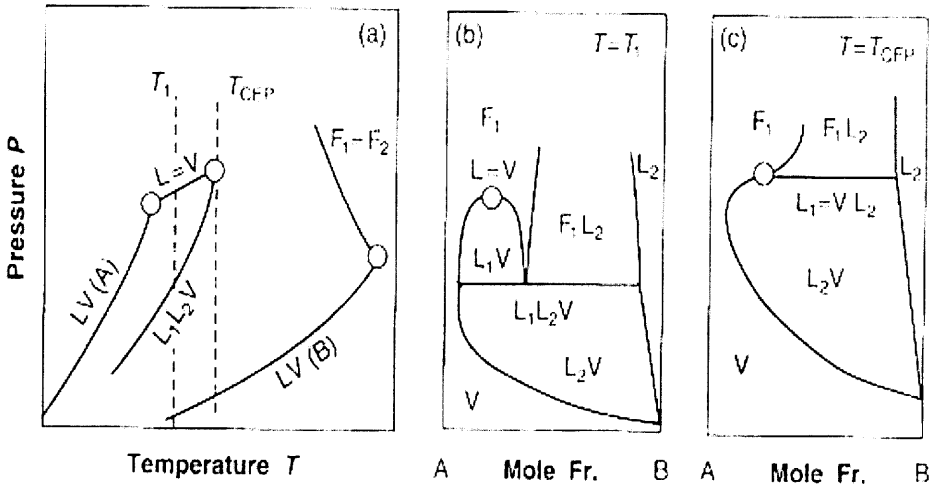

Figure 2.12 The graphs shows cases where critical line does not remain constant due to volatility of solute as well as solvent and additional phase separation occurs in liquid phase.

In many applications, the volatilities of solute and supercritical solvent are very different. In those cases, the critical line usually does not remain connected, and additional phase separation may occur in the liquid phase. Figure 2.12 shows a P-T projection and in two partial P-x sections near and at the critical end point. This type of phase behavior occurs in mixture with large difference in volatility, and in which the attractions between unlike pairs are weaker than the average of those of like pairs. In this type, the involatile solute has only limited solubility in the near-critical solvent. The critical line breaks off at a critical end point (CEP). Additional solute added

collects in a second liquid phase. A three-phase LLV line extends downwards from the critical endpoint. At the solute critical point, a critical line starts that can either move almost straight up to higher pressures, or may first appear to move to lower temperature, but ultimately turns over and moves to higher pressures. On this critical line, it is possible for both temperature and pressure to both is higher than those of the solute. In that case, the critical line is said to be gas-gas, even though the two coexisting supercritical phases may be quite dense due to the high pressures.

Applications of Supercritical Fluids

As supercritical fluid exists in a single phase with several advantageous properties of both liquids and gases, SC fluids have numerous applications in various fields; few of them are discussed here briefly.

Pharmaceutical Applications of Supercritical Fluids:

Supercritical Fluid technology is very attractive for manufacturing therapeutic particles, either of pure active compounds or mixtures of excipient and active compounds. Drug formulation and Particle design using Supercritical Fluids can be operated by several different processes, the choice between them depending on the aimed particle structure, morphology and size distribution, opening new ways for solving drug delivery problems [4].

Organic Synthesis in Supercritical Fluids: The use of supercritical fluids in synthetic organic chemistry remains the subject of increasing interest in the scientific community.

Hydrogenation, Friedel-Crafts alkylation, Etherification, Hydroformylation are few of the types of organic synthesis.

Micelles and Micro emulsions:

Micro emulsions are clear, thermodynamically stable solutions that generally contain water, a surfactant, and "oil". The "oil" in this case is the supercritical fluid phase. The water micro domains have characteristic structural dimensions between 5 and 100 nm. Aggregates of this size are poor scatterers of visible light and hence these solutions are optically clear. Water-in-"oil" (w/o) micro emulsions can have a multitude of different microscopic structures including sphere, rod, or disc shaped aggregates. Micro emulsions dramatically improve the solvent properties of CO_2 and other supercritical fluids to allow the dissolution of a wide range of polar species. Its use by industry has been limited because, by itself, it will dissolve only a small number of compounds having low polarity and low molecular weight. A micro emulsion overcomes the major limitations of CO_2 or other supercritical fluids by making it possible to dissolve highly polar, ionic, high molecular weight species. Following picture shows an example of extraction using micro emulsion.

2.2 Supercritical CO_2 as Antisolvent

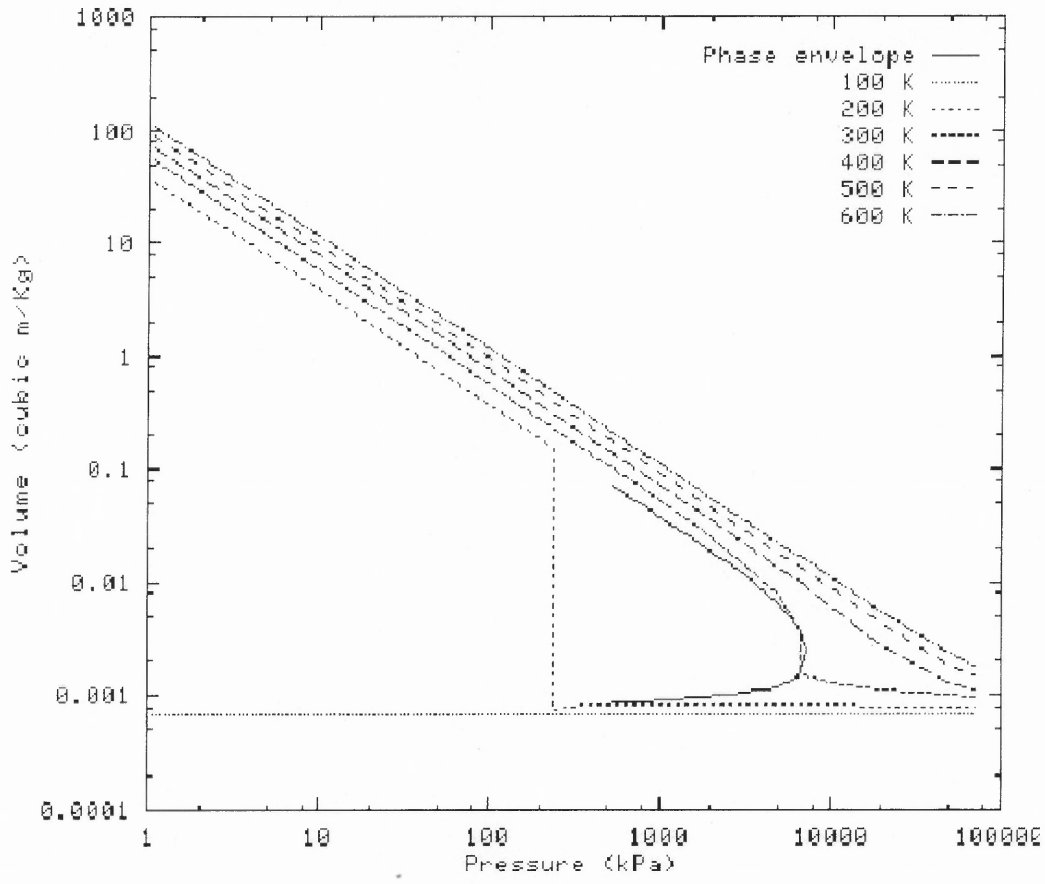

Figure 2.13 Phase diagram (Volume – Pressure) of CO_2.

Carbon Dioxide is most commonly used as an antisolvant because of its "ideal" physical properties. As can be seen in Figure 2.13, it has very low critical temperature (T_c=31.1°C) and pressure (P_c=73.8 bar) [5]. It is also a good solvent, non toxic, non flammable, inexpensive, convenient critical temperature, cheap, chemically stable, non flammable, stable in radioactive applications, easy to remove from the product and environmentally benign. Very significant changes in density and hence solvating properties can be achieved by comparatively small pressure and / or temperature changes (Figure 2.14), particularly around the critical point [6, 7, 8, 9]. Its polar

character as a solvent is intermediate between a truly non – polar solvent such as hexane and weakly polar solvents. Pure CO_2 can be used for many organic solute molecules even if they have some polar characters. It has particular affinity for fluorinated compounds and is useful for working with fluorinated compounds and is useful for working with fluorinated metal complexes and fluoropolymers [10]. These properties make it suitable for extracting. Large amount of CO_2 released accidentally could constitute a working hazard, but hazard detectors are available.

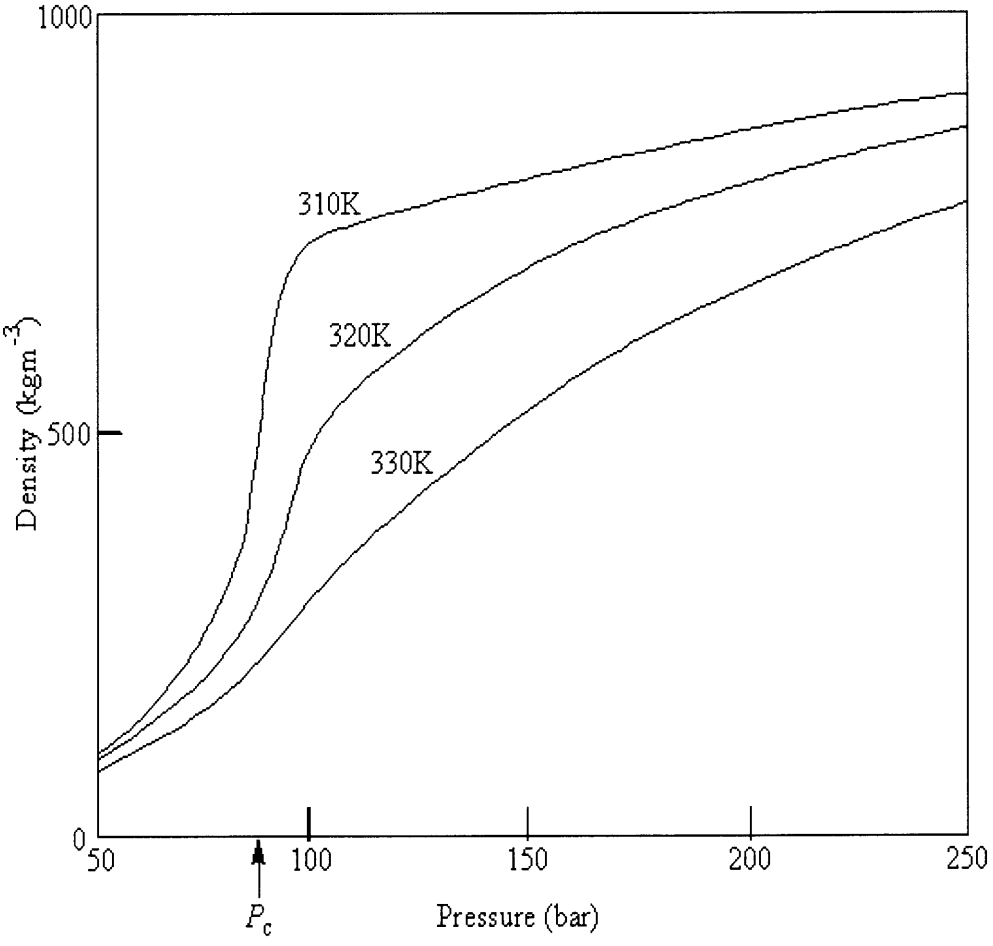

Figure 2.14 Variation of carbon dioxide density with pressure.

Some properties [2] are listed below:

Average mixture critical properties

Critical compressibility : 0.274

Critical density : 10.650 kgmol/m^3

Critical pressure : 7380.000 kPa

Critical temperature : 304.100 K

Normal freezing point : 216.600 K

Mixture properties at 308.15 K and 73.80 Bar

vapor density : 5.978 kgmole/m3

liquid density : 5.978 kgmole/m3

vapor enthalpy : 4195.590 kJ/kgmol

liquid enthalpy : 4195.590 kJ/kgmol

vapor heat capacity : 217.063 kJ/kgmol-K

liquid heat capacity : 217.063 kJ/kgmol-K

feed molecular weight : 44.010 kg/kgmol

vapor molecular weight : 44.010 kg/kgmol

liquid molecular weight : 44.010 kg/kgmol

2.3 Particle Formation Using Supercritical Fluids

Various techniques for the formation of micro/nano particles are described in the literature. Most of them, such as organic phase separation [11, 12], spray drying [13] or solvent evaporation [14], are based on the use of organic solvents for microsphere preparation. The investigation of alternatives to organic solvents, especially in its supercritical state, has attracted considerable interest recently because of its several advantages (discussed in chapter 2.3.1) over traditional techniques.

Two main principles based on supercritical carbon dioxide for microsphere production can be distinguished, namely its use as solvent or as anti-solvent. In the RESS (rapid expansion of supercritical solutions) and SFN (supercritical fluid nucleation) a polymer solution in a supercritical fluid is expanded across a nozzle at supersonic velocities, leading to instantaneous particle formation by precipitation. Again, SFN can be subdivided into various techniques like GAS, SAS, PCA, ASES, PGSS, and SEDS. These techniques are discussed in this chapter.

2.3.1 Methods of Particle Formation Using Supercritical Fluids

Rapid Expansion of Supercritical Fluid Solution: In the RESS process, the supercritical fluid solution expands rapidly through a narrow capillary or orifice nozzle, to a low pressure and low temperature state, which leads to a very high supersaturation at an ultra-short time interval of about 10^{-7} s. The steep increase of supersaturation and rapid density drop prompt an outburst of homogeneous nuclei, and ultra-fine particles with a narrow size distribution are expected to form [15].

Merits and Demerits: This process is relatively easy to implement and simple at least at small scale when a single nozzle can be used. But to form larger number of particles, it needs to have a multi nozzle device instead of single nozzle, which makes it costly and difficult to maintain. Instead of using multi nozzle, one can use a porous sintered disk through which pulverization occurs. But in both the cases, particle size distribution is not easy to control, and may be much wider than in the case of a single nozzle. Moreover, particle harvesting is complex, as it is in any process leading to very small particles. The biggest limitation of RESS development lies in the too low solubility of compounds in supercritical fluids, what precludes production at acceptable costs, as, in most cases, use of a co-solvent to increase solubility in the fluid is not feasible. Its application is restricted to products that present a reasonable solubility in supercritical carbon dioxide (low polarity compounds) [2, 16].

Gas Antisolvent (Supercritical Fluid as Antisolvent): In this method, the solvent power of a polar liquid solvent in which the substrate is dissolved is decreased by saturating it with carbon dioxide in supercritical conditions, causing the substrate precipitation or recrystallization. A batch of solution is expanded by mixing with a dense gas in a vessel. Due to the dissolution of the compressed gas, the expanded

solvent has a lower solvent strength than the pure solvent. The mixture becomes supersaturated and solute precipitates in micro or nano particles. CO_2 is kept flowing through vessel conforming that obtained particles will be dry [16, 17, 18]. In the GAS process, mass transfer typically occurs at low *Re* (<500) by the mechanism of convection and molecular diffusion, leading to relatively small supersaturation for many solutes.

Merits and Demerits: Although, theoretically, very slow expansion in the GAS process should produce a homogeneous supersaturated solution, such expansion is very difficult to control. In addition, it is impossible to achieve high supersaturation levels in the GAS because of the faster process of nucleation [17]. This processes will be having a bright future, especially for drug delivery systems, as it permit to monitor the properties and composition of the particles with a great flexibility and for almost any kind of compounds.

Aerosol Solvent Extraction System: The method involves spraying the solution through an atomization nozzle as fine droplets into compressed carbon dioxide. The dissolution of the supercritical fluid into the liquid droplets is accompanied by a large volume expansion and, consequently, a reduction in the liquid solvent power, causing a sharp rise in the supersaturation within the liquid mixture, and the consequent formation of small and uniform particles. The supercritical fluid is pumped to the top of the high pressure vessel by a high pressure pump. Once the system reaches steady state (temperature and pressure), the active substance solution is introduced into the high pressure vessel through a nozzle. To produce small liquid droplets in the nozzle, the liquid solution is pumped at a pressure higher (typically ~20 bar) than the vessel operating pressure. Particles are collected on a filter at the bottom of the vessel. The

fluid mixture (supercritical fluid plus solvent) exits the vessel and flows to a depressurization tank where the conditions (temperature and pressure) allow gas-liquid separation. After collection of a sufficient amount of particles, liquid solution pumping is stopped and pure supercritical fluid continues to flow through the vessel to remove residual solvent from the particles [16].

Merits and Demerits: The extraction properties of the gas depend on pressure, temperature and the adjusted density. While particles can be produced with nearly every kind of polymer using other methods, ASES seems to be limited to a small number of slow degrading polymers, such as L-PLA and b-PHB only. Fast degrading PLG does not lead to particle formation at all. The reasons for this behavior are not clear.

PGSS: This acronym refers to `Particles from Gas-Saturated Solutions (or Suspensions). This process consists in dissolving a supercritical fluid into a liquid substrate, or a solution of the substrate(s) in a solvent, or a suspension of the substrate(s) in a solvent followed by a rapid depressurization of this mixture through a nozzle causing the formation of solid particles or liquid droplets according to the system.

As the solubility of compressed gases in liquids and solids like polymers are usually high, and much higher than the solubilities of such liquids and solids in the compressed gas phase, the process consists in solubilizing supercritical carbon dioxide in melted or liquid-suspended substance(s), leading to a gas-saturated solution / suspension that is further expanded through a nozzle with formation of solid particles. Typically, this process allows one to form particles from a great variety of substances that need not to be soluble in supercritical carbon dioxide, especially with

some polymers that absorb a large concentration (10–40 wt.%) of CO_2 that either swells the polymer or melts it at a temperature much below (~10–50°C) its melting/glass transition temperature [3, 19]. This process can also be used with suspensions of active substrate(s) in a polymer or other carrier substance leading to composite microspheres.

Particle design using the PGSS concept is already widely used at large scale, at the difference with other process concepts presently under development yet. The simplicity of this concept, leading to low processing costs, and the very wide range of products that can be treated (liquid droplets or solid particles from solid material or liquid solutions or suspensions) open wide avenues for development of PGSS applications, not only for high-value materials but also perhaps for commodities, in spite of limitations related to the difficulty to monitor particle size [16].

SEDS: A specific implementation of ASES consists in co-pulverizing the substrate(s) solution and a stream of supercritical carbon dioxide through appropriate nozzles [20].

This method is used in order to achieve smaller droplet size and intense mixing of supercritical fluid and solution for increased transfer rates. Indeed the supercritical fluid is used both for its chemical properties and as `spray enhancer' by mechanical effect: a nozzle with two coaxial passages allows introducing the supercritical fluid and a solution of active substance(s) into the particle formation vessel where pressure and temperature are controlled. The high velocity of the supercritical fluid allows breaking up the solution into very small droplets. Moreover, the conditions are set up so that the supercritical fluid can extract the solvent from the solution at the same time as it meets and disperses the solution [16].

PCA: In the PCA-type process, the mass transfer is faster than in the GAS, however it relies on the mixing between jet and reservoir fluid, which may not be fast enough to compete with the nucleation and particle growth.

2.3.2 Particle Formation Using SAS

The experimental apparatus mainly consists of two high-pressure pumps that deliver the liquid and the antisolvent. An injection nozzle is used to produce a spray of the liquid solution and a precipitation chamber with a stainless steel filter at the bottom collecting the precipitated powder. A second vessel located after the precipitator is operated at low pressures and used to recover the liquid solvent [21].

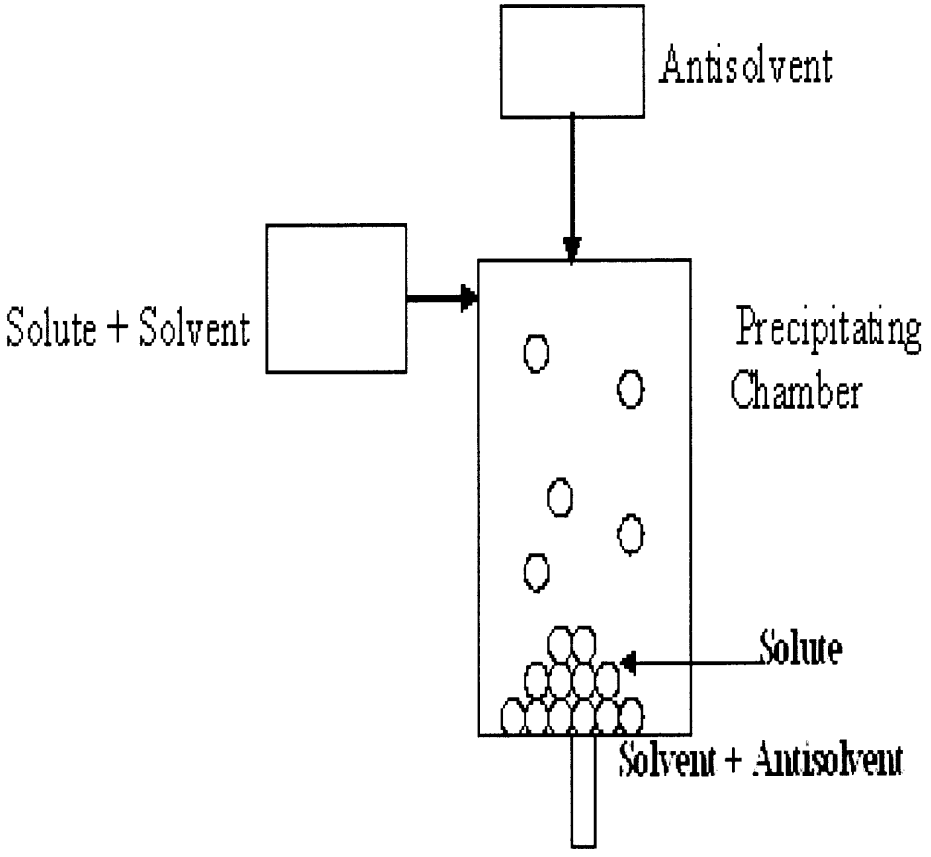

Figure 2.15 Schematic diagrams for SAS process.

In antisolvent processes, solute of interest is dissolved in a suitable organic phase. This organic phase is then contacted with an antisolvent with a low affinity for solutes and appreciable mutual solubility with the organic phase [1]. The principle of

these processes is to decrease the solvent power of a liquid by addition of an antisolvent in which the solute is insoluble. In this process, the mass transfer of the SF into the sprayed droplet determines the rate of particle formation, whereas particle agglomeration and aggregation phenomena are influenced by the rate of solvent mass transfer into the SF from the droplet [2]. Supercritical CO_2 is preliminarily fed to the precipitator at a constant flow rate. An experiment starts when the liquid solvent is fed to the precipitation chamber through the nozzle. The scope of this operation is to assure steady state concentration of the supercritical solution in the precipitator at the beginning of the precipitation process. After few minutes, the liquid solvent is stopped and the liquid solution is fed through the injector. Supercritical CO_2 continues to flow through the chamber to wash the supercritical solution containing the liquid solvent. This operation is very long (20 – 60 min) to avoid the re-condensation of the liquid inside the chamber [21].

Nucleation and growth of crystals from this solute–organic–antisolvent system is governed by two mechanisms: diffusion of the antisolvent inside the organic phase and the evaporation of the organic solvent into the antisolvent phase. Antisolvent diffusion decreases the solute solubility within the organic phase, whereas the solvent evaporation increases its concentration. Therefore, high supersaturation can be achieved. Morphology can be controlled by manipulating process variables, such as temperature, flow rate, agitation rate and pressure. Crystals of small size and of narrow size distribution are usually obtained when solute are consumed mainly by nucleation, thus for concentrated solutions or large diffusion rates. On reverse, crystals of larger average size and sizes distribution will be formed in conditions where only few nuclei are formed and grown [1].

The SAS process has better control on particle size and size distribution than traditional methods and as it's a one step process better quality of the particles can be maintained easily.

2.3.3 Factors Influencing Particle Properties For SAS Technique

Different researchers have done many experiments. Different approaches and designs have been considered to get micro / nano particles with narrow size distribution. Though the morphology of the resulting solid material depends on the material structure (crystalline or amorphous, composite or pure etc.) [16], the particle size varies with process parameters. So the effects of parameters on particle size and particle size distribution is being studied and presented in different papers. Here the effect of parameters on particle size and different approaches used by different researchers are discussed.

1. ***Pressure:*** Effect of pressure on particle size is being studied by varying pressure in large units. Pressure as low as 90 bar to as high as 400 bar is used to study the effect on particle size by different researchers. Many researchers concluded that as working pressure increases, particle size decreases [22, 23, 24, 25 and 26] but there are contradictions to these statements. M Rantakyala [37] showed that if pressure increases, the particle size increases. D. Dixon showed that there would not be any effect of pressure on particle size above 120 Bar [24]. Thus there is no conviction in results but a general conclusion can be drawn which will be agreed by most of people that as pressure increases particle size decreases. This statement may be contradictory for few solutes but in general these results can be defended.

2. ***Temperature:*** Temperature is always being a special concern as very high temperature would be unfavorable as it may exceed glass transition temperature affecting crystallinity. Most of the time, 35^0C is used when antisolvent is CO_2 in the process. Particle size seems to have a strong correlation with temperature. An explanation for the strong temperature effect on particle size is that the assumption of one agglomerated particle developing from each droplet is not adequate. The droplets are possibly colliding with each other and combining or some droplets are breaking up. Another explanation may be that several particles, which later agglomerate, are born inside each droplet. Therefore, the final particle size is possibly determined more by the mass transfer of CO_2 into the droplet. The change of temperature affects the density of CO_2 and therefore also the mass transfer between liquid and CO_2 [27]. So, studies shows as increase in temperature results in increases in particle size [27, 28] but is contradicted by K. Krober [36]. E. Reverchon affirmed first particle size increases with increase in temperature but then decreases with further increase in temperature [6].

3. ***CO_2 density:*** Effect of CO_2 density on particle size is studied in different experimentations using different materials and solvents. Perhaps, there are many inconsistencies in the results. D. Dixon as well T. Randolf [25, 28] stated that as density of CO_2 is directly proportional to particle size that is, if density increases particle size increases. But this statement is contradicted by M. Rantaklya, who showed exact opposite results in a paper [27]. There may be upcoming results, which can focus well on the relation between CO_2 density and particle size.

4. ***Reynolds Number:*** B. Shekunov has focused on the influence of Reynolds number on particle size. He concluded that particle size decreases due to establishment of super saturation profile at $Re<10^4$. At higher Re, particle size increases as Re increases [27, 29].

5. ***Initial Drop Formed*:** As particles formed by disintegration of drops, drop size is important for final particle size. But it is been found that there is no effect of initial droplet formed at nozzle end on final particle size. Equation is been formulated and proved by M. Rantaklya [27].

6. ***Nucleation:*** Particle size is inversely proportional to nucleation. If nucleation and crystal growth takes place at slow rate then particle size increases [30]. Thus it is favorable to have nucleation as fast as possible to get smaller particle size.

7. ***Solution Flow Rate:*** Particle size depends on CO_2 diffusion in solution. To have good diffusion between solution and CO_2 it is desirable to have lower concentration of solution. Lower flow rate helps better diffusion of CO_2 in solution. Thus, lower particle size can be obtained by lowering flow rate [30, 31].

8. ***Velocity difference:*** Velocity difference between solution and CO_2 does not play any important role in particle size [27].

9. ***Nozzle Diameter:*** As far as nozzle is of same shape, there is no effect of nozzle diameter in particle size or morphology [23]. Apart from just showing relations between different process parameters and particle size, researchers are now using different techniques like using co-axial nozzles, ultrasonic nozzles, nozzles having pre mixing facilities etc. Also formulas are getting derived showing relations between different parameters and particle size.

2.4 Effect of Jet Breakup Processes on The Particle Formation

To study whether the diameter of particles formed in Supercritical As Antisolvent (SAS) process as a result of droplet disintegration is depend on diameter of droplets and uniform diameter size distribution of droplets, jet behavior, droplet disintegration regime and droplet disintegration is studied by changing various parameters like nozzle diameter, velocity of jets, temperature and pressure. The study of relationship between particle diameter and size distribution with operating conditions is being special interest of research in this area. So a detailed analysis of the jet flow is the first step in the development of a comprehensive model capable of facilitating the design and optimization of the SAS technology.

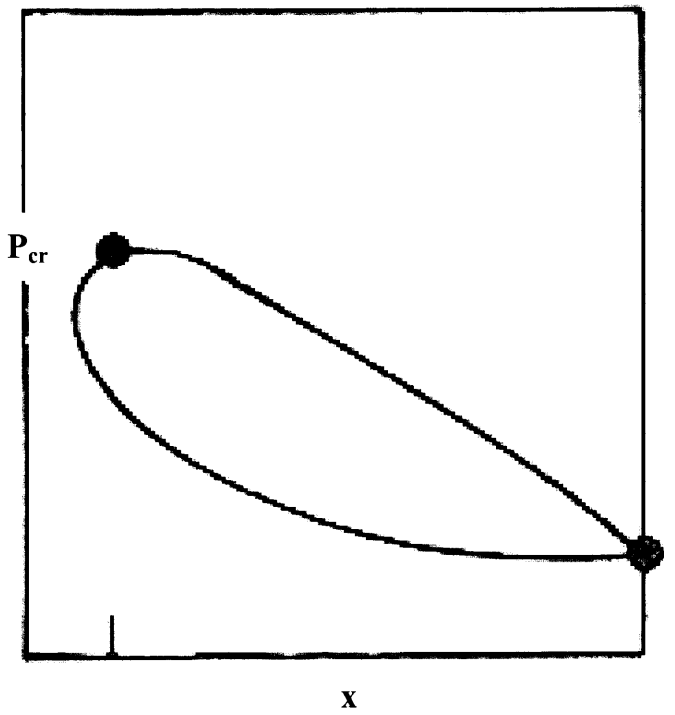

Figure 2.16 The isothermal phase diagram of a binary mixture, P vs. molar composition, x, for a temperature above the critical temperature of the light component A, but below the critical temperature of the heavy component, B.

Figure 2.16 shows the simplest isothermal phase diagram of a binary mixture in terms of pressure, P versus molar composition x, for a temperature above the critical temperature of the light component, but, still below the critical temperature of the heavy component [32]. The fluids are completely miscible for a pressure greater than the critical pressure of a mixture, $P_{cr,m}$ but are only partially miscible for a pressure lower than $P_{cr,m}$. If the heavy component is injected into a chamber containing the light component at a pressure below $P_{cr,m}$, the jet pattern typical of two immiscible fluids can be expected. On the other hand, if the chamber pressure is above $P_{cr,m}$ the jet pattern typical of two miscible fluids is expected. While numerous previous studies have demonstrated this drastic difference in the jet behavior below and above the critical pressure, very little information is available in the literature on the transformation of the jet structure from a two-phase pattern typical of immiscible fluids to a single-phase pattern typical of miscible fluids with an increase in the chamber pressure over a pressure range close to the critical point of a mixture.

The pressure-composition diagram at the operating temperature of 35°C (being above the critical temperature of CO_2) calculated with the use of Soave-Redlich-Kwong equation of state, and plotted in Figure 2.17.

$$P = \frac{RT}{V - b_m} - \frac{(\alpha a)_m}{V(V + b_m)} \tag{2.1}$$

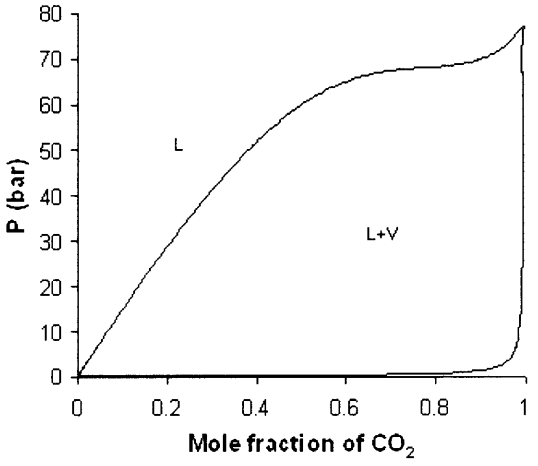

Figure 2.17 Equilibrium phase diagram "pressure vs. CO_2 mole fraction" at 308 K computed for the carbon dioxide-ethanol mixture.

Considering Ethanol – CO_2 system for example, as can be seen in Figure 2.18, the solubility of CO_2 in liquid ethanol and the solubility of ethanol vapor in gaseous CO_2 are relatively low at low pressure. With increasing the pressure, the solubility of carbon dioxide in ethanol increases sharply whereas the solubility of ethanol vapor in CO_2 does not exceed at a reduced pressure of $P/P_{cr,m}$ =0.9. Above the critical pressure of a mixture, ethanol and carbon dioxide become completely miscible.

Flow regimes of ethanol injected into stagnant carbon dioxide for the chamber pressure below the critical pressure of a mixture were found to be typical of jets when a liquid is injected into another immiscible liquid [33, 34, 35]. In particular, presented in Figure 2.18 images show the appearance of liquid jets at various velocities for subcritical chamber pressure, $P/P_{cr,m}$ ==0.83. At low flow rates [Figure 2.18] drops are formed individually at the tip of the nozzle, and break off when they attain a particular size (dripping flow). At larger velocities, jetting flow forms [Figure 2.18]. For velocities below approximately 4-5 m/s, drops detach the jet tip at some distance downstream of the nozzle because of the growth of long-wavelength

disturbances. These disintegration regimes correspond to the Rayleigh and wind-induced breakup [35]. Presented in Figure 2.18 photos taken at various distances below the nozzle demonstrate that drops formed at subcritical pressure do not dissolve in CO_2, as they fall down, for at least several seconds.

Presented in Figure 2.19 photos show the flow patterns of ethanol injected at various velocities into carbon dioxide for the chamber pressure above the critical pressure of a mixture, $P/P_{cr,m}$ =1.15. These images strongly resemble a cone-like structure of single-phase jets (the jet width increases nearly proportional to the distance from the nozzle orifice) when a gas injected into gas [36]. The thread-like surfaces disturbances ("ligaments") grow downstream but in contrast to jets for subcritical pressure do not break up into drops under these conditions. The observed cone-like jet structures are consistent with the appearance of jets of cryogenic liquids injected into supercritical surroundings [37] and jets in binary systems above the critical pressure of a mixture when both fluids are miscible [38, 39].

Images presented in Figure 2.20 show flow patterns of ethanol injected at different velocities at the chamber pressure slightly above the critical pressure of a mixture, $P/P_{cr,m}$ =1.03. They appear to be similar to those observed for subcritical chamber pressures, varying from dripping to jetting with the Rayleigh and wind-induced breakup regimes, as the jet velocity increases [Figure 2.18] the injected liquid disintegrates into drops, which gradually disappear as they fall down. With increasing the velocity, the drops become smaller and disappear faster. Comparison of flow structures presented in Figures 2.18 and 2.20 shows that the disappearance of falling drops is the main difference in the flow structures of ethanol injected below and slightly above the critical pressure of a mixture. This similarity in the flow patterns clearly demonstrates the presence of a transient surface tension at the liquid-

surroundings interface slightly above $P_{cr,m}$. This fact is consistent with data on the development of instabilities at the interface between two miscible liquids at atmospheric pressure for a variety of hydrodynamic situations [40], which indicate the presence of a transient surface tension governing these processes, whereas the equilibrium surface tension at this interface is zero.

Experimental data on the dependence of the jet breakup length, L, on the jet velocity, U, for the range of chamber pressures below and slightly above $P_{cr,m}$ when jets disintegrate into drops, i.e., exhibit behavior typical of immiscible fluids, are presented in Figure 2.21. Beyond the dripping flow regime, the jet length at first increases with increasing the jet velocity (Rayleigh's breakup) and then, reaching a maximum, decreases (the wind-induced breakup).

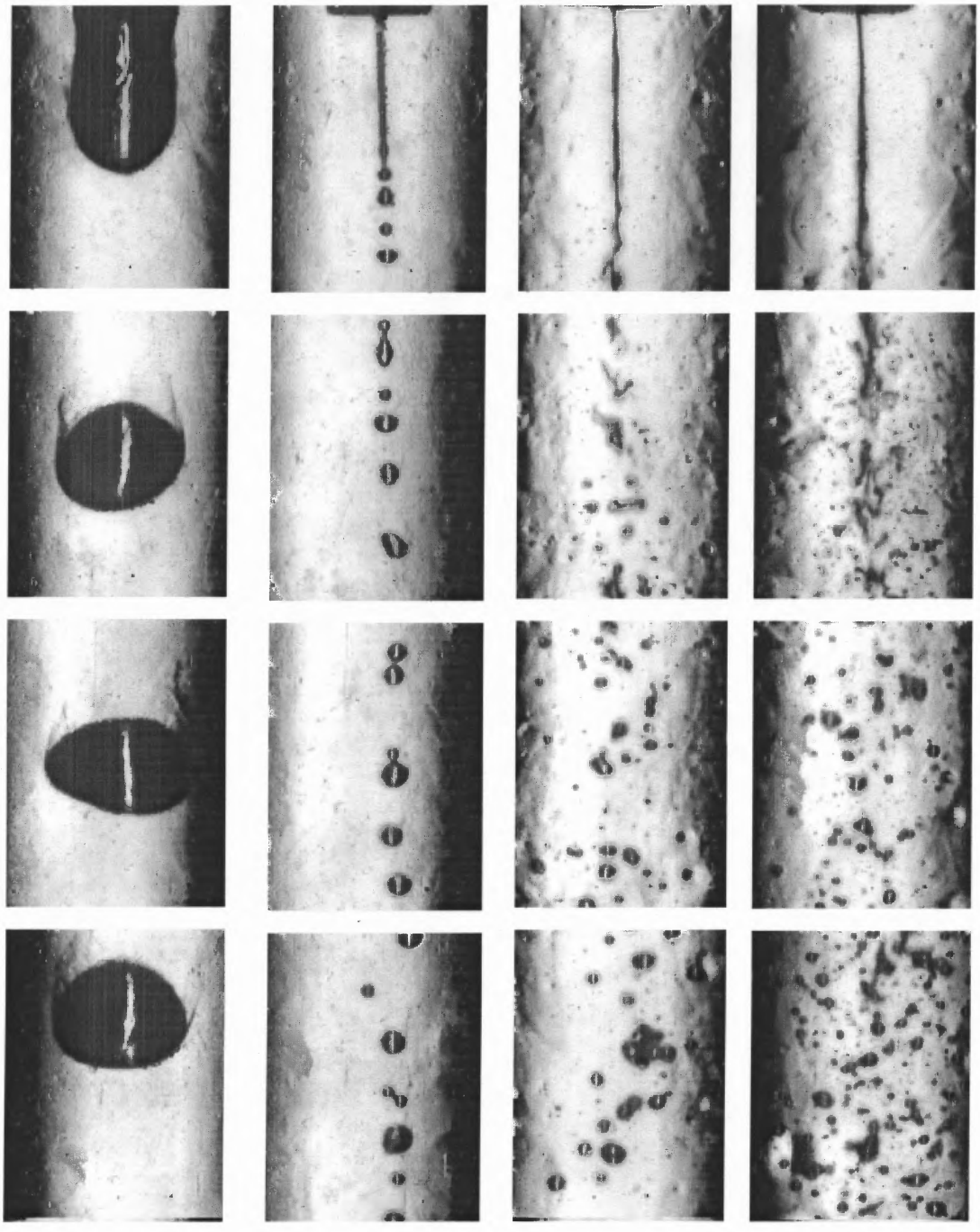

A	B	C	D
0.50 m/s	0.64 m/s	2.50 m/s	4.05 m/s

Figure 2.18 Photos of ethanol injected into carbon dioxide at 70 bar and 35° C for velocities: (A) 0.50 m/s, (B) 0.64 m/s, (C) 2.50 m/s, and (D) 4.05 m/s, which were taken at different locations below the nozzle: 0 (1st row); 4 mm (2nd row); 8 mm (3rd row); and 12 mm (4th row). The nozzle diameter is 127 μm.

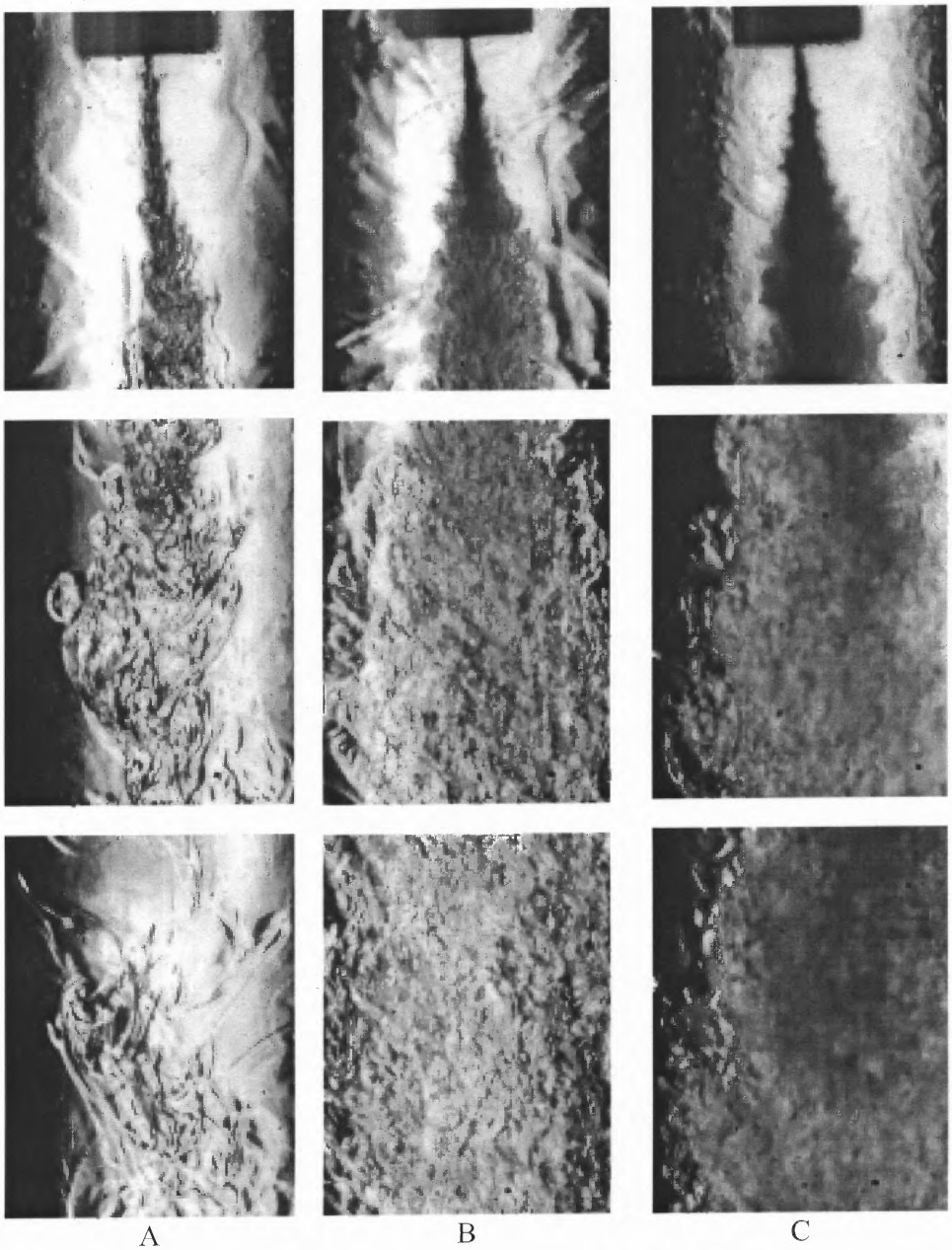

Figure 2.19 Photos of ethanol injected into carbon dioxide at 35° C and pressure 90 bar for velocities: (A) 0.22 m/s, (B) 1.45 m/s, and (C) 2.50 m/s, which were taken at different locations below the nozzle: 0 (1st row); 4 mm (2nd row); 8 mm (3rd row); a 12 mm (4th row). The nozzle diameter is 127 μm.

Data for 80 bar

(A) 0.78 m/s

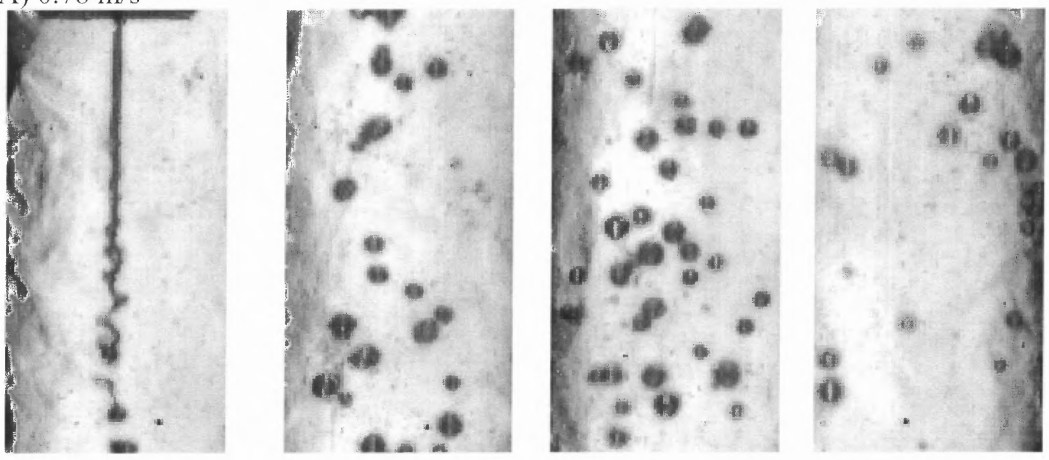

0 4 mm 8 mm 12 mm

(B) 1.25 m/s

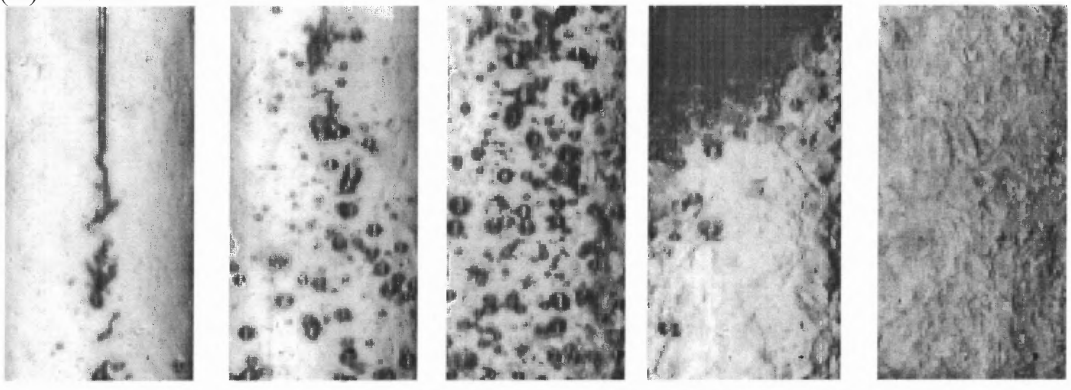

0 4 mm 8 mm 12 mm 16 mm

Figure 2.20 Photos of ethanol injected into carbon dioxide at 35° C and pressures 80 bar for velocities: (A) 0.78 m/s which were taken at 0, 4 mm, 8 mm, and 12 mm below the nozzle, and (B) 1.25 m/s which were taken at 0, 4 mm, 8 mm, 12 mm, and 16 mm below the nozzle. The nozzle diameter is 127 μm.

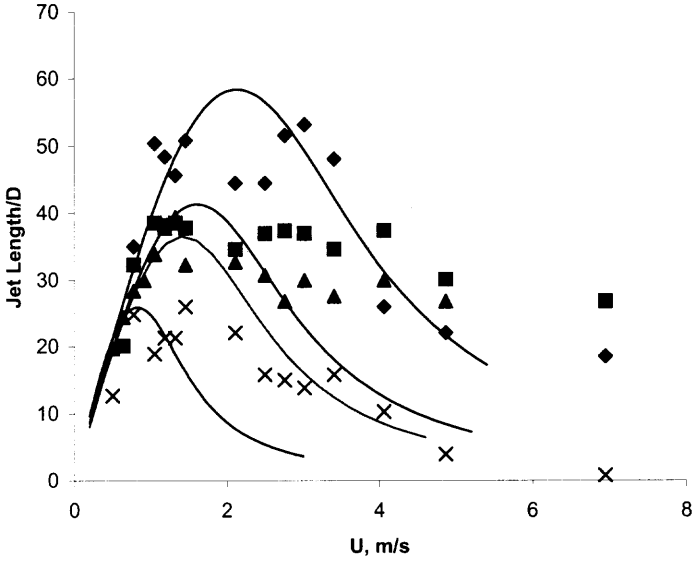

(a)

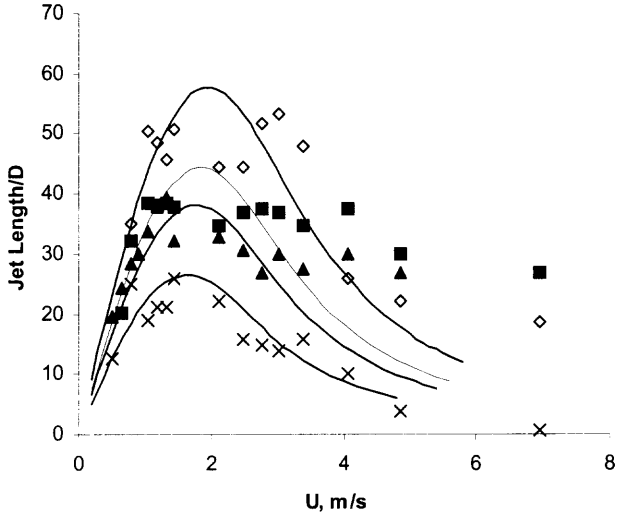

(b)

Figure 2.21 Experimental data (symbols) on the dependence of the jet length, L/D, on the jet velocity, U, for 57 bar (diamonds), 70 bar (squares), 74 bar (triangles), and 80 bar (crosses). D = 127μm is the nozzle diameter. Predictions (solid lines) obtained by using (a) σ_2 and (b) σ_3 for surface tension in the equation for the growth of disturbances.

Experiments performed on the disintegration of ethanol injected into a pressurized carbon dioxide over a pressure ranging from below to above the critical point of the ethanol-carbon dioxide mixture, $P_{cr,m}$, indicate that the flow patterns below $P_{cr,m}$ appear to be the same as those typical of immiscible fluids (varying from dripping flow to the Rayleigh and wind-induced breakup and then to spraying with increasing the jet velocity), whereas the jet structures far above $P_{cr,m}$ strongly resemble a cone-like structure of single-phase gaseous jets. However, the flow patterns for pressures slightly above $P_{cr,m}$ were found to be similar to those observed below $P_{cr,m}$.

Due to a short pre-breakup period, $\sim 1-2\mu s$ the effect of the mass transfer between the liquid and the surroundings on the jet stability was found to be insignificant. Therefore, a classical theory for the breakup of a viscous liquid jet was invoked for interpreting experimental data on the Rayleigh and wind-induced breakup. The diffusion of carbon dioxide into falling drops was shown to play the major role in mass transfer for subcritical chamber pressures, thereby leading to slowly mixing of the injected liquid with CO_2. The faster mixing of injected liquid at pressures above $P_{cr,m}$ was found to be caused by a significant increase in diffusion when the liquid becomes miscible with the surroundings and by additional hydrodynamic mixing since, under these conditions, the mass transfer is not limited by diffusion inside drops.

CHAPTER 3

EXPERIMENTAL RESULTS OF JET BEHAVIOR OF LIQUIDS IN BINARY SYSTEM

3.1 Experimental Setup

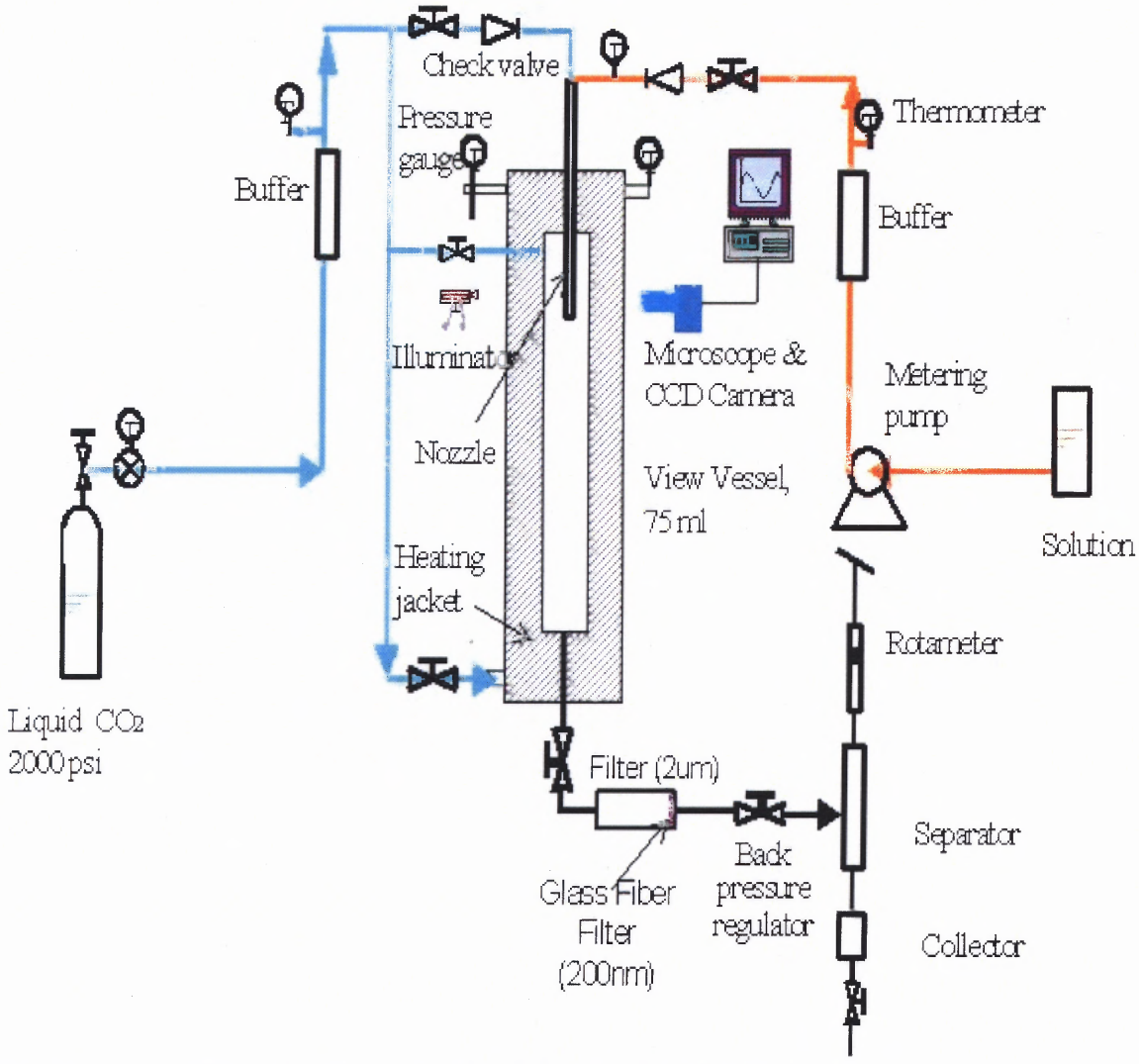

Figure 3.1 A setup equipped with a flow visualization system.

An experimental setup [Figure 3.1 and Figure 3.2] comprises of two systems – particle formation system and visualization system. The particle formation system consists of high-pressure view cell, which can sustain high-pressure upto 3000 psi. A *red*

flow line represents the flow path of solution and *aqua* represents for the flow path of CO_2. A high pressure-metering pump (Prep 100, Scientific Systems) pumps solution into view cell (with a cross-sectional area of 12.7mm × 12.7mm) of 75 ml in capacity (Jerguson Gauge, T19-32). The view cell has double-sided (front and back) sapphire windows (320mm × 16mm) for flow visualization. The view cell can withstand pressures of up to 200 atm (3,000 psi) and temperatures up to 200°C. Velocity of injected solution can be adjusted from 0.1 ml/min to 100 ml/min. The flow rate of supercritical CO_2 is controlled by backpressure regulator (max 4000 psi, Tescom). A cyclone separator located after the backpressure regulator is used to recover the liquid that is accumulated in a collector placed at the bottom of the separator. Rotameter (VA22440, Dwyer) is put in the flow line of CO_2 to measure the quantity of CO_2 delivered. Heating pads (SRFG-512 and FGH051-060, Omega) are attached to the view cell, which keeps the temperature of view cell constant. Heating tapes are wounded to the CO_2 and solution buffers (SS316L-50DF4-150, Swagelok) to increase the temperature to desire value through proportional-integral-derivative controllers (D85011, Dwyer). Pressure gauges are connected to view cell to read pressure and pressure regulator is connected to CO_2 cylinder (Bone-dry, 99.9%, supplied by Messer Inc) to control pressure. A high-pressure pump (M1/3, HP, Haskel) is connected to CO_2 flow line before CO_2 heating buffer to increase CO_2 pressure to desired value. Thermocouples (SMPW-T-M, Omega) are connected in view cell as well as after buffers to read temperature of CO_2 and solution after passing through buffers and in the view cell. A flexible tube is connected between filter and pressure regulator to remove and connect filter with ease. Whole setup is wounded with insulating tape to control the temperature.

Figure 3.2 Photograph showing experimental setup.

The optical visualization system is comprised of microscope lens (Zoom 160, Optem), a high-speed CCD camera (LaVision, Germany) and a computer with the image capture software (Davis 6.5, LaVision, Germany). The view field varies from 0.3 mm × 0.4 mm to 20 mm × 27 mm; the working distance can be adjusted from 52 mm to 114 mm. Two different high-speed cameras were used. The first one employs a uniform illumination by a diffused light and takes pictures at the rate of 85 frames per

second in an exposure time less than 100 μs. The pixel resolution is 648 × 484 per frame. The second one (LaVision, Germany) employs an Nd: YAG dual cavity pulsed laser (Solo 50 PIV, New Wave Research) and takes double shots with an exposure time of 0.5 μs and a 15-μs delay. The images have a pixel resolution of 1280 × 1024 per frame. A relatively large difference in refractive indexes between the solution and CO_2 (1.05 - 1.25, depending on density) provides with a capability of visualizing the jet structure with a resolution of several microns.

Modifications Done In the Experimental Setup

The major problem in the field of supercritical fluids is particle collection. Many researchers are adopting different methods to make particle collection effective. The methods include in-line filters, collecting particles on sticky tapes, collecting them on glass rods etc. In all the methods, biggest problem is particles agglomerate. In the existing setup in our lab, we have in-line filter. It was difficult to collect particles as in-line filter being blocking due to particle segregation. To avoid blocking, an auxiliary glass fiber filter (200 ήm) is placed in front of stainless steel filter (2 μm) so that it could be easily replaced every time. The filter is made horizontal so that collected particles can slide on each other giving way to CO_2 to flow thought filter without blocking it. Also while depressurizing the chamber, some solution used to come out of nozzle, dissolving particles on the filter. To exterminate this problem, a valve is placed in between the chamber and the filter so that by closing the valve, filter can be taken out without depressuring chamber and particles are collected successfully.

Also, few proposals are been made to modify flow lines to reduce the distance between buffer and nozzle for solution and increase in CO_2 buffer as exist buffer is too small for current experiments. The CO_2 flow line could be modified by using

flexible metal tube to allow CO_2 flow through nozzle as well as existing way. By this modification it would be easy to get rid of solution in the nozzle to eliminate nozzle-blocking problems. In combination with this, both of the in-line valves can be placed very near to nozzle so that CO_2 as well as solution would not be accumulating in the lines before nozzle causing nozzle blocking.

3.2 Breakup of the Ethanol Jet Injected Into CO_2

As a first step of studying effect of jet breakup process on particle formation break up of ethanol jet into CO_2 is studied at different injection velocities at different CO_2 pressures and temperatures as stated in Chapter 2.4. The complete data of the experiment is presented quantitatively in this chapter including snap shots of jet break up for different process parameters showing different kinds of jets and graph of jet lengths at different process parameters. Four different jet patterns are investigated for every pressure, namely, dripping flow, symmetric jet, sinusoidal jet and spray. For every pressure, every kind of jet pattern is shown in following photographs. According to pressure, the velocity of jet for which the pattern changes, changes. To avoid repetition, photographs of dripping flow are not shown for every pressure.

Snapshots for pressure 34, 57 and 60 bar for temperature 35°C are shown below. For all other operating conditions, they are placed in the Appendix.

3.2.1 Snap Shots of Ethanol Jets

1. For Temperature = 35°C,

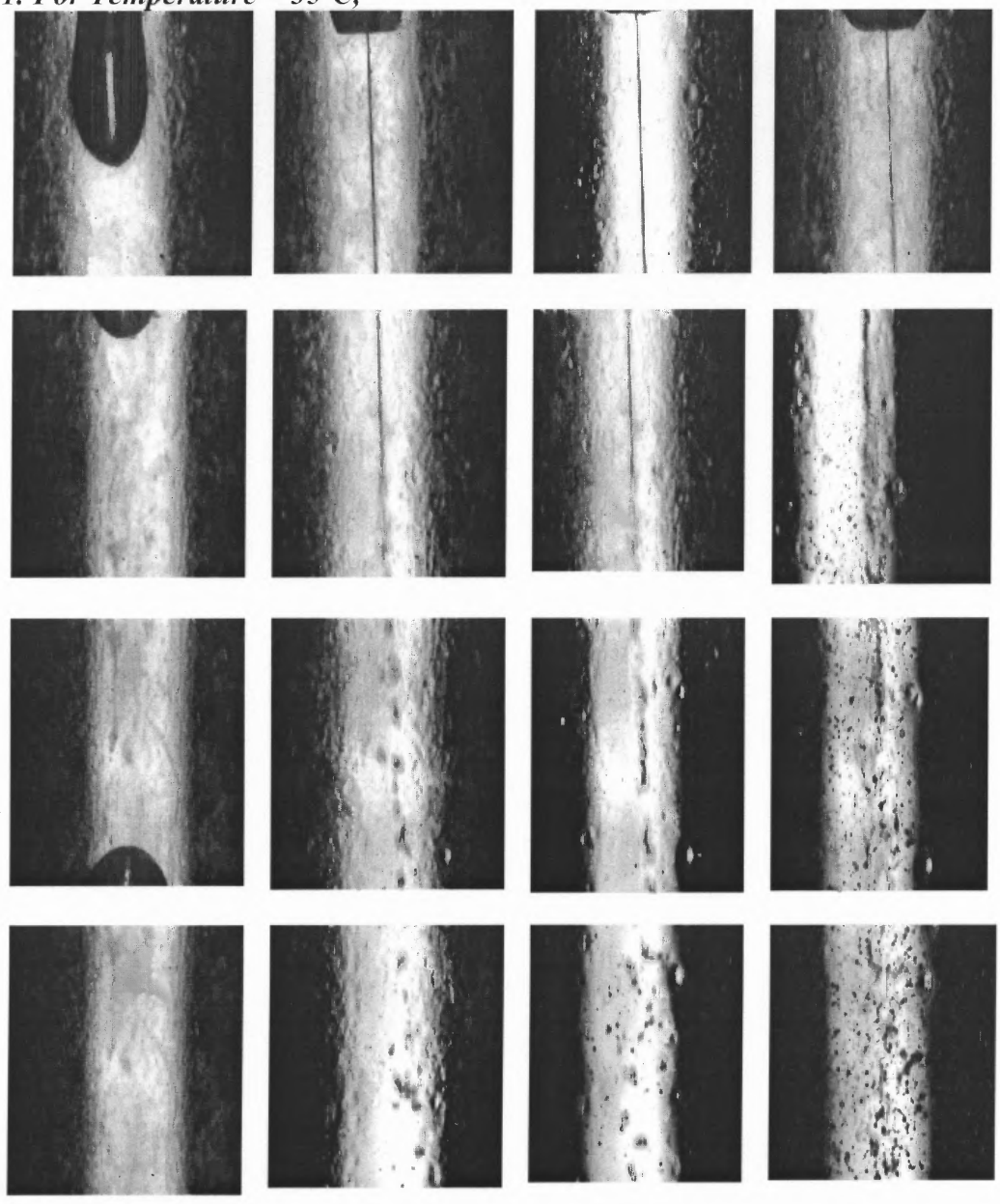

(A) v = 0.5 m/s (B) v = 1.27 m/s (C) v = 2.05 m/s (D) v = 7.78 m/s

Figure 3.3 Photos of ethanol injected into carbon dioxide at 34 bar and 35° C for velocities: (A) 0.50 m/s, (B) 1.27 m/s, (C) 2.05 m/s, and (D) 7.78 m/s, which were taken at different locations below the nozzle: 0 (1st row); 4 mm (2nd row); 8 mm (3rd row); and 12 mm (4th row). The nozzle diameter is 127 μm.

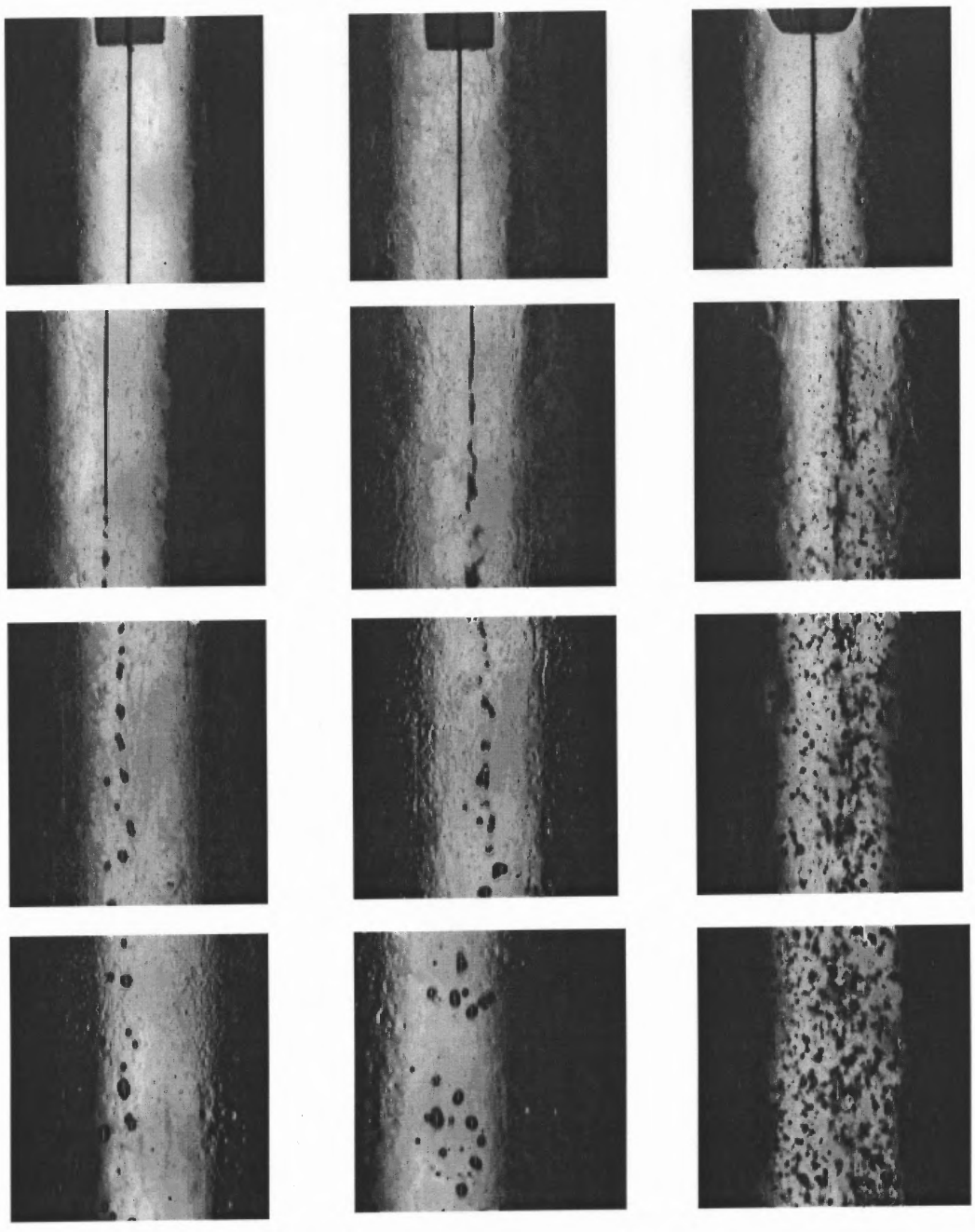

(A) v = 1.45 m/s (B) v = 2.37 m/s (C) v = 5.43 m/s

Figure 3.4 Photos of ethanol injected into carbon dioxide at 57 bar and 35° C for velocities: (A) 1.45 m/s, (B) 2.37 m/s, (C) 5.43 m/s, which were taken at different locations below the nozzle: 0 (1st row); 4 mm (2nd row); 8 mm (3rd row); and 12 mm (4th row). The nozzle diameter is 127 μm.

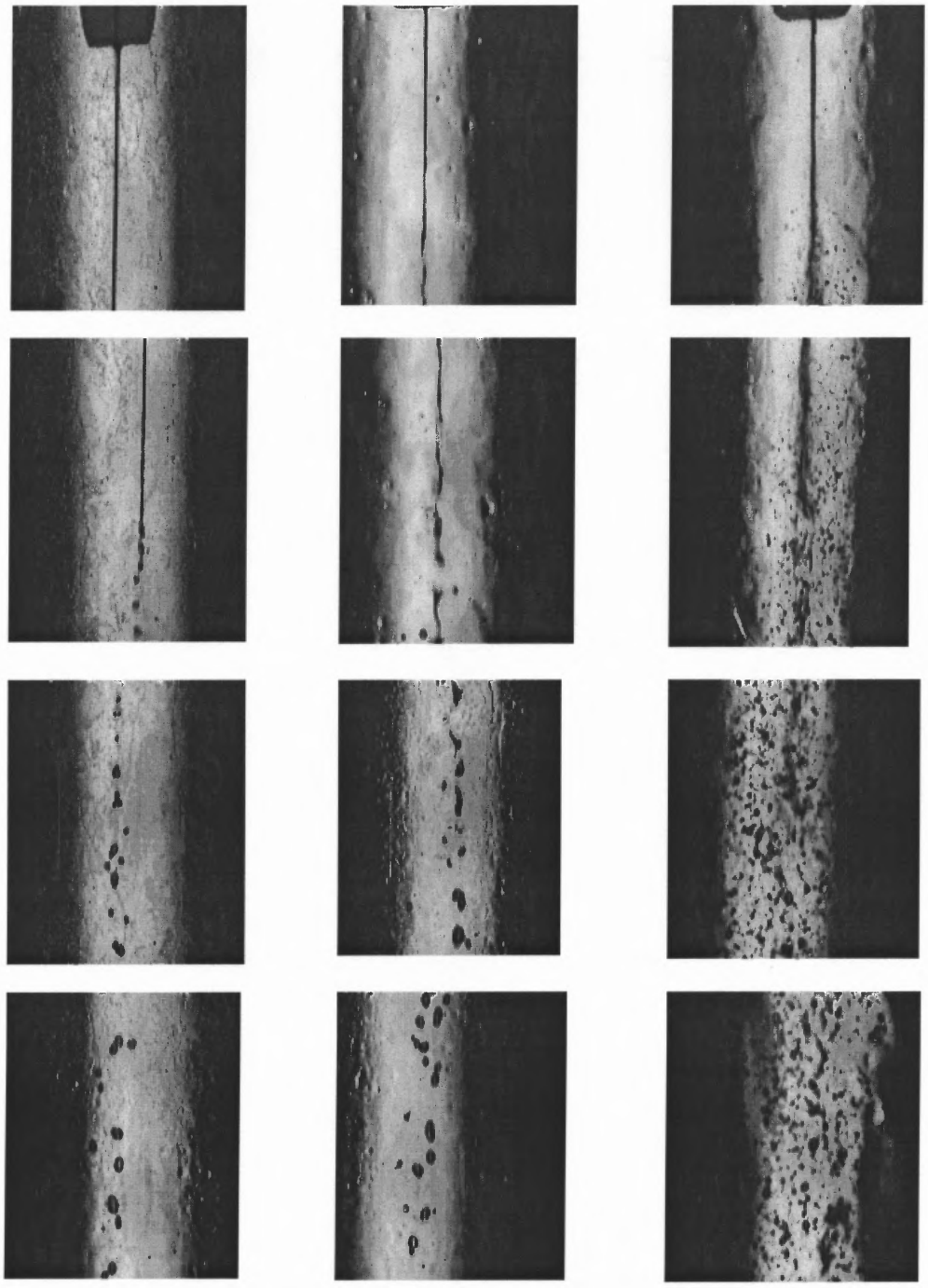

(A) v = 1.32 m/s (B) v = 2.88 m/s (C) v = 5.43 m/s

Figure 3.5 Photos of ethanol injected into carbon dioxide at 60 bar and 35° C for velocities: (A) 1.32 m/s, (B) 2.88 m/s, (C) 5.43 m/s, which were taken at different locations below the nozzle: 0 (1st row); 4 mm (2nd row); 8 mm (3rd row); and 12 mm (4th row). The nozzle diameter is 127 μm.

3.2.2 Graphs of Jet Lengths at Different Pressures

The systematic study of jet behavior is carried out and graph of liquid jet is plotted with L/D_{nozzle} ratio versus injection velocity (in m/s). In this chapter graph of ethanol jet at different pressures and temperatures is been presented and certain conclusions are drawn accordingly showing the relation between jet length and temperature.

Graphs for pressure 7, 34, 57 and 60 bar for temperature 35°C are shown below. For all other operating conditions are placed in Appendix.

1. **For Temperature *35° C***

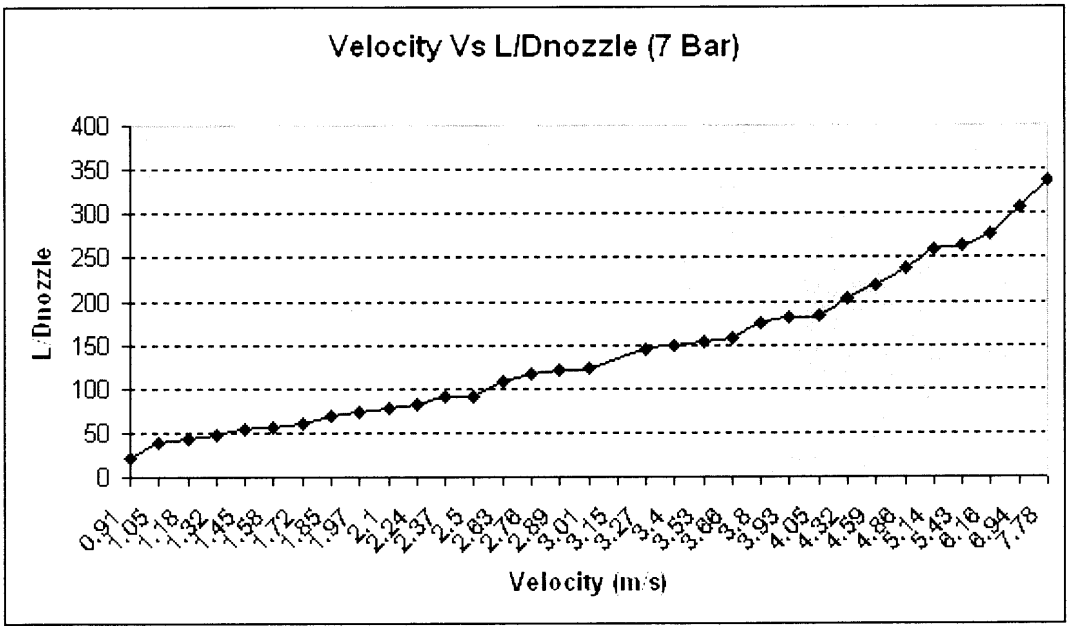

Figure 3.6 Pressure = 7 Bar, Temperature = 35 C, Velocity of injected ethanol varies from 0.91 m/s to 7.78 m/s.

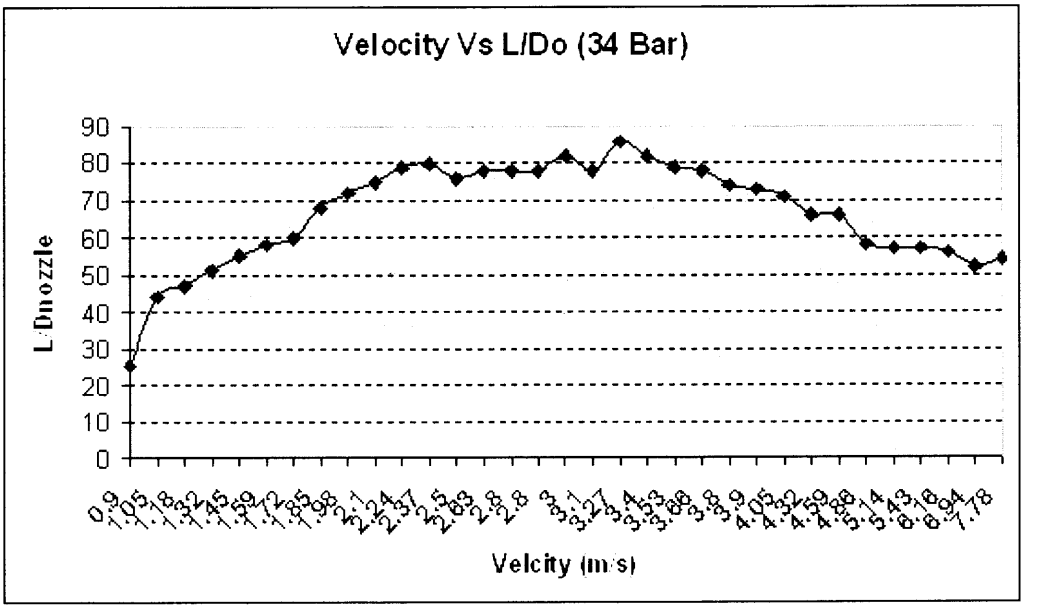

Figure.3.7 Pressure = 34 Bar, Temperature = 35 C, Velocity of injected ethanol varies from 0.9 m/s to 7.78 m/s.

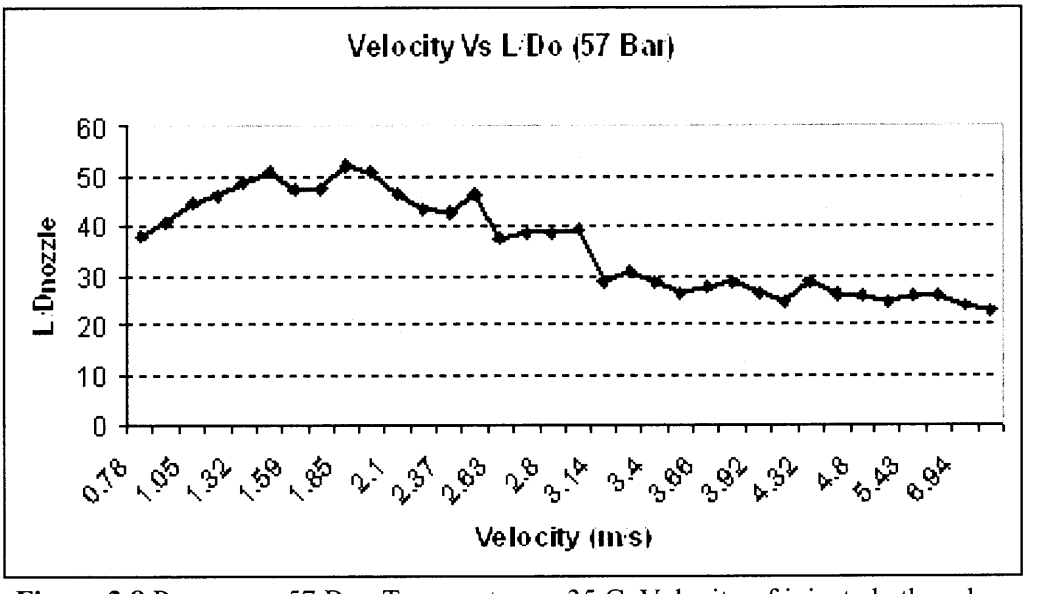

Figure 3.8 Pressure = 57 Bar, Temperature = 35 C, Velocity of injected ethanol varies from 0.78 m/s to 7.78 m/s.

3.2.3 Effect of Parameters on Jet Length

The main results of the experiments are as follows:

1. As pressure increases, jet length for any injection velocity decreases, also, highest jet length for the particular pressure and temperature also decreases.

2. For a given pressure, as velocity increases, jet length increases till certain velocity and then decreases, change in jet pattern is observed when jet length starts decreasing after achieving maximum jet length.

3. As temperature increases, jet length increases for the injection velocity and the pressure.

4. As pressure increases, highest length of jet shifts towards lower velocity.

5. For ethanol, at 88 bar, liquid jet changes to gas like jet.

6. Pressure increases, all four types of jet flows (dripping, systematic, wavy, spread) shifts towards lower velocity.

7. After a particular injection velocity, jet turns into spray. This critical velocity reduces with increase in pressure.

3.3 Breakup of the Acetone Jet Injected Into CO_2

For many solutes, acetone is an alternative as a solvent instead of ethanol so it was been necessary to collect information about acetone – CO_2 system as a first step of studying effect of jet breakup process on particle formation break up of acetone jet into CO_2. So this phenomenon is studied at different injection velocities at different CO_2 pressures and temperatures. The complete data of the experiment is presented quantitatively in this chapter including snap shots of jet break up for different process parameters showing different kinds of jets and graph of jet lengths at different process parameters. Four different jet patterns are investigated for every pressure, namely, dripping flow, symmetric jet, sinusoidal jet and spray. For every pressure, every kind of jet pattern is shown in following photographs. According to pressure, the velocity of jet for which the pattern changes, changes. To avoid repetition, photographs of dripping flow are not shown for every pressure.

Snapshots for pressure 57 and 60 bar for temperature 35°C are shown below. For all other operating conditions, they are placed in Appendix.

3.3.1 Snap Shots of Jets

1. For Temperature = 35°C,

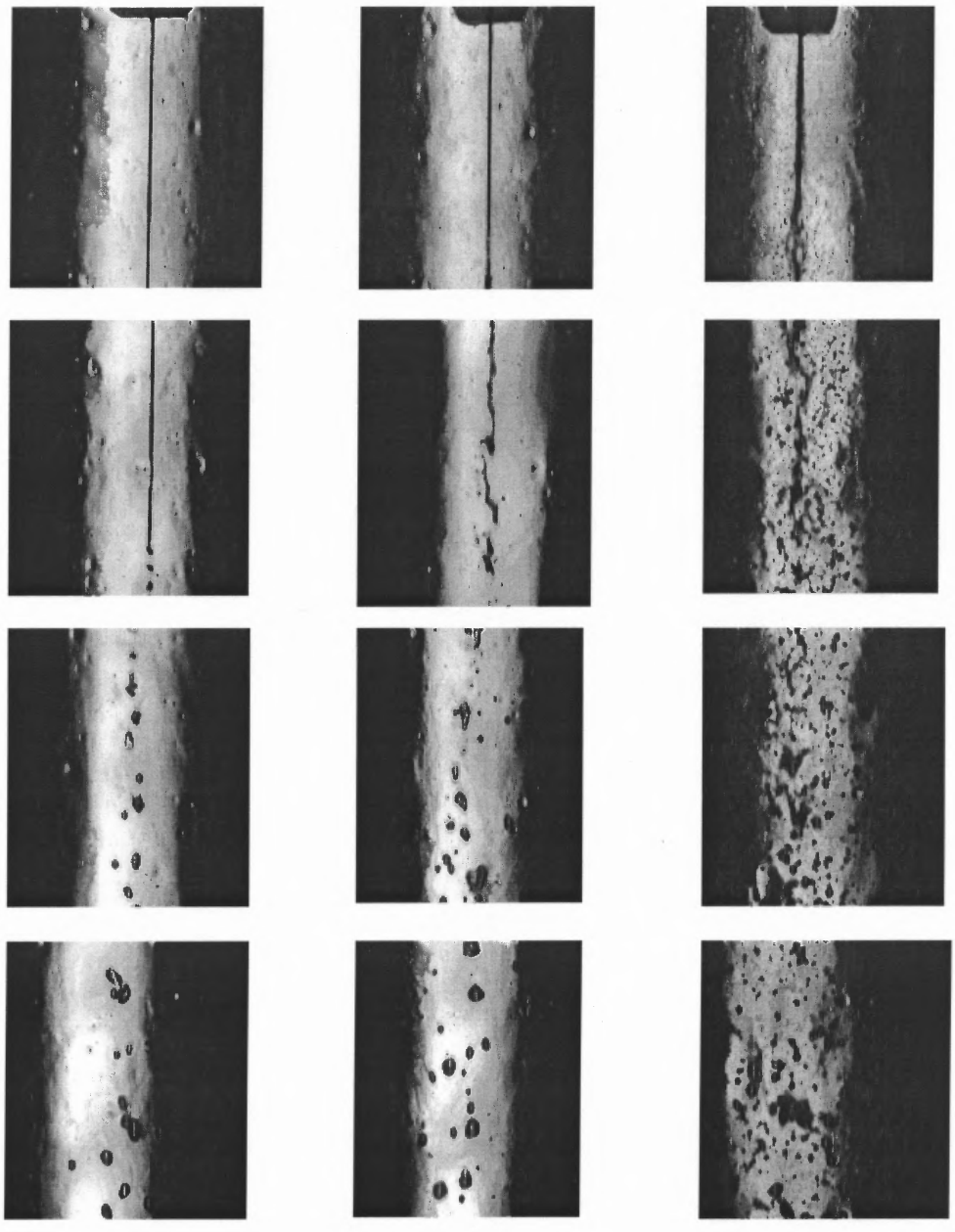

(A)v = 1.19 m/s (B) v = 1.98 m/s (C) v = 4.59 m/s

Figure 3.9 Photos of acetone injected into carbon dioxide at 57 bar and 35° C for velocities: (A) 1.19 m/s, (B) 1.98 m/s, (C) 4.59 m/s, which were taken at different locations below the nozzle: 0 (1st row); 4 mm (2nd row); 8 mm (3rd row); and 12 mm (4th row). The nozzle diameter is 127 μm.

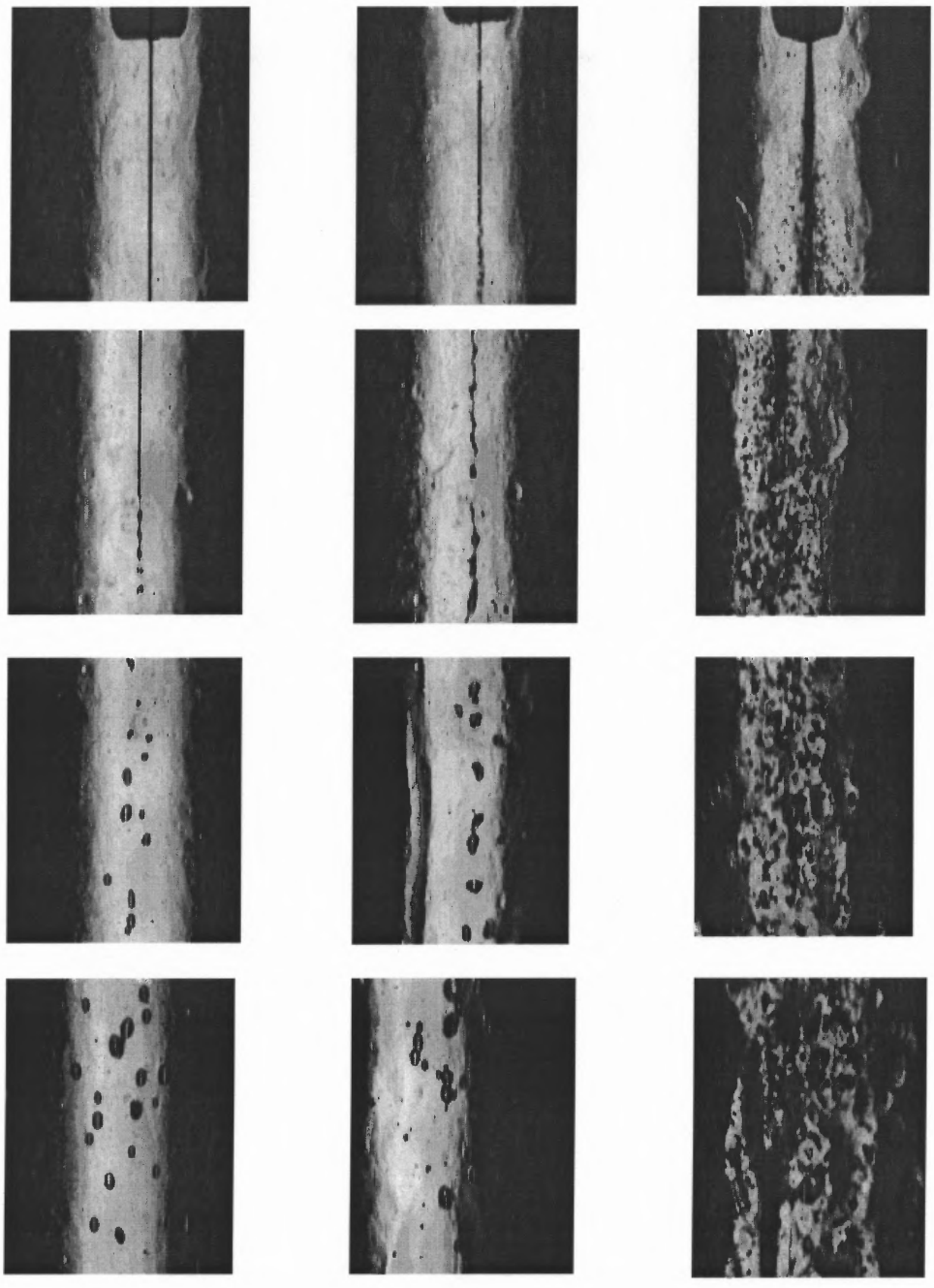

v = 0.91 m/s v = 1.72 m/s v = 5.14 m/s

Figure 3.10 Photos of acetone injected into carbon dioxide at 60 bar and 35° C for velocities: (A) 0.91 m/s, (B) 1.72 m/s, (C) 5.14 m/s, which were taken at different locations below the nozzle: 0 (1st row); 4 mm (2nd row); 8 mm (3rd row); and 12 mm (4th row). The nozzle diameter is 127 μm.

3.3.2 Graphs of Jet Length at Different Pressures

Acetone jet length is studied at different pressures for 35°C and comparison is made between ethanol jet length and acetone jet length for this temperature.

Graphs for pressure 57 and 60 bar for temperature 35°C are shown below. For all other operating conditions are placed in Appendix.

Temperature = 35 C

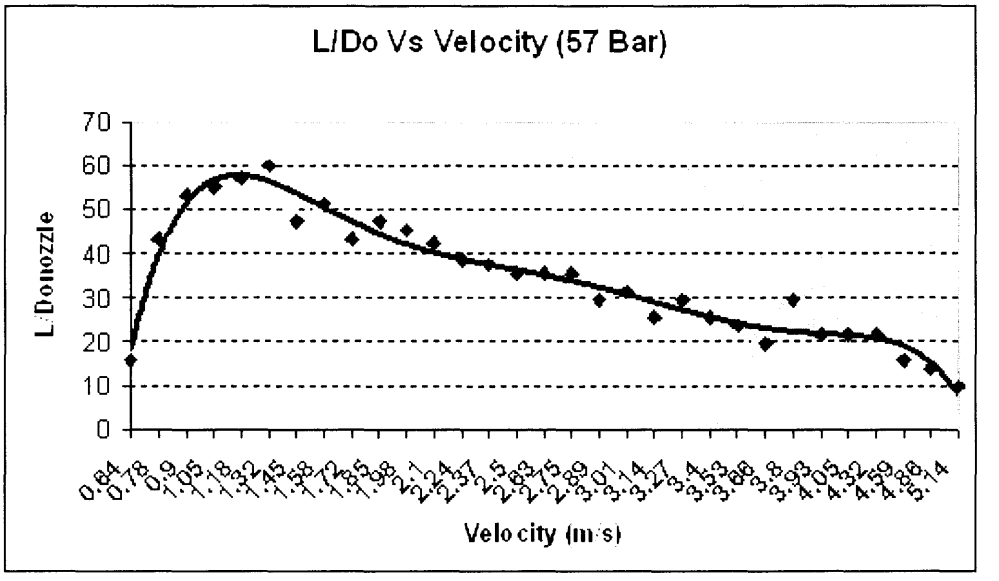

Figure 3.11 Pressure = 57 bar, Temperature = 35 C, Velocity of injected ethanol varies from 0.64 m/s to 5.14 m/s.

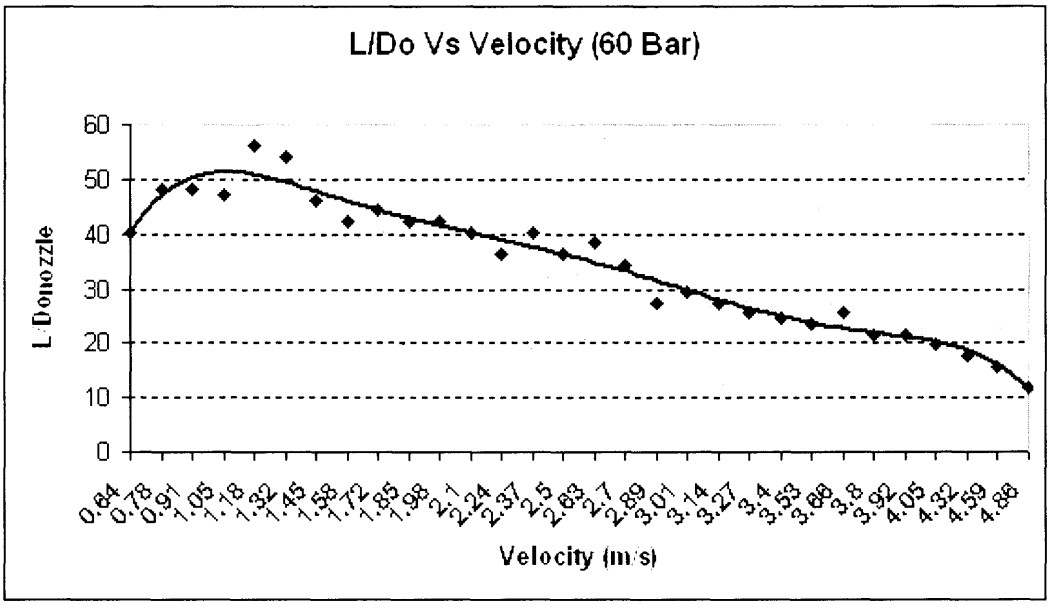

Figure 3.12 Pressure = 60 Bar, Temperature = 35 C, Velocity of injected ethanol varies from 0.64 m/s to 4.88 m/s.

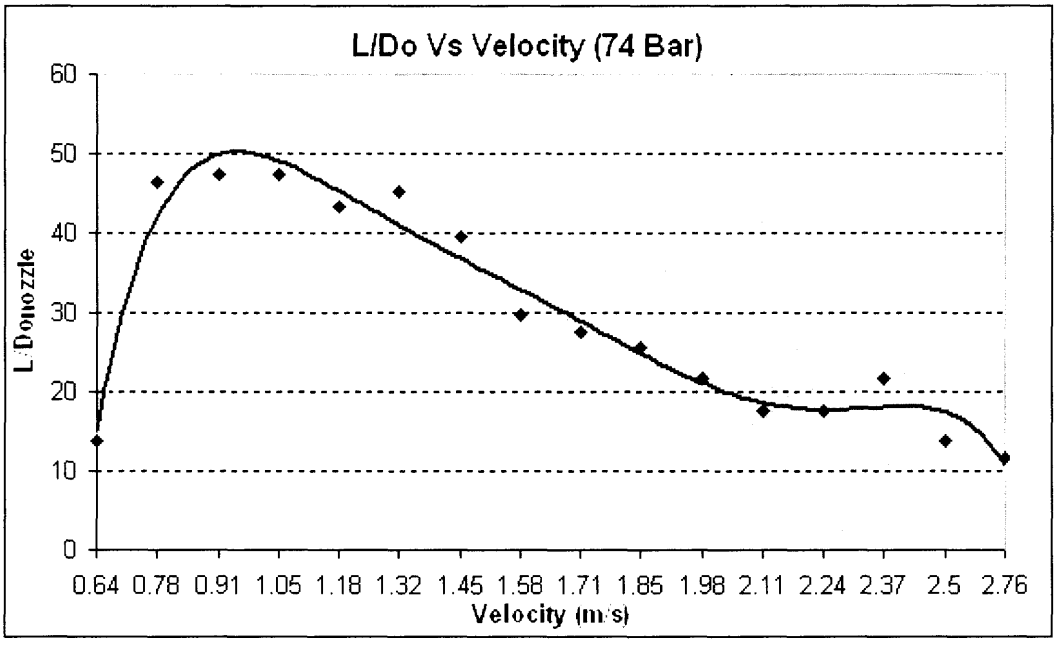

Figure 3.13 Pressure = 74 bar, Temperature = 35 C, Velocity of injected ethanol varies from 0.64 m/s to 2.76 m/s.

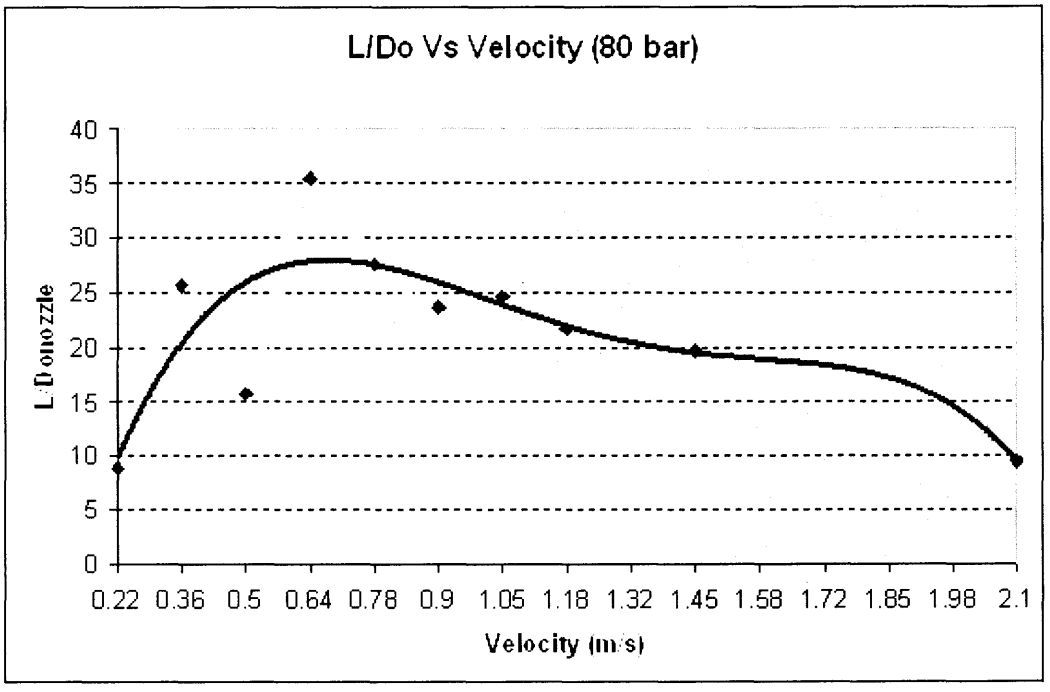

Figure 3.14 Pressure = 80 Bar, Temperature = 35 C, Velocity of injected ethanol varies from 0.22 m/s to 2.10 m/s.

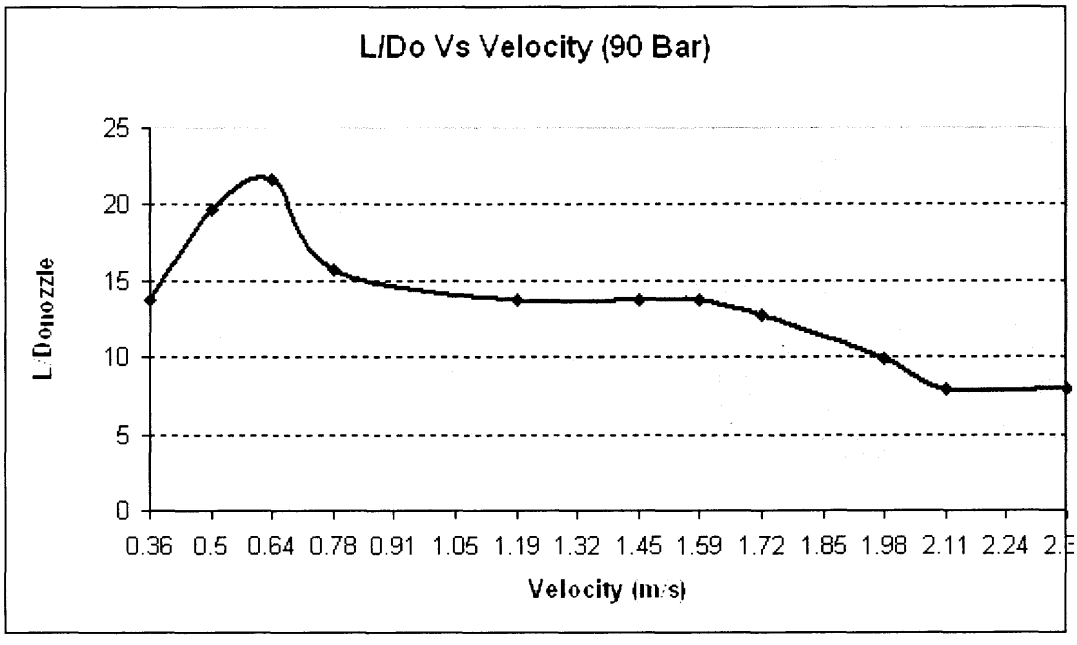

Figure 3.15 Pressure = 90 Bar, Temperature = 35 C, Velocity of injected ethanol varies from 0.36 m/s to 2.30 m/s.

3.3.3 Effect of Parameters on Jet Length

The main results of the experiments are as follows:

1. As pressure increases, jet length for any injection velocity decreases, also, highest jet length for the particular pressure and temperature also decreases.

2. For a given pressure, as velocity increases, jet length increases till certain velocity and then decreases, change in jet pattern is observed when jet length starts decreasing after achieving maximum jet length.

3. As temperature increases, jet length increases for the injection velocity and the pressure.

4. As pressure increases, highest length of jet shifts towards lower velocity.

5. Pressure increases, all four types of jet flows (dripping, systematic, wavy, spread) shifts towards lower velocity.

6. After a particular injection velocity, jet turns into spray. This critical velocity reduces with increase in pressure.

CHAPTER 4

THE SAS METHOD FOR THE PARTICLE FORMATION

As described previously in Section 2.3.1, solution is injected in supercritical antisolvent and dry particles are collected. The major advantage of this process over others is ease in controlling particle size and size distribution.

Numerous researchers, to understand the process of particle formation performed various experiments by `using combinations of different polymers and solvents. The process parameters like pressure, solution injection velocity were widely varied synthesis nano/micro particles. So to understand the process and relations between process parameters and physical properties of particles, different polymers like polylactic acid and its co-polymers, eudragit, chitosan, polyethylene glycol, lidocaine, dextran are used with the combination of different solvents like dichloromethane, ethanol, acetone, dimethyl sulfoxide and chloroform to study the process of particle formation. Using visualization system, the process of particle formation and effect of process parameters are studied carefully and certain conclusions are drawn.

Few experiments and the results are listed below. For whole list of experiments please refer Appendix.

Characterization of particles formed in lab and snapshots of the process for Polylactic Acid – Dichloromethane – CO_2 systems

Polylactic Acid (Birmingham Polymers, Inc.) is used as a solute and Dichloromethane (Acros, new jersey. 99.6 % purity) is used as a solvent. Liquid carbon dioxide is bought from Messer, PA. 99.5 %.

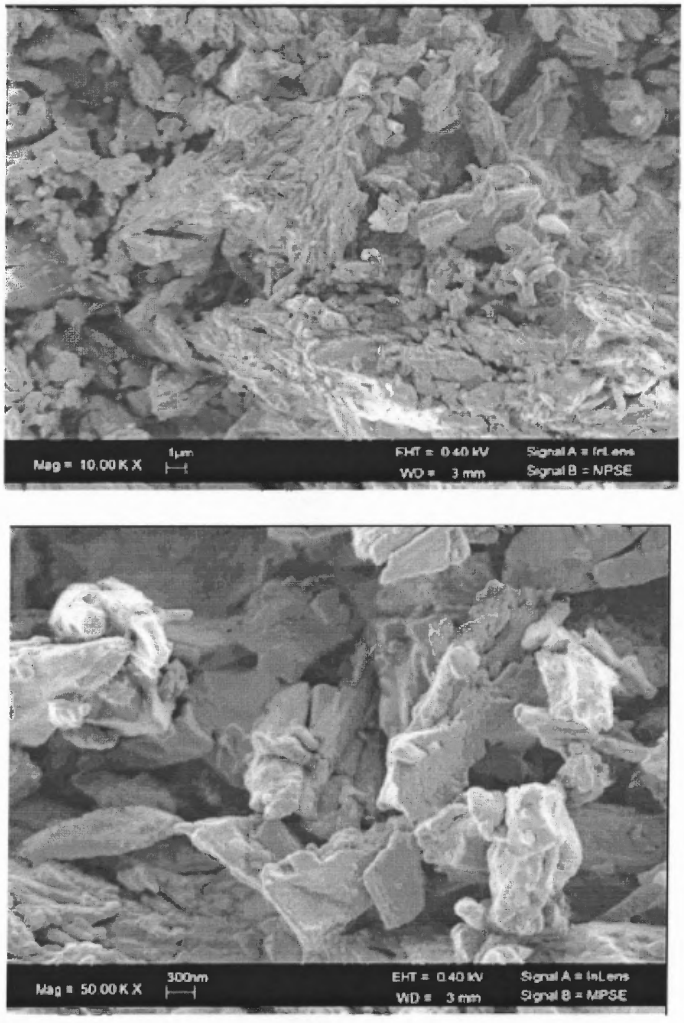

Figure 4.1 Original powder of L-PLA from Birmingham.

Condition 1

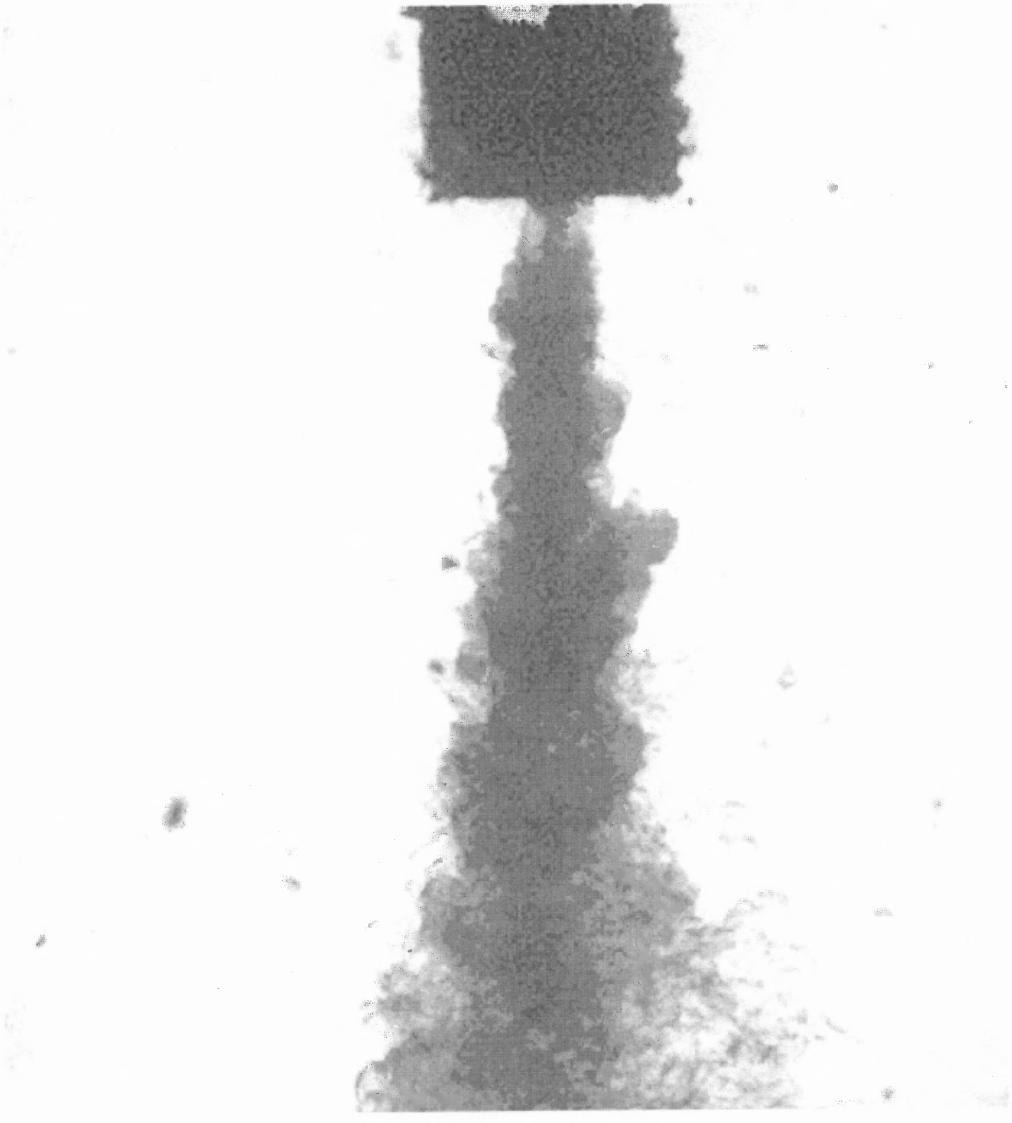

Figure 4.2 Injection of solution into the view cell P = 100 Bar, T = 35 C, Vsol = 0.4 ml/min, v = 1.18 m/s, D_{nozzle} = 127 μm, V_{CO2} = 60, (CO_2 pulsations are not induced).

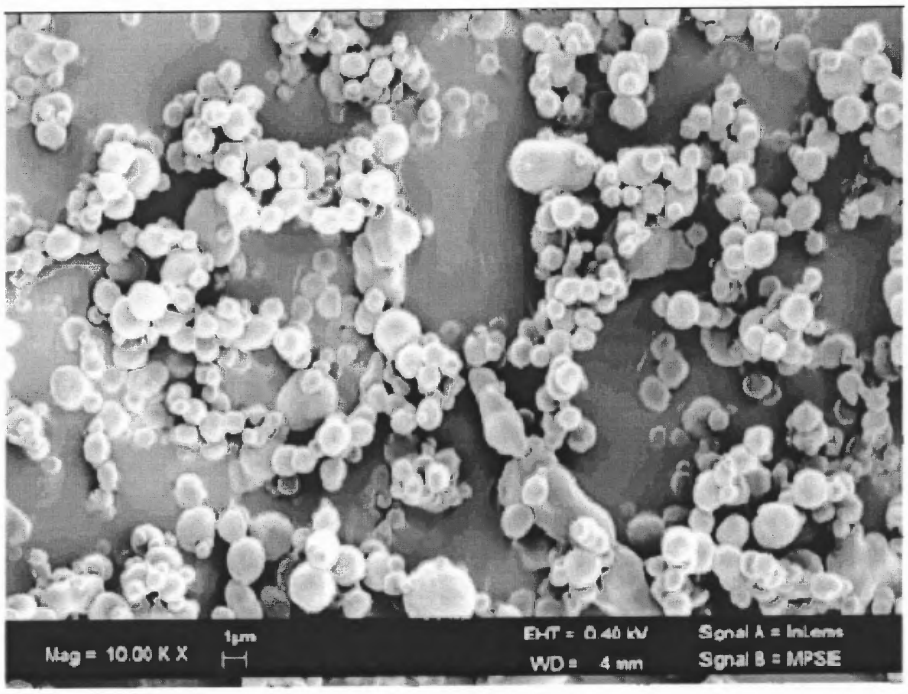

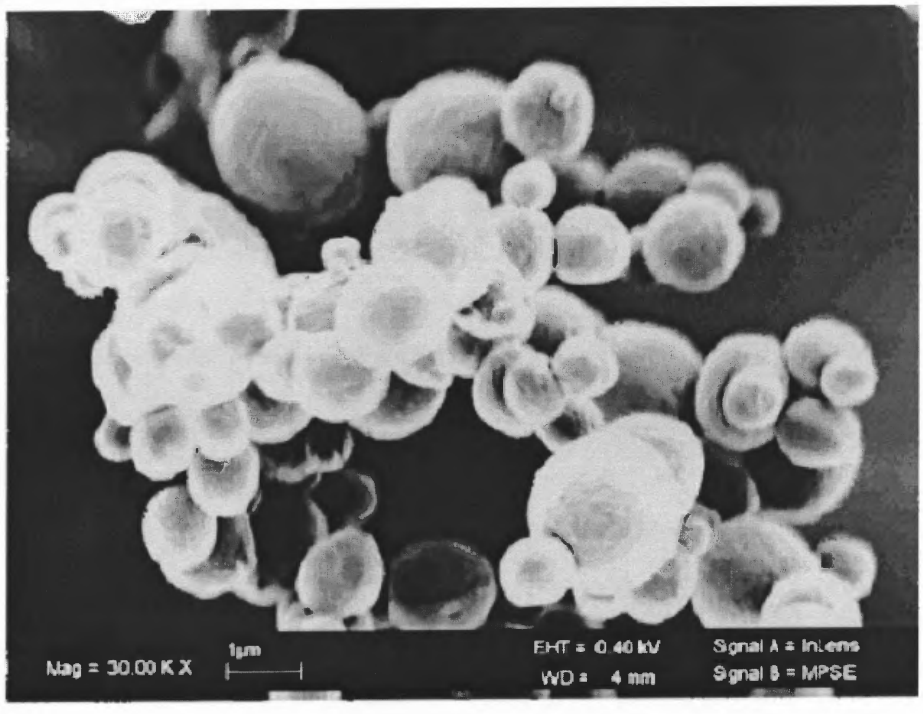

Figure 4.3 SEM images of particles formed P = 100 Bar, T = 35 C, V_{sol} = 0.4 ml/min, v = 1.18 m/s, D_{nozzle} = 127 µm, V_{CO2} = 60, (CO_2 pulsations are not induced).

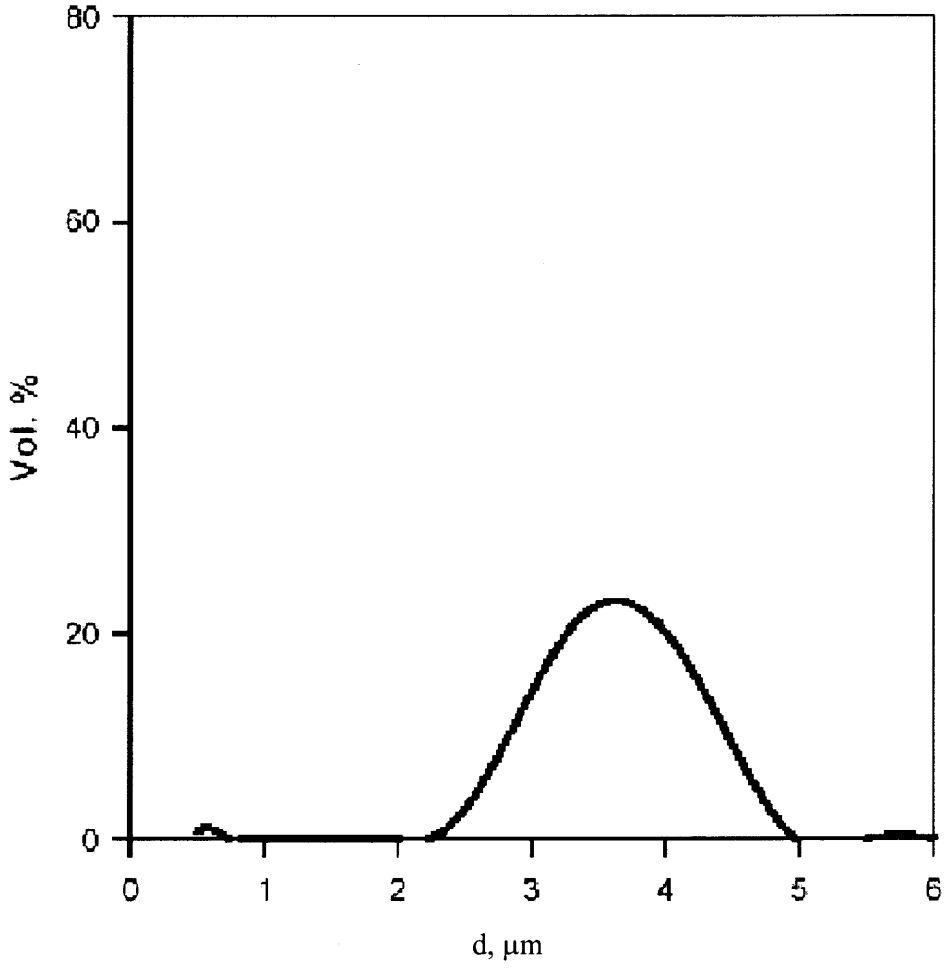

Figure 4.4 Particle size distribution (LS 200 microscope) P = 100 Bar, T = 35 C, Vsol = 0.4 ml/min, v = 1.18 m/s, D_{nozzle} = 127 μm, V_{CO2} = 60, (CO_2 pulsations are not induced).

CHAPTER 5

CONCLUSION

A detailed study of ethanol and acetone injection in supercritical as well as subcritical CO_2 is done. Effect of process parameters on jet length and jet pattern is studied.

Based on experiments done for particle formation using SAS method, it is found that particles form with injection of gas like jet and not liquid jet. Critical pressure for ethanol as well as acetone is investigated experimentally for which the liquid jet changes to gas like jet. Effect of process parameters on particle size and shape are studied. Less agglomerated particles formed when CO_2 as well as solution is injected in pulsations rather than continuous injection.

APPENDIX A

BREAKUP OF THE ETHANOL JET INJECTED INTO CO_2

Studying effect of jet breakup process on particle formation break up of ethanol jet into CO_2 is studied at different injection velocities at different CO_2 pressures and temperatures. The complete data of the experiment is presented quantitatively including snap shots of jet break up for different process parameters showing different kinds of jets at different process parameters. For every pressure, every kind of jet pattern is shown in following photographs. According to pressure, the velocity of jet for which the pattern changes, changes. To avoid repetition, photographs of dripping flow are not shown for every pressure.

1. For Temperature = 35°C,

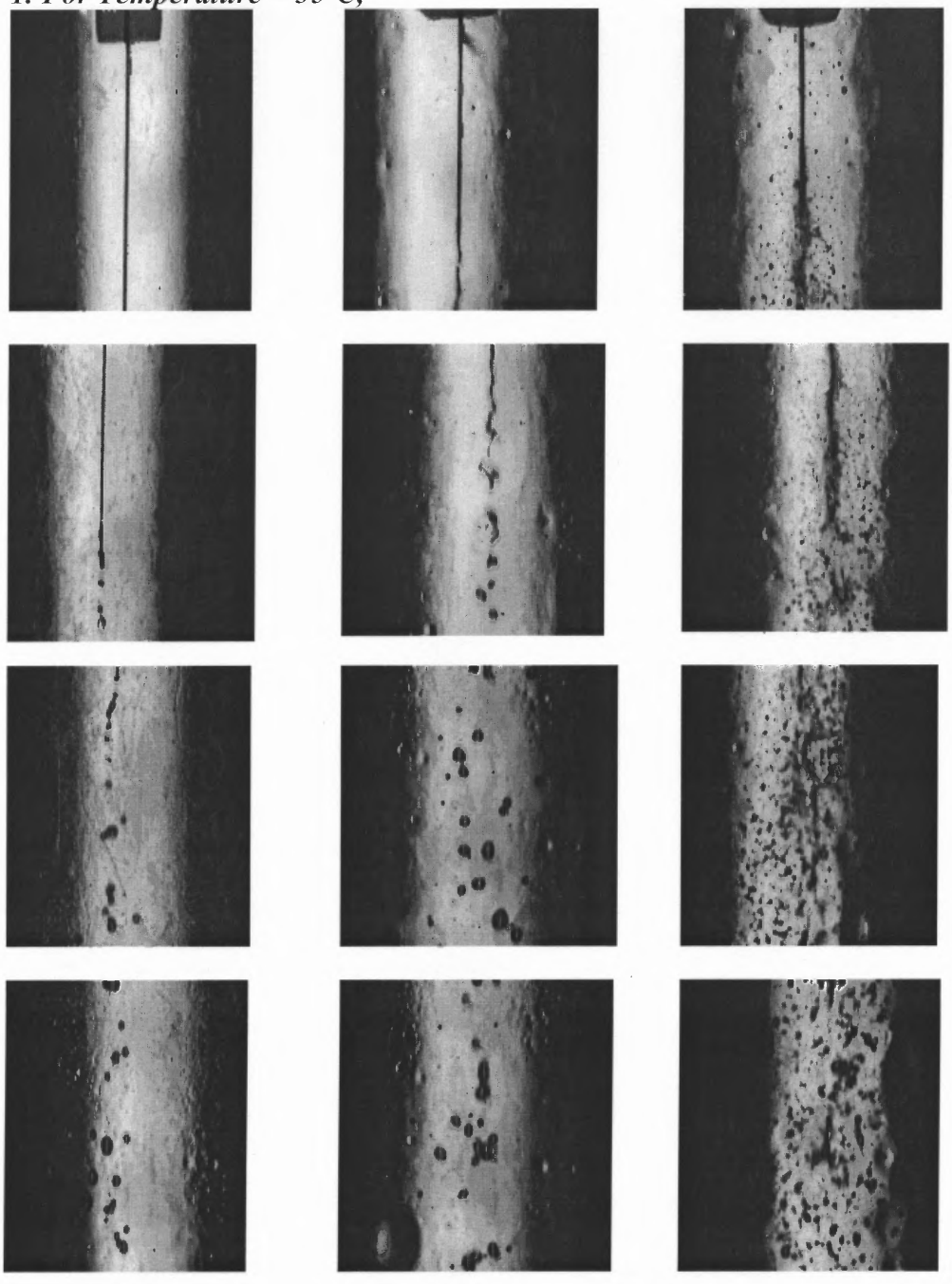

v = 1.32 m/s v = 2.5 m/s v = 5.43 m/s

Figure A.1 Photos of ethanol injected into carbon dioxide at 65 bar and 35° C for velocities: (A) 1.32 m/s, (B) 2.5 m/s, (C) 5.43 m/s, which were taken at different locations below the nozzle: 0 (1st row); 4 mm (2nd row); 8 mm (3rd row); and 12 mm (4th row). The nozzle diameter is 127 μm.

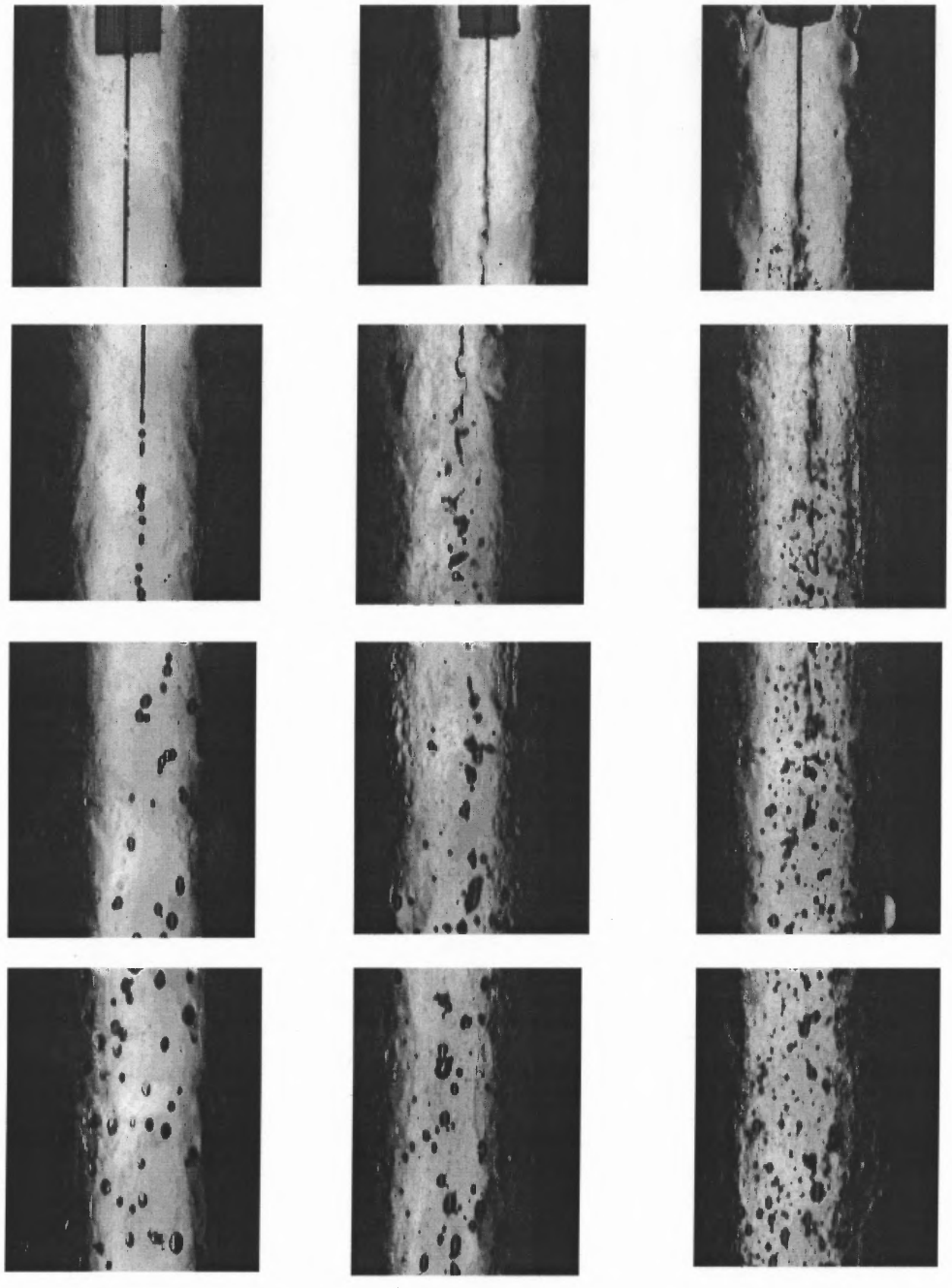

v = 0.78 m/s v = 2.24 m/s v = 3.27 m/s

Figure A.2 Photos of ethanol injected into carbon dioxide at 70 bar and 35° C for velocities: (A) 0.78 m/s, (B) 2.24 m/s, (C) 3.273 m/s, which were taken at different locations below the nozzle: 0 (1st row); 4 mm (2nd row); 8 mm (3rd row); and 12 mm (4th row). The nozzle diameter is 127 μm.

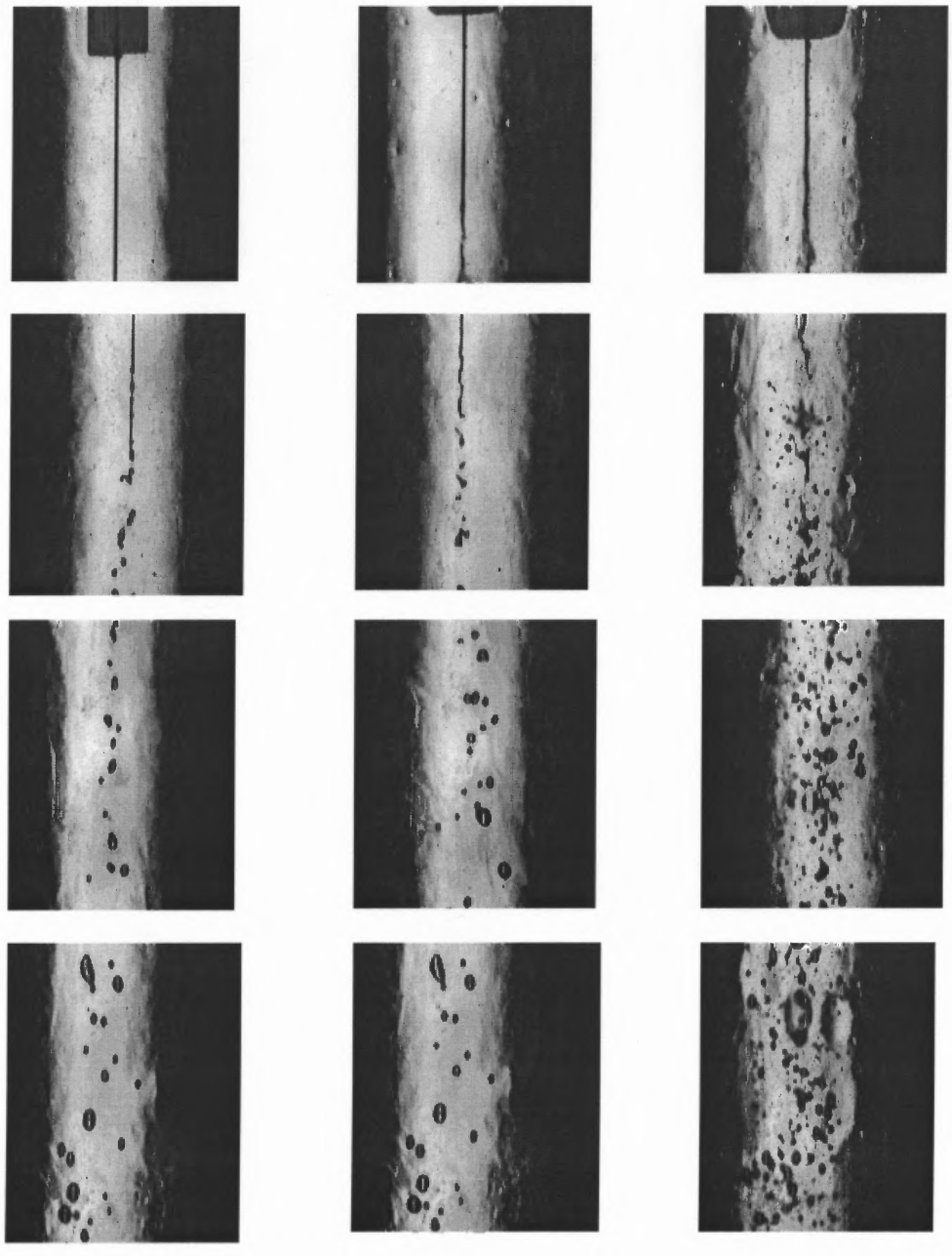

v = 1.05 m/s v = 1.32 m/s v = 3.01 m/s

Figure A.3 Photos of ethanol injected into carbon dioxide at 74 bar and 35° C for velocities: (A) 1.05 m/s, (B) 1.32 m/s, (C) 3.01 m/s, which were taken at different locations below the nozzle: 0 (1st row); 4 mm (2nd row); 8 mm (3rd row); and 12 mm (4th row). The nozzle diameter is 127 μm.

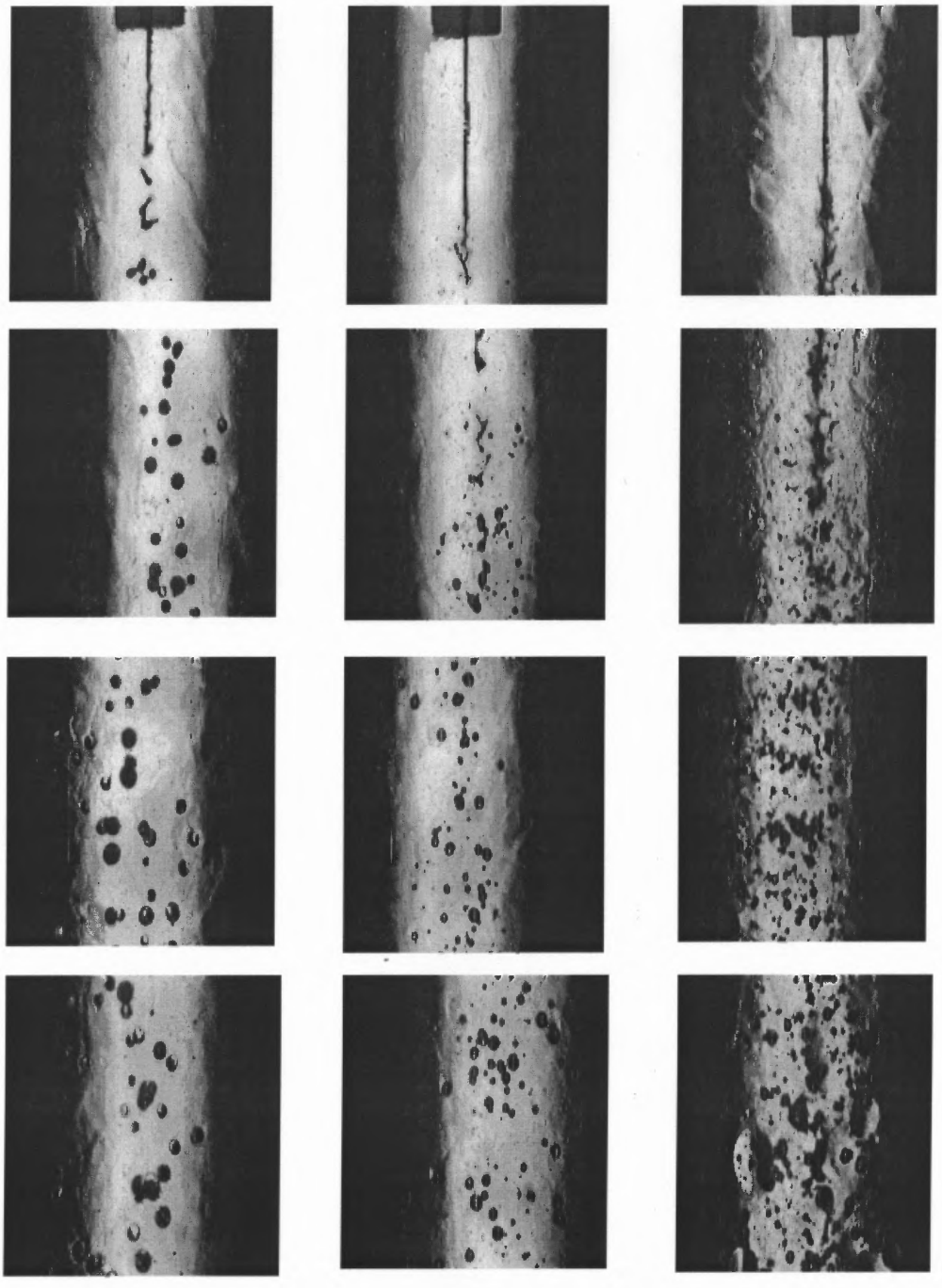

v = 0.78 m/s v = 1.2 m/s v = 2.89 m/s

Figure A.4 Photos of ethanol injected into carbon dioxide at 80 bar and 35° C for velocities: (A) 0.78 m/s, (B) 1.2 m/s, (C) 2.89 m/s, which were taken at different locations below the nozzle: 0 (1st row); 4 mm (2nd row); 8 mm (3rd row); and 12 mm (4th row). The nozzle diameter is 127 μm.

2. For Temperature = 40° C,

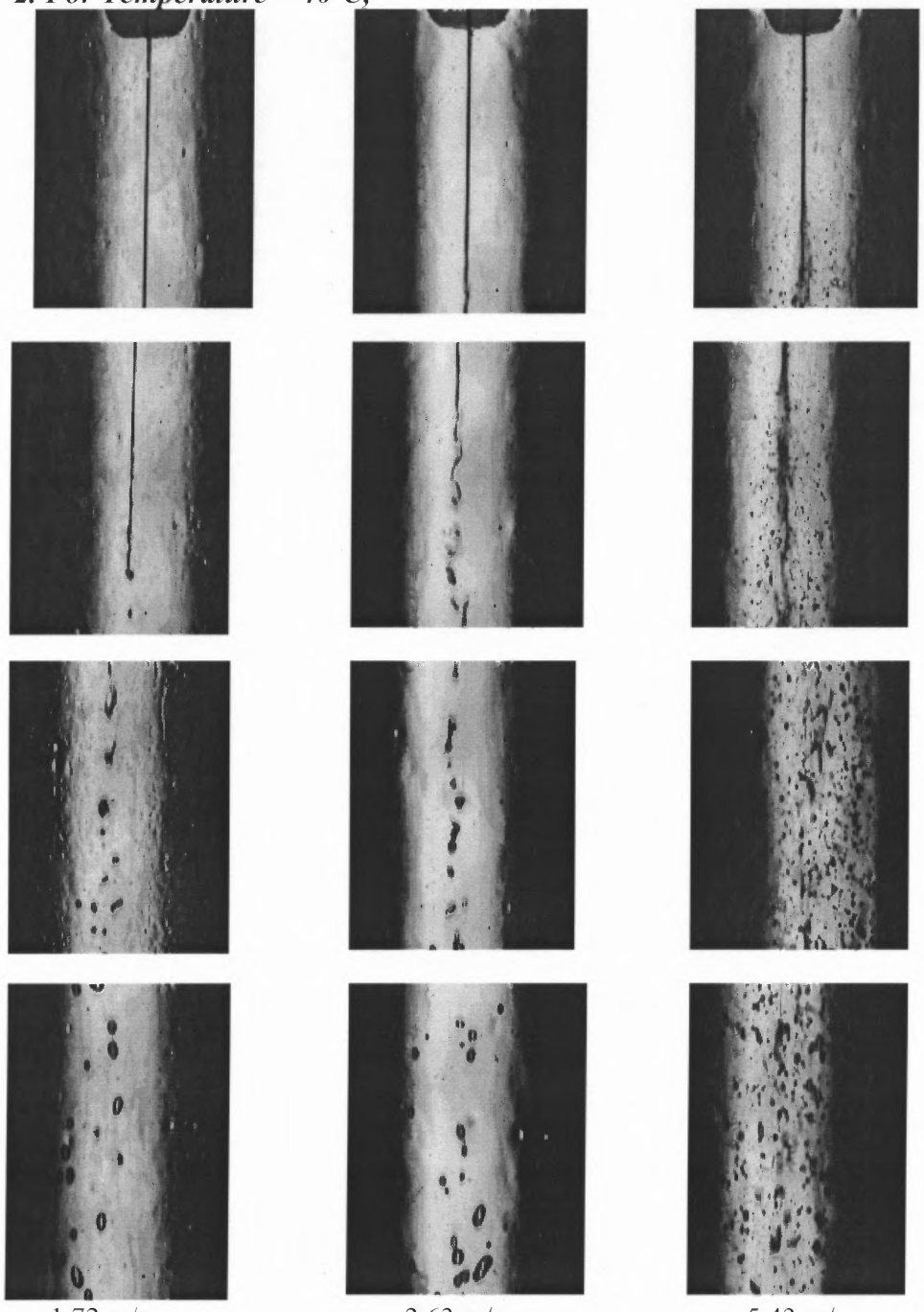

v = 1.72 m/s v = 2.63 m/s v = 5.43 m/s

Figure A.5 Photos of ethanol injected into carbon dioxide at 57 bar and 40° C for velocities: (A) 1.72 m/s, (B) 2.63 m/s, (C) 5.43 m/s, which were taken at different locations below the nozzle: 0 (1st row); 4 mm (2nd row); 8 mm (3rd row); and 12 mm (4th row). The nozzle diameter is 127 μm.

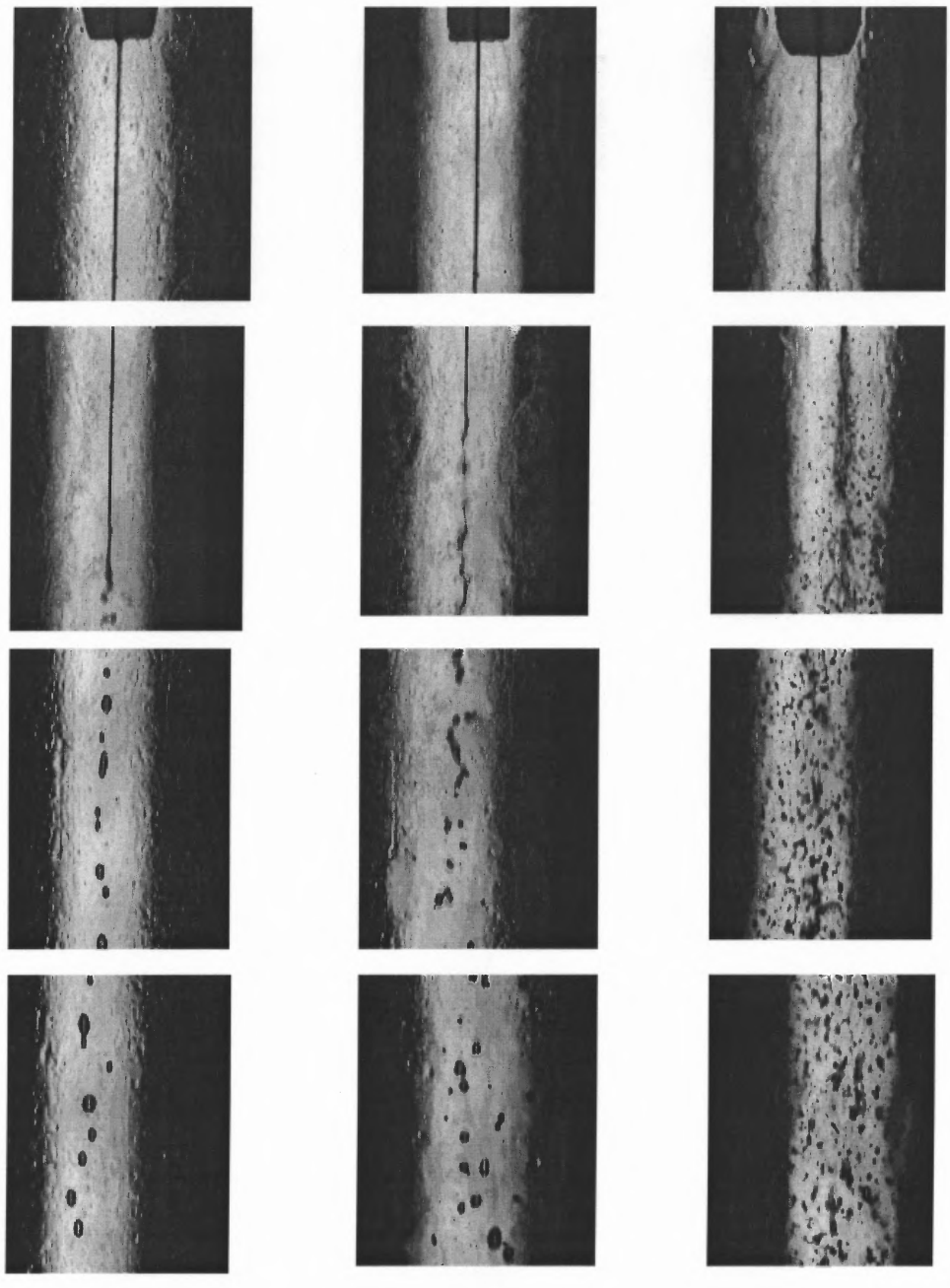

v = 1.97 m/s v = 2.5 m/s v = 5.43 m/s

Figure A.6 Photos of ethanol injected into carbon dioxide at 60 bar and 40° C for velocities: (A) 1.97 m/s, (B) 2.5 m/s, (C) 5.43 m/s, which were taken at different locations below the nozzle: 0 (1st row); 4 mm (2nd row); 8 mm (3rd row); and 12 mm (4th row). The nozzle diameter is 127 μm.

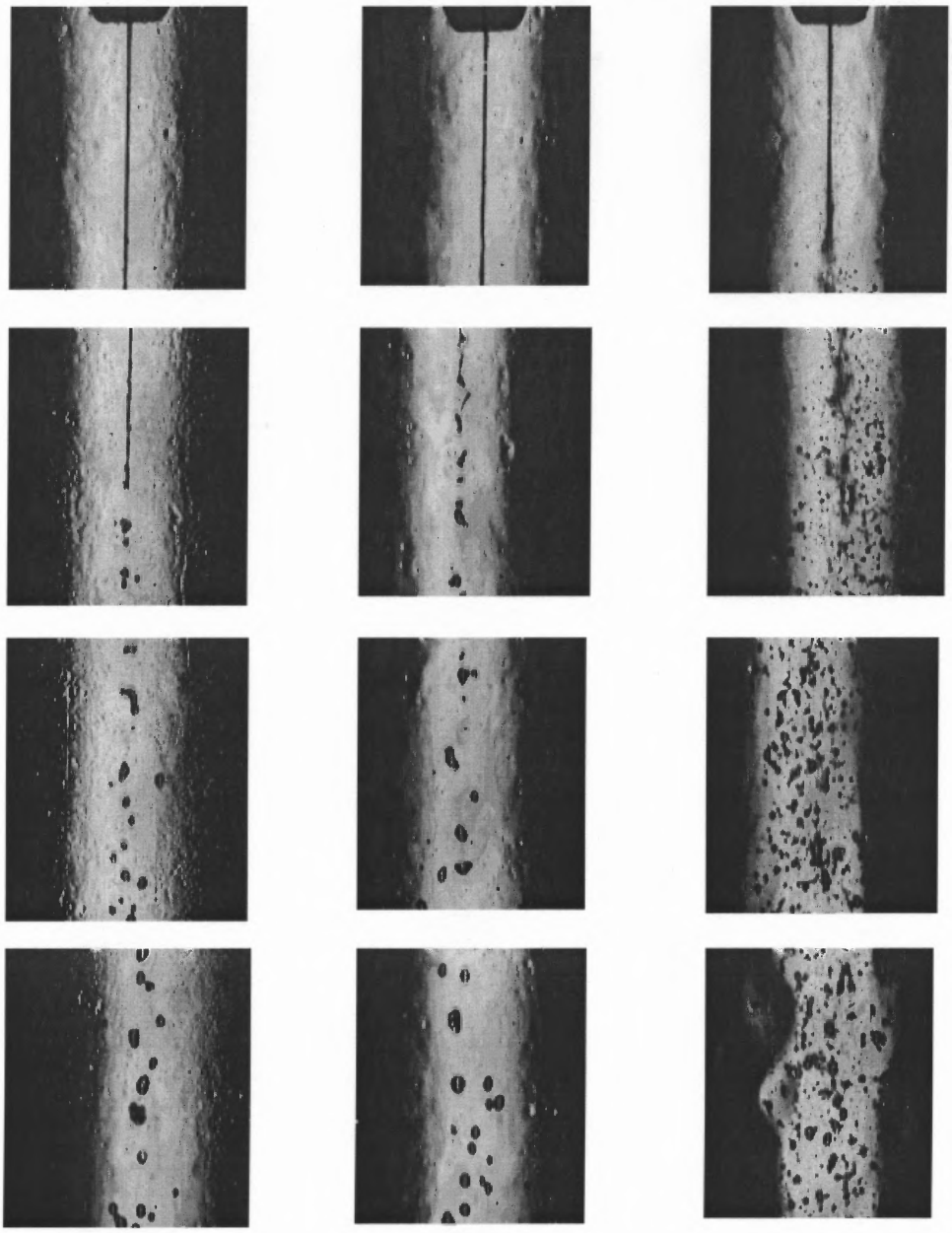

v = 1.45 m/s v = 2.11 m/s v = 4.32 m/s

Figure A.7 Photos of ethanol injected into carbon dioxide at 70 bar and 40° C for velocities: (A) 1.45 m/s, (B) 2.11 m/s, (C) 4.32 m/s, which were taken at different locations below the nozzle: 0 (1st row); 4 mm (2nd row); 8 mm (3rd row); and 12 mm (4th row). The nozzle diameter is 127 μm.

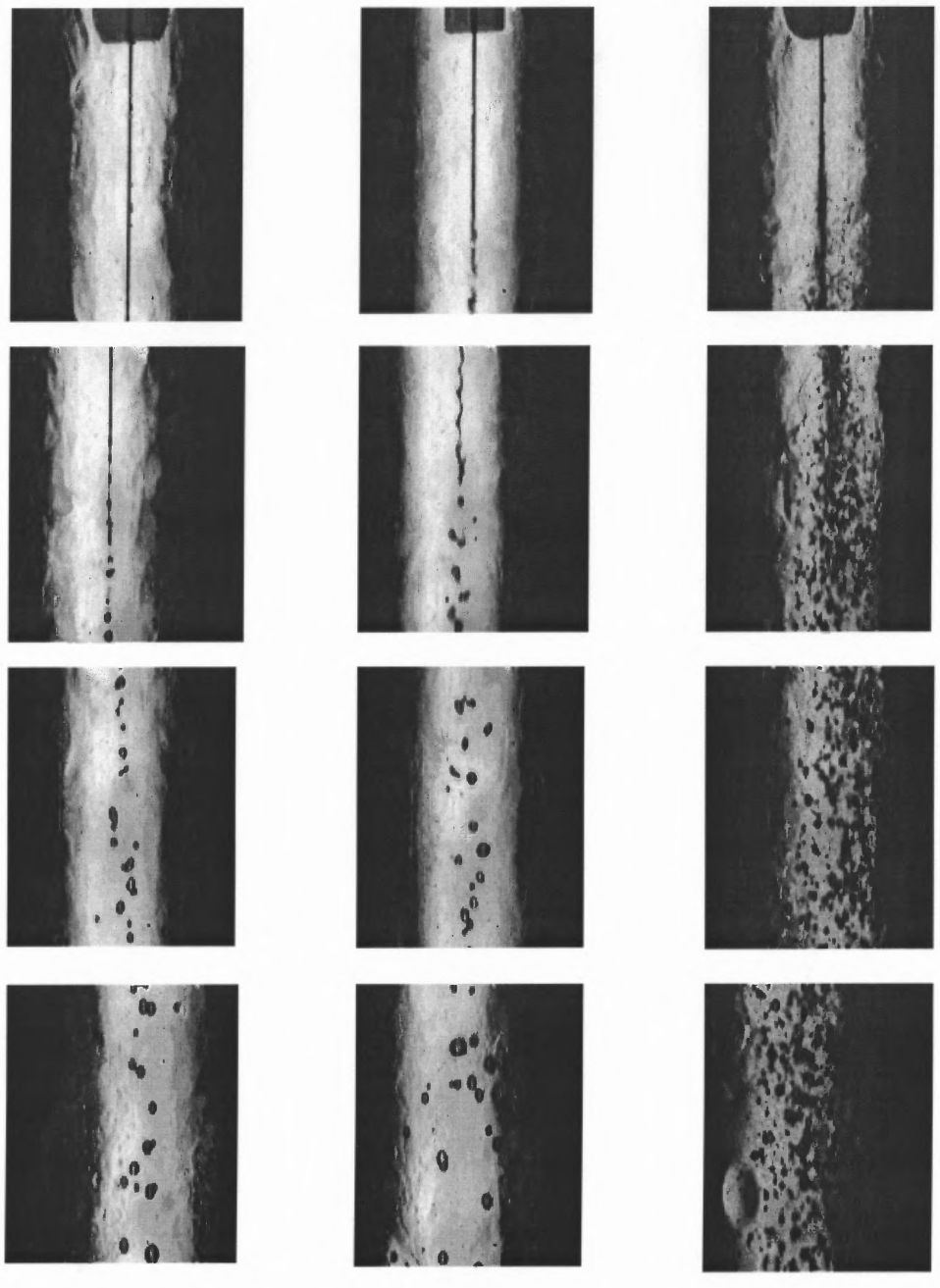

V = 1.18 m/s v = 1.85 m/s v = 4.59 m/s

Figure A.8 Photos of ethanol injected into carbon dioxide at 74 bar and 40° C for velocities: (A) 1.18 m/s, (B) 1.85 m/s, (C) 4.59 m/s, which were taken at different locations below the nozzle: 0 (1st row); 4 mm (2nd row); 8 mm (3rd row); and 12 mm (4th row). The nozzle diameter is 127 μm.

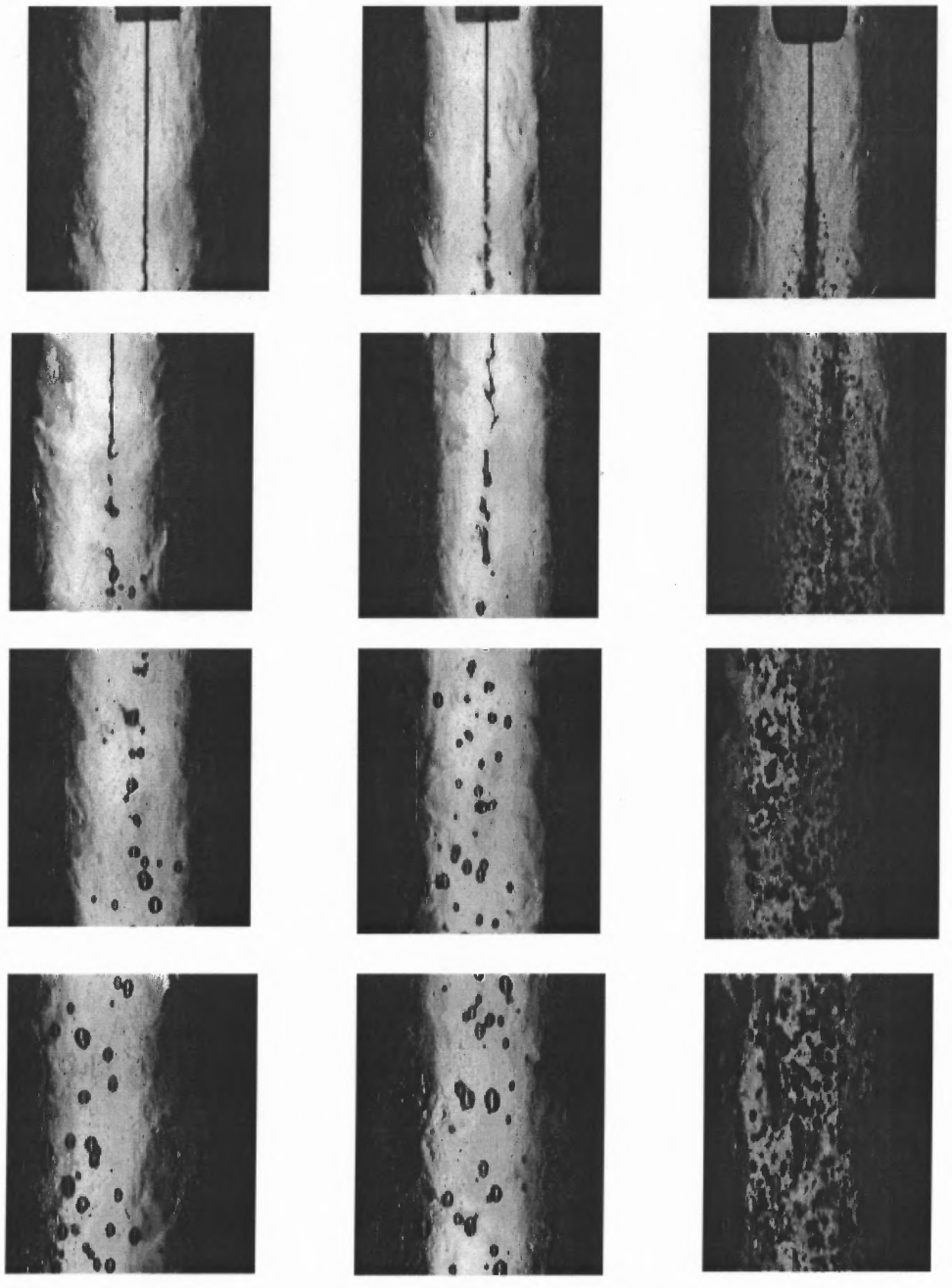

v = 1.32 m/s v = 1.59 m/s v = 3.4 m/s

Figure A.9 Photos of ethanol injected into carbon dioxide at 80 bar and 40° C for velocities: (A) 1.32 m/s, (B) 1.59 m/s, (C) 3.4 m/s, which were taken at different locations below the nozzle: 0 (1st row); 4 mm (2nd row); 8 mm (3rd row); and 12 mm (4th row). The nozzle diameter is 127 μm.

APPENDIX B

GRAPHS OF ETHANOL JET LENGTHS AT DIFFERENT PRESSURES

Graphs of jet lengths of ethanol into supercritical CO_2 are shown for different pressures and temperatures with wide velocity range.

1. For Temperature 35^oC

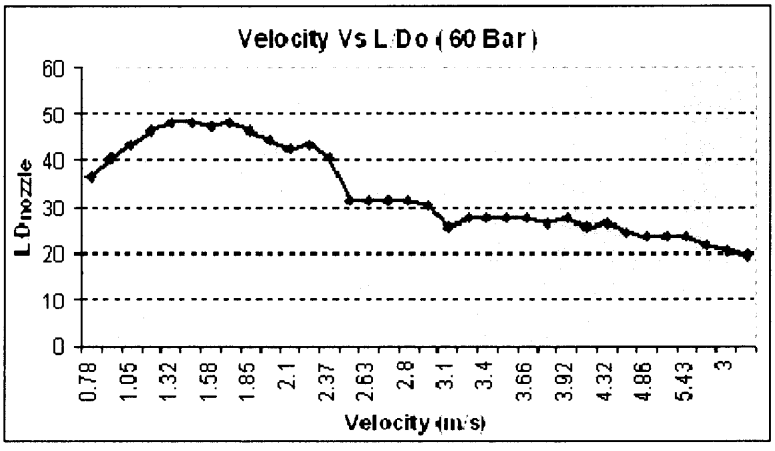

Figure B.1 Pressure = 60 Bar, Temperature = 35 C, Velocity of injected ethanol varies from 0.78 m/s to 7.78 m/s.

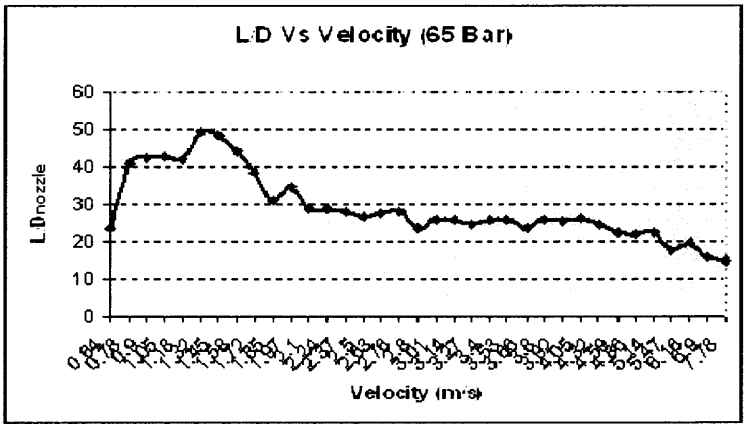

Figure B.2 Pressure = 65 Bar, Temperature = 35 C, Velocity of injected ethanol varies from 0.84 m/s to 7.78 m/s.

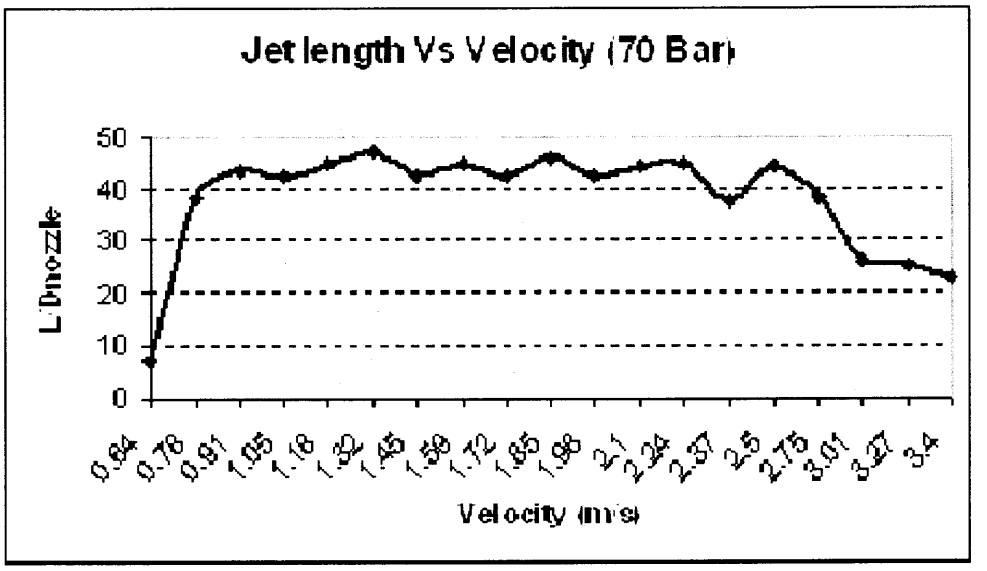

Figure B.3 Pressure = 70 Bar, Temperature = 35 C, Velocity of injected ethanol varies from 0.64 m/s to 3.40 m/s.

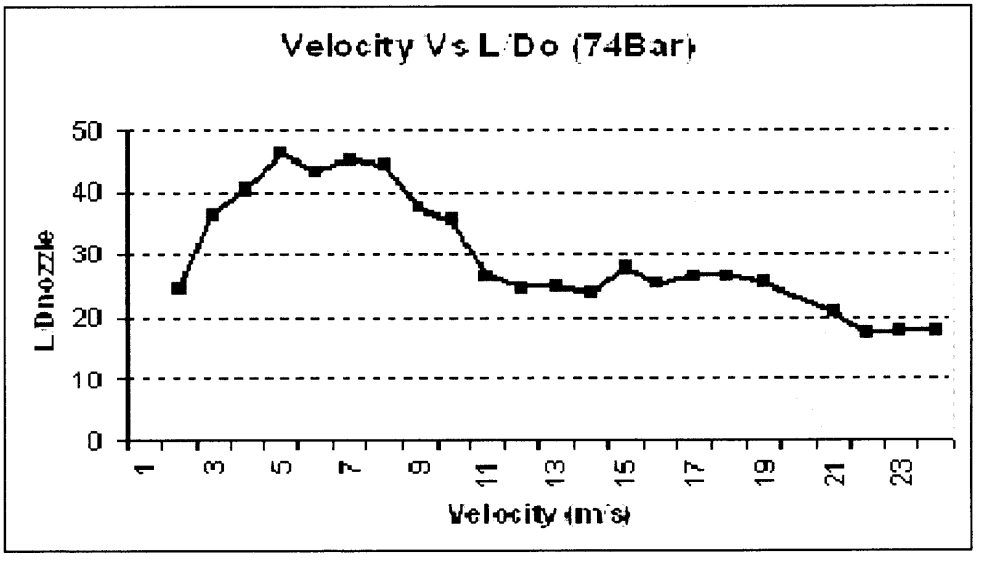

Figure B.4 Pressure = 74 Bar, Temperature = 35 C, Velocity of injected ethanol varies from 0.64 m/s to 7.78 m/s.

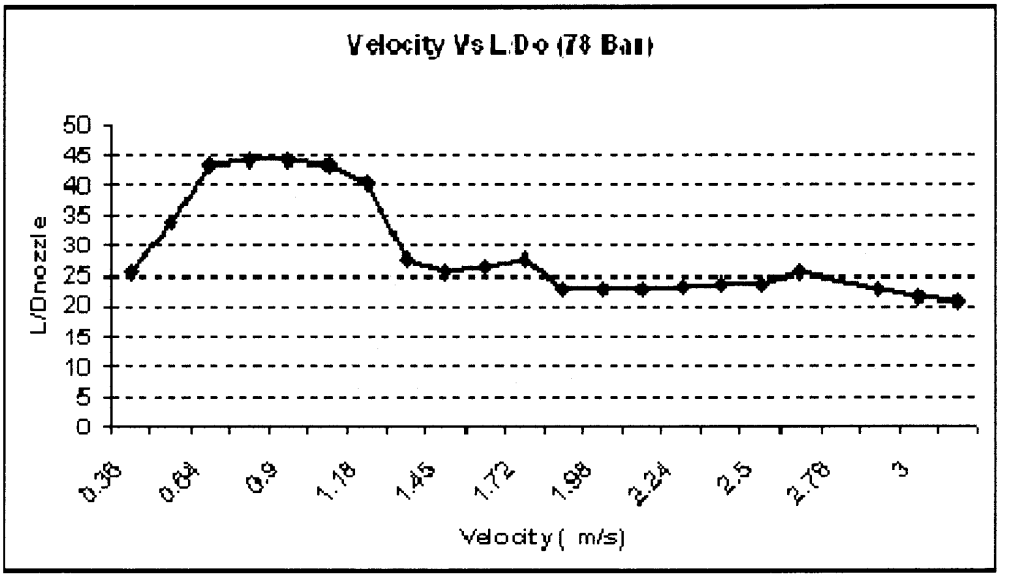

Figure B.5 Pressure = 78 Bar, Temperature = 35 C, Velocity of injected ethanol varies from 0.38 m/s to 3.20 m/s.

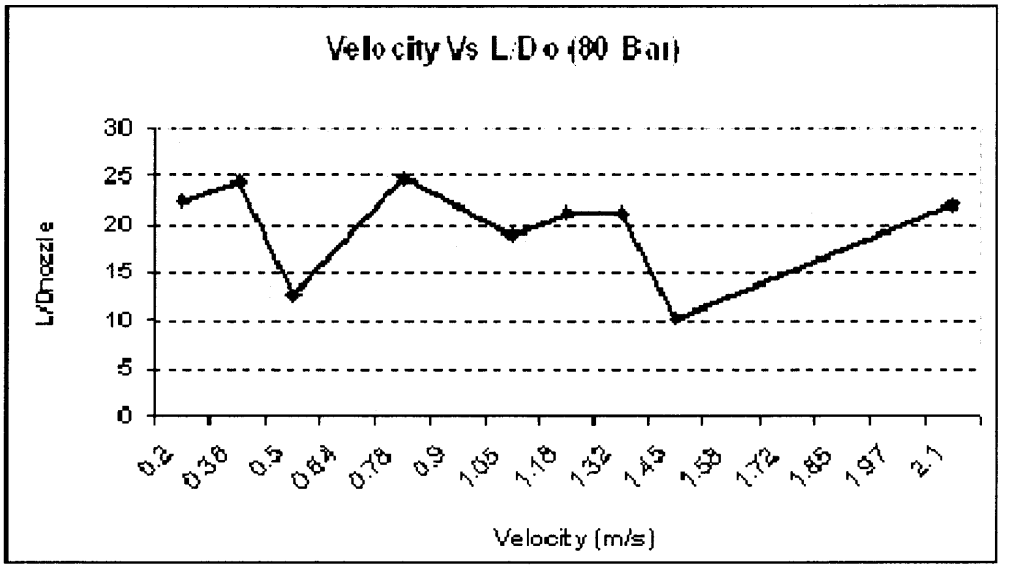

Figure B.6 Pressure = 80 Bar, Temperature = 35 C, Velocity of injected ethanol varies from 0.20 m/s to 2.20 m/s.

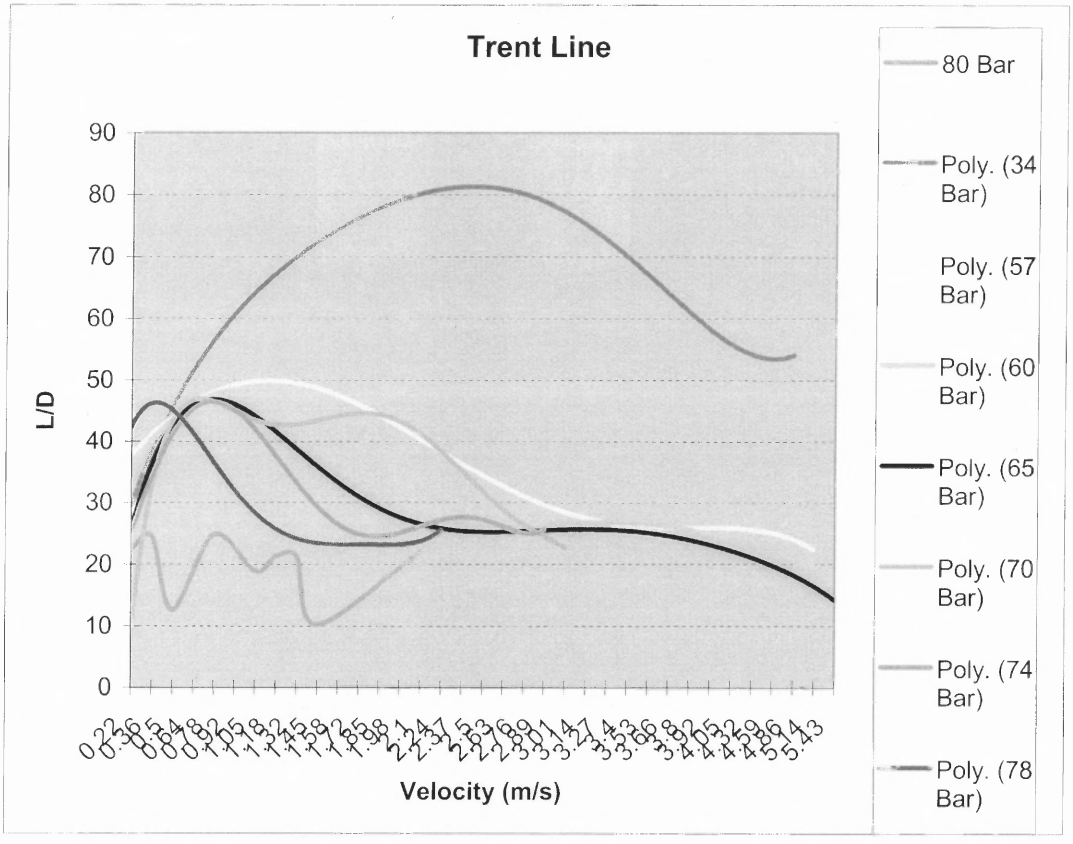

Figure B.7 Comparison of Jet Lengths at Different Pressures for Temperature = 35°C.

2. **For Temperature** $40^{o}C$

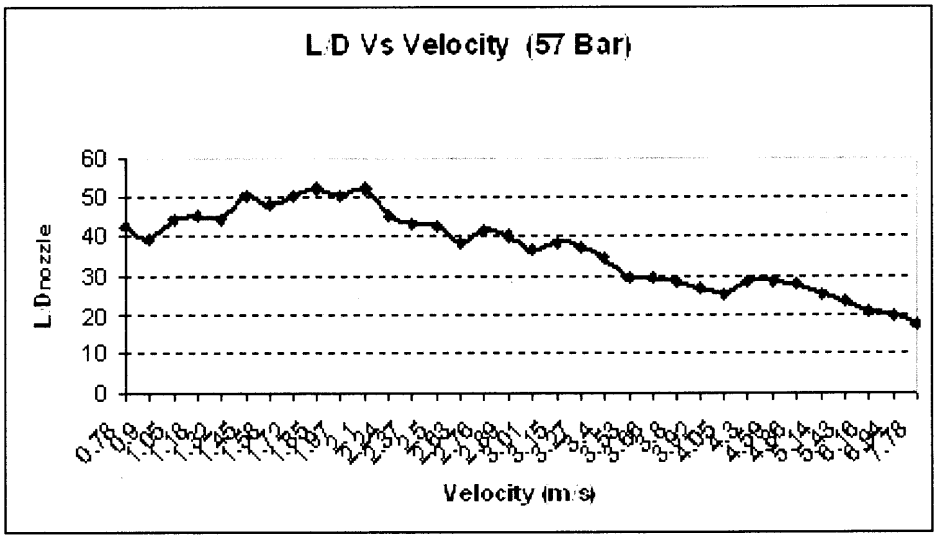

Figure B.8 Pressure = 57 Bar, Temperature = 40C, Velocity of injected ethanol varies from 0.78 m/s to 7.78 m/s.

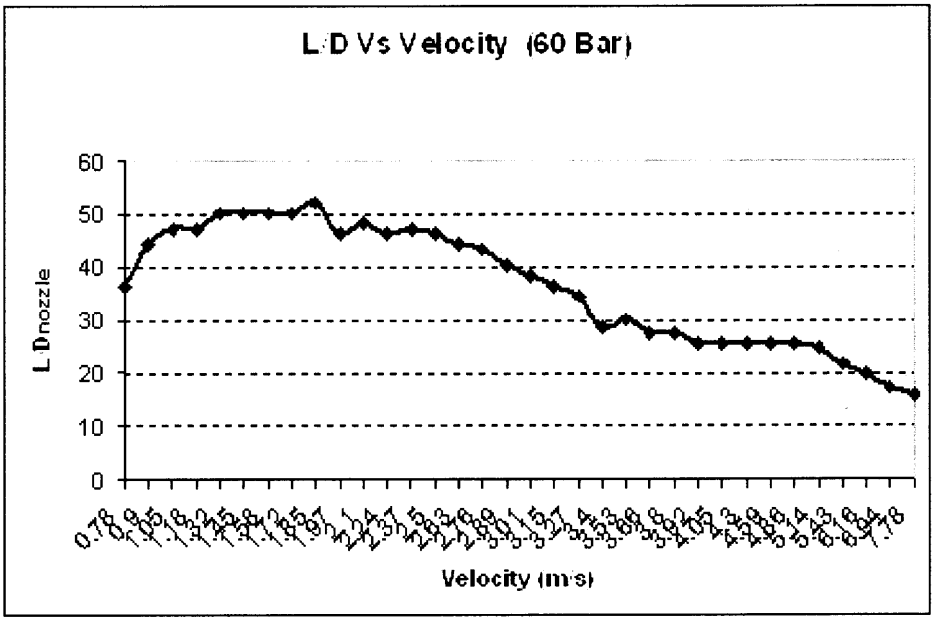

Figure B.9 Pressure = 60 Bar, Temperature = 40C, Velocity of injected ethanol varies from 0.78 m/s to 7.78 m/s.

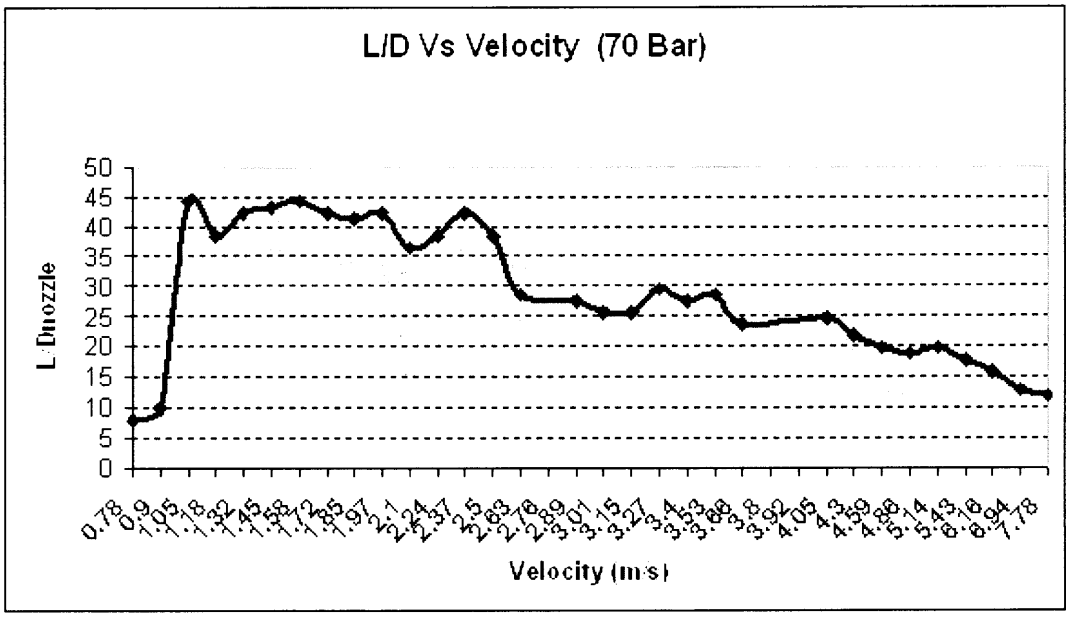

Figure B.10 Pressure = 70 Bar, Temperature = 40C, Velocity of injected ethanol varies from 0.78 m/s to 7.78 m/s.

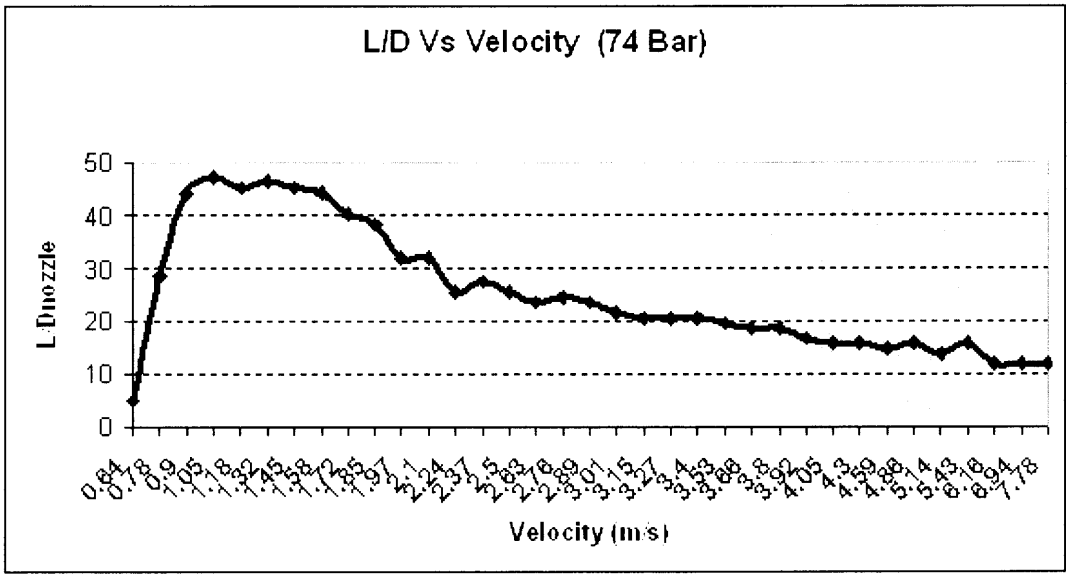

Figure B.11 Pressure = 74Bar, Temperature = 40C, Velocity of injected ethanol varies from 0.64 m/s to 7.78 m/s.

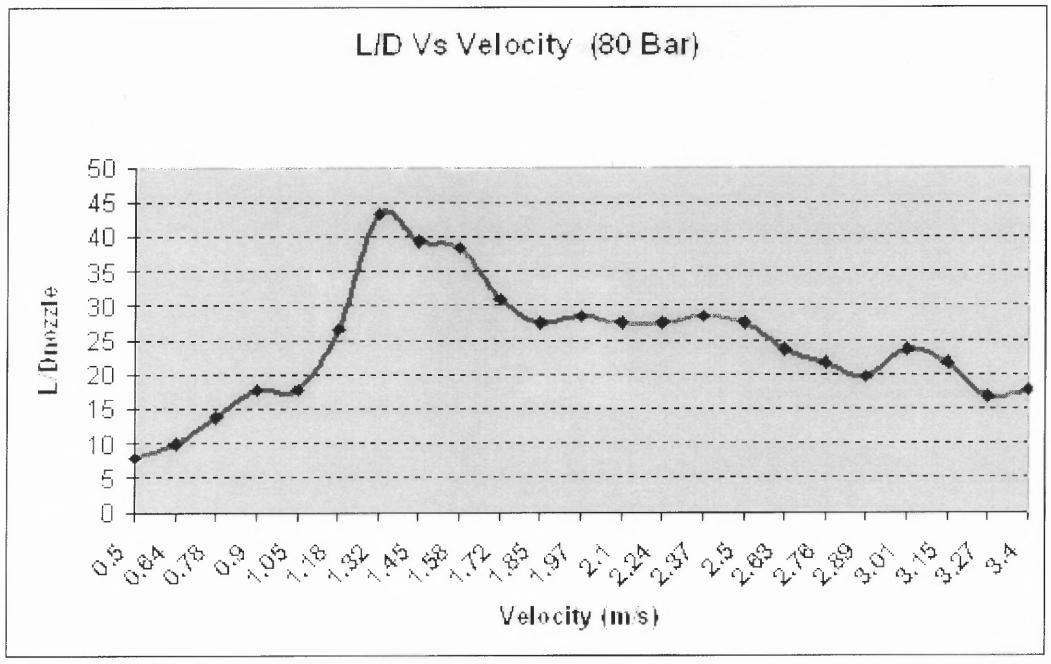

Figure B.12 Pressure = 80 Bar, Temperature = 40C, Velocity of injected ethanol varies from 0.50 m/s to 3.40 m/s.

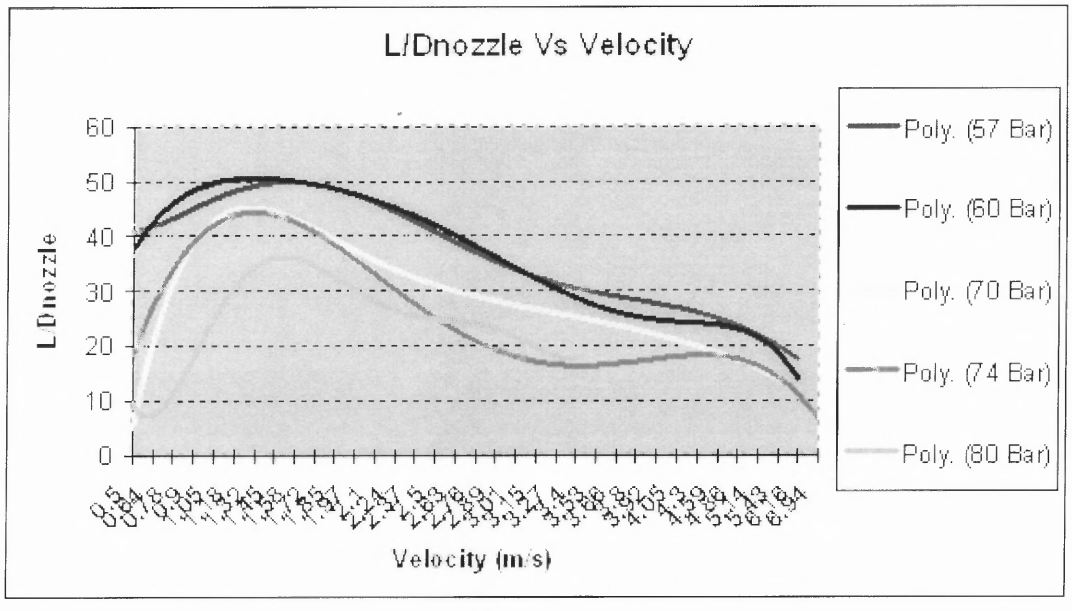

Figure B.13 Comparison between jet lengths at different pressures.

3. For Temperature $50^{o}C$

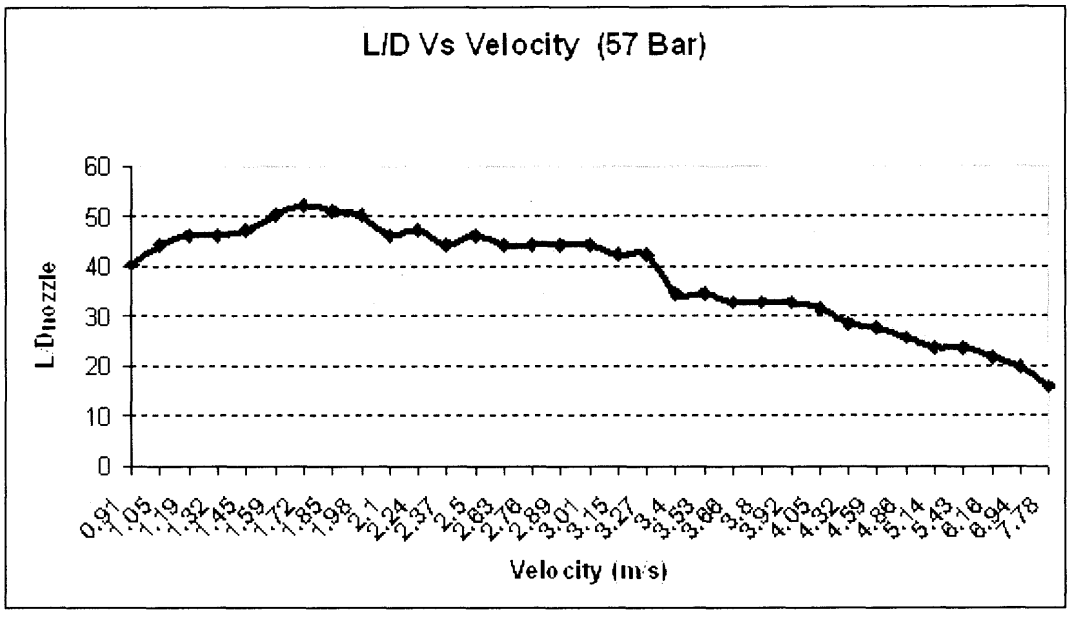

Figure B.14 Pressure = 57 bar, Temperature = 50C, Velocity of injected ethanol varies from 0.91 m/s to 7.78 m/s.

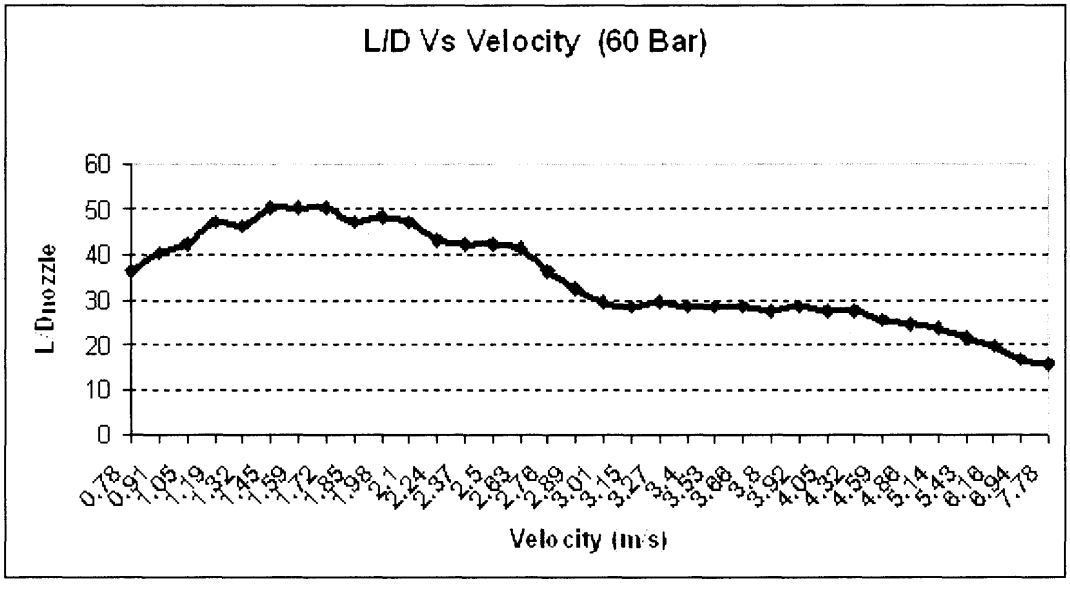

Figure B.15 Pressure = 60 Bar, Temperature = 50C, Velocity of injected ethanol varies from 0.78 m/s to 7.78 m/s.

Comparison of Jet Lengths at Different Temperatures

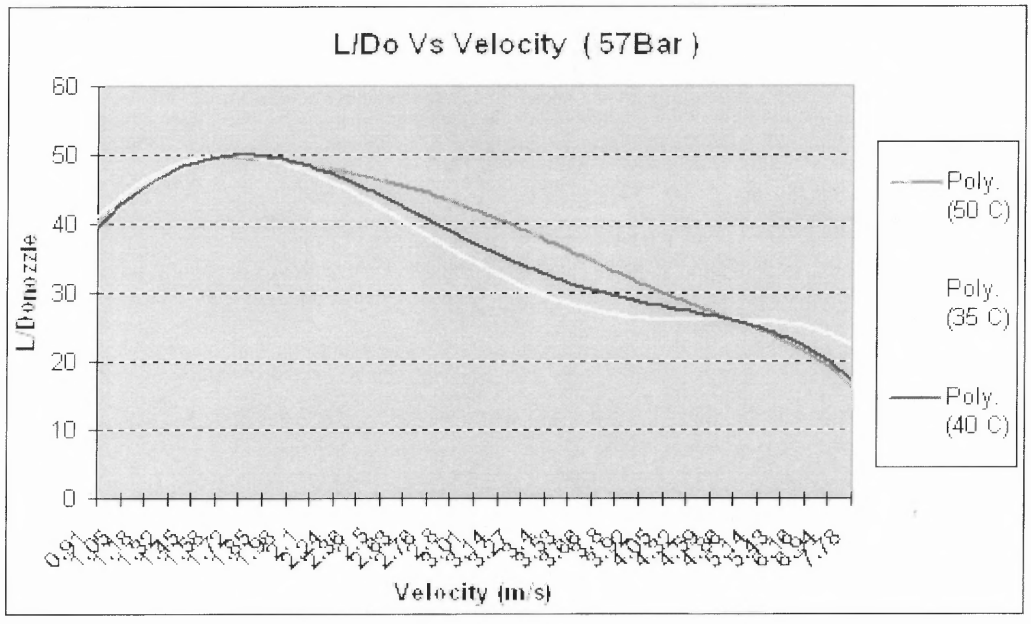

Figure B.16 Pressure = 57 Bar, Temperatures = 35, 40, 50C, Velocity of injected ethanol varies from 0.91 m/s to 7.78 m/s.

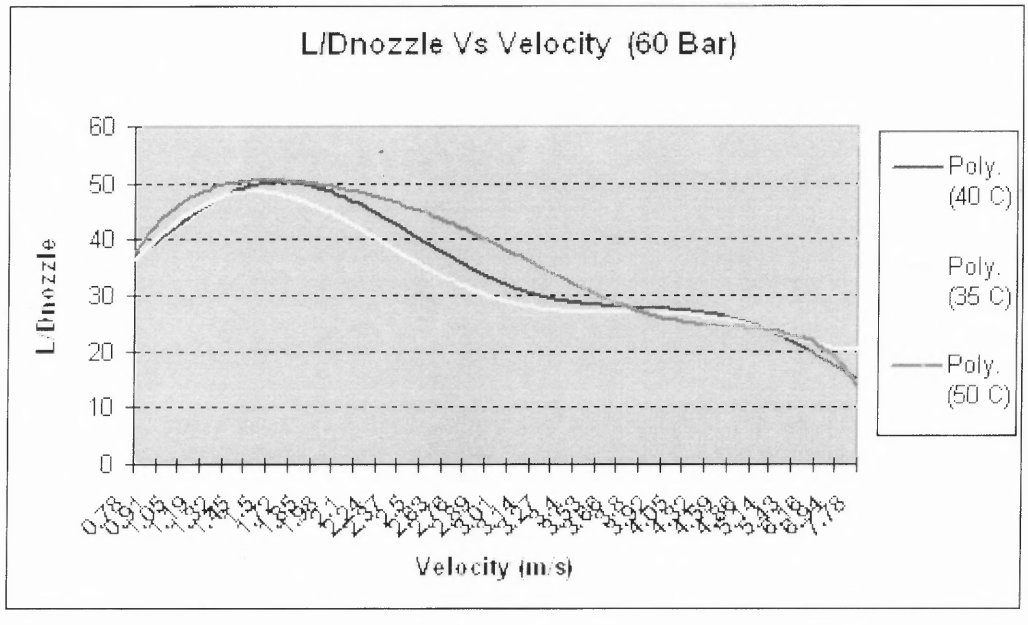

Figure B.17 Pressure = 60 Bar, Temperatures = 35, 40, 50C, Velocity of injected ethanol varies from 0.78 m/s to 7.78 m/s.

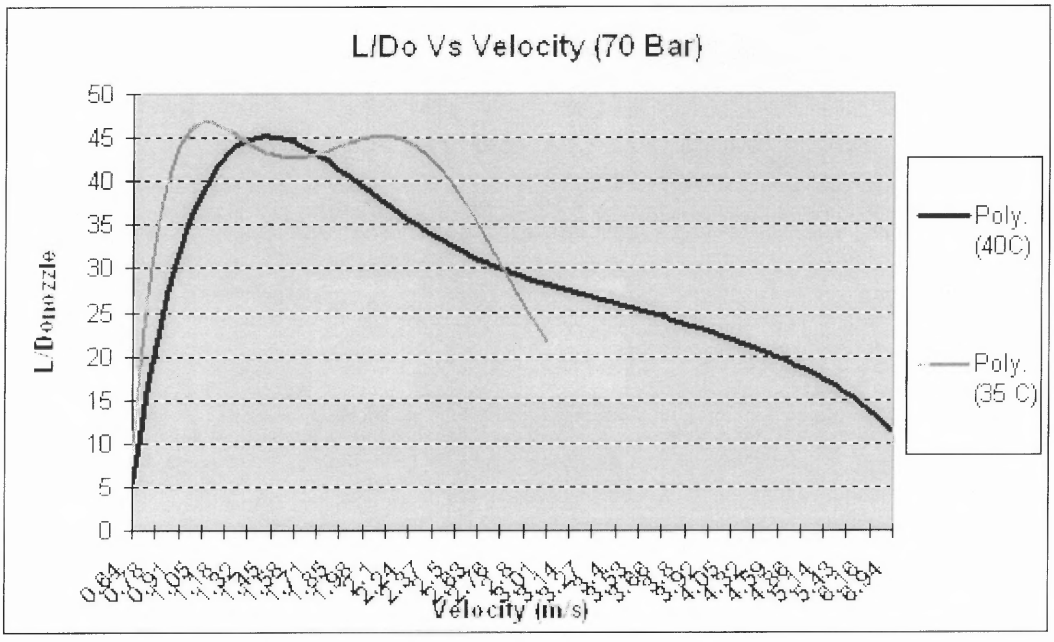

Figure B.18 Pressure = 70 Bar, Temperatures = 35, 40°C Velocity of injected ethanol varies from 0.64 m/s to 6.94 m/s.

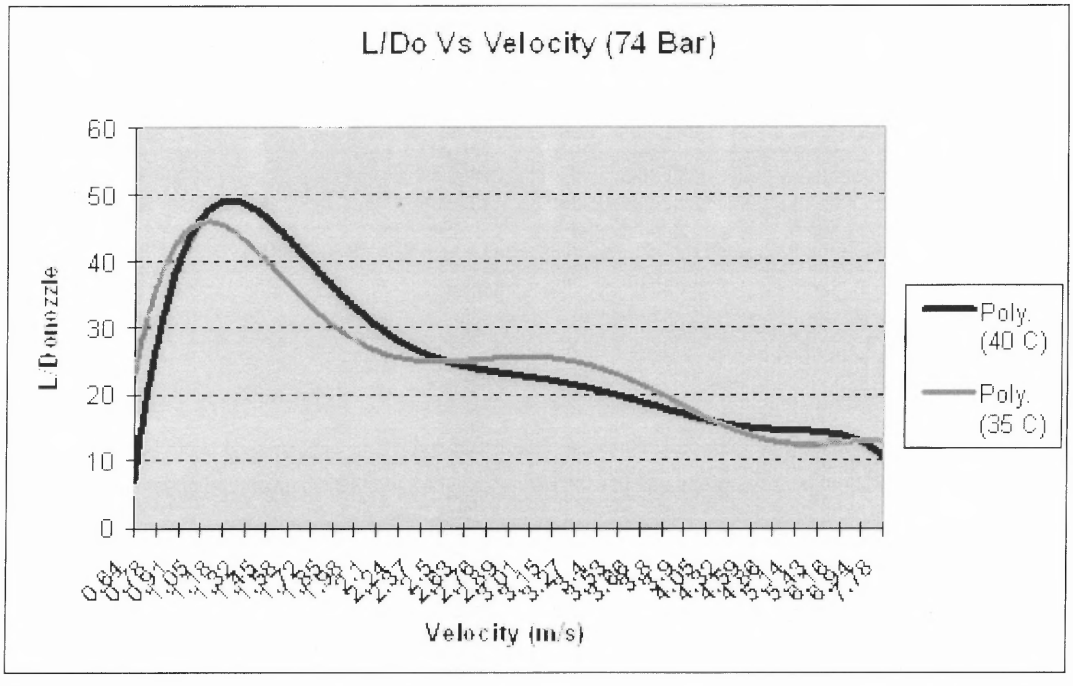

Figure B.19 Pressure = 74 Bar, Temperatures = 35, 40°C, Velocity of injected ethanol varies from 0.64 m/s to 7.78 m/s.

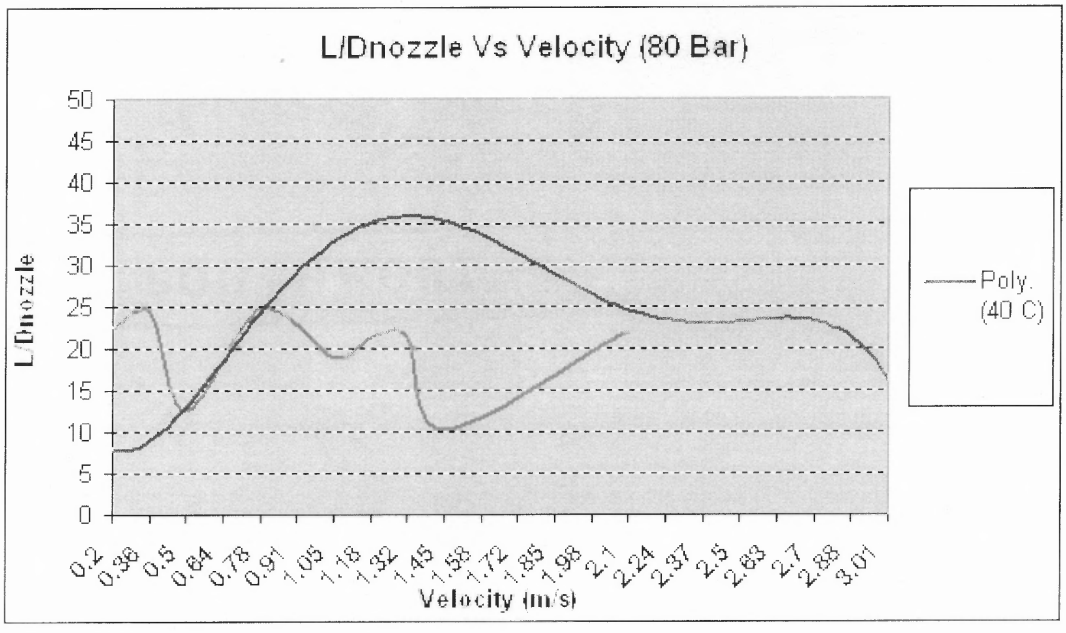

Figure B.20 Pressure = 80 bar, Temperatures = 35, 40C, Velocity of injected ethanol varies from 0.20 m/s to 3.01 m/s.

APPENDIX C

BREAKUP OF THE ACETONE JET INJECTED INTO CO_2

Studying effect of jet breakup process on particle formation break up of acetone jet into CO_2 is studied at different injection velocities at different CO_2 pressures and temperatures. The complete data of the experiment is presented quantitatively including snap shots of jet break up for different process parameters showing different kinds of jets at different process parameters. For every pressure, every kind of jet pattern is shown in following photographs. According to pressure, the velocity of jet for which the pattern changes, changes. To avoid repetition, photographs of dripping flow are not shown for every pressure.

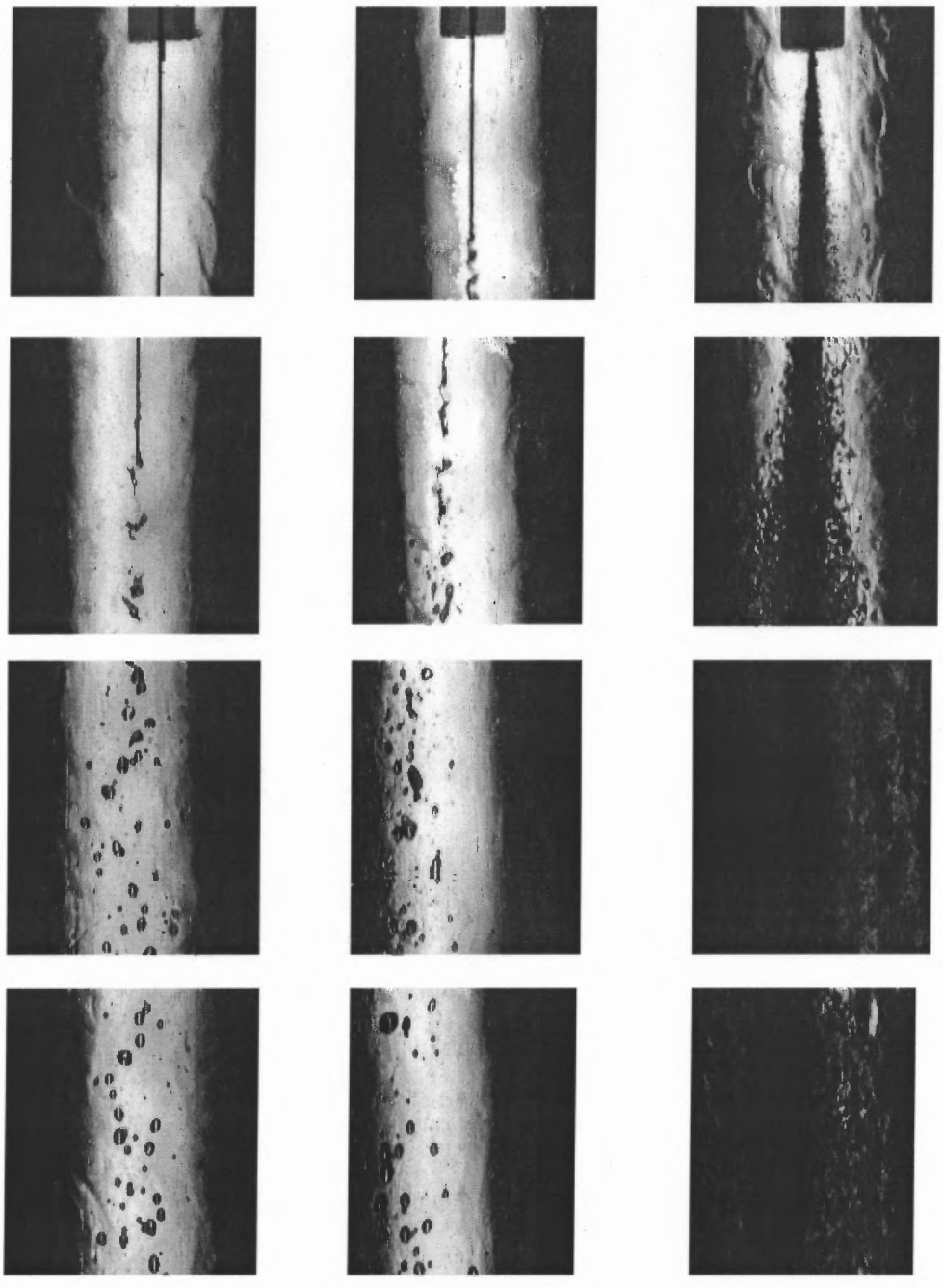

(A) v = 0.78 m/s (B) v = 1.05 m/s (C) v = 4.59 m/s

Figure C.1 Photos of acetone injected into carbon dioxide at 74 bar and 35° C for velocities: (A) 0.78 m/s, (B) 1.05 m/s, (C) 4.59 m/s, which were taken at different locations below the nozzle: 0 (1st row); 4 mm (2nd row); 8 mm (3rd row); and 12 mm (4th row). The nozzle diameter is 127 μm.

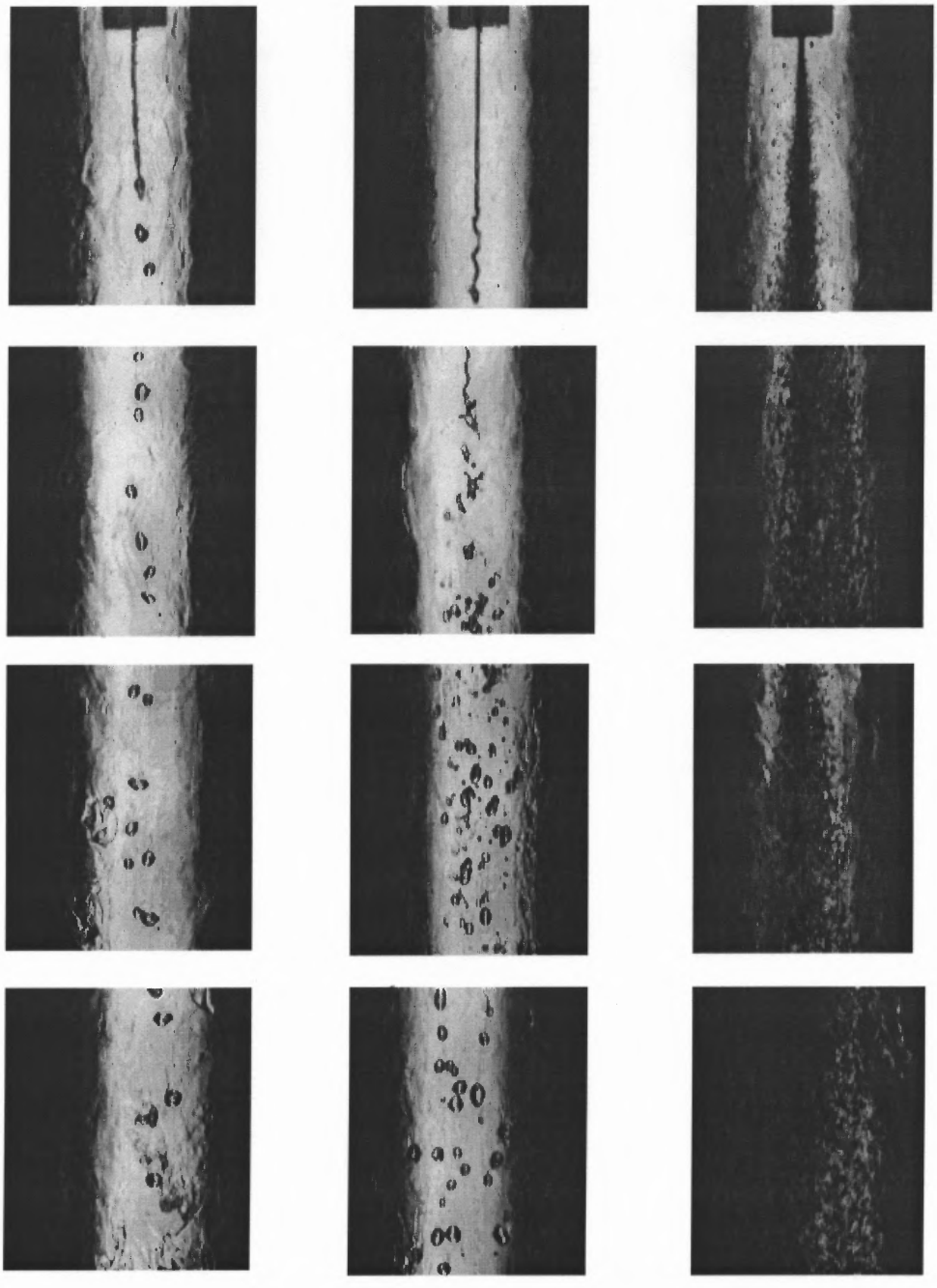

(A) v = 0.5 m/s (B) v = 0.64 m/s (C) v = 5.43 m/s

Figure C.2 Photos of acetone injected into carbon dioxide at 80 bar and 35° C for velocities: (A) 0.5 m/s, (B) 0.64 m/s, (C) 5.43 m/s, which were taken at different locations below the nozzle: 0 (1st row); 4 mm (2nd row); 8 mm (3rd row); and 12 mm (4th row). The nozzle diameter is 127 μm.

APPENDIX D

COMPARISON OF ACETONE AND ETHANOL JET LENGTHS FOR 35^{O}C

Graphs of jet lengths of acetone into supercritical CO_2 are shown for different pressures and temperatures with wide velocity range.

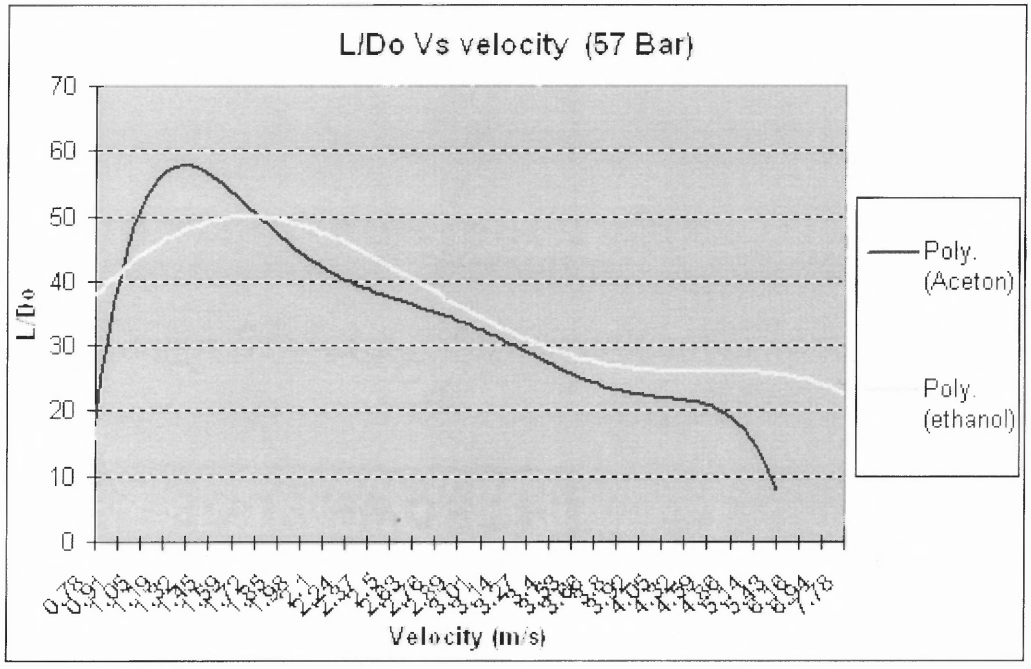

Figure D.1 Pressure = 57 Bar, Temperature = 35C, Velocity of injected ethanol and acetone varies from 0.78 m/s to 7.78 m/s.

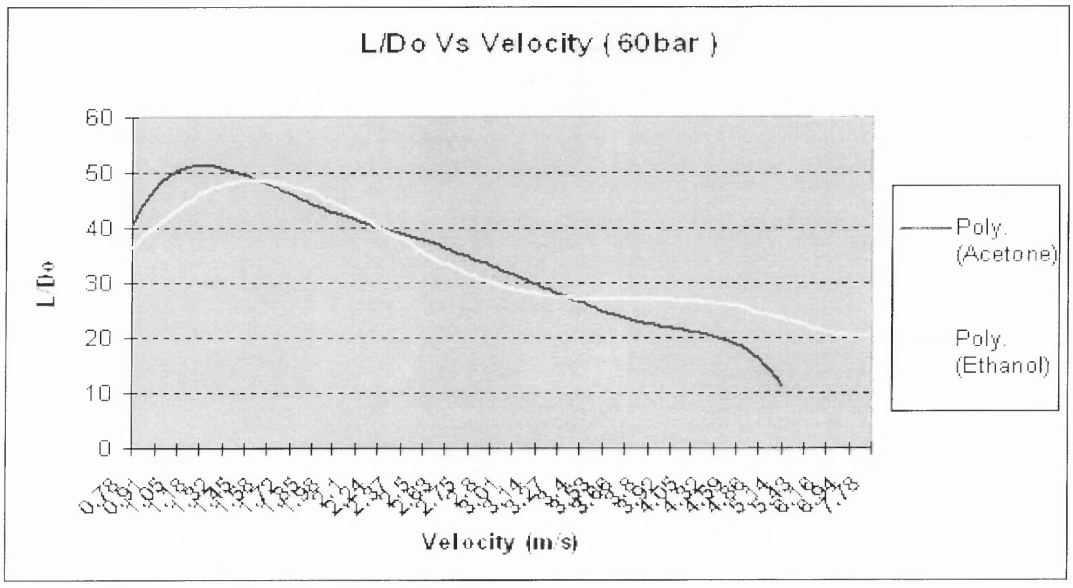

Figure D.2 Pressure = 60 Bar, Temperature = 35C, Velocity of injected ethanol and acetone varies from 0.78 m/s to 7.78 m/s.

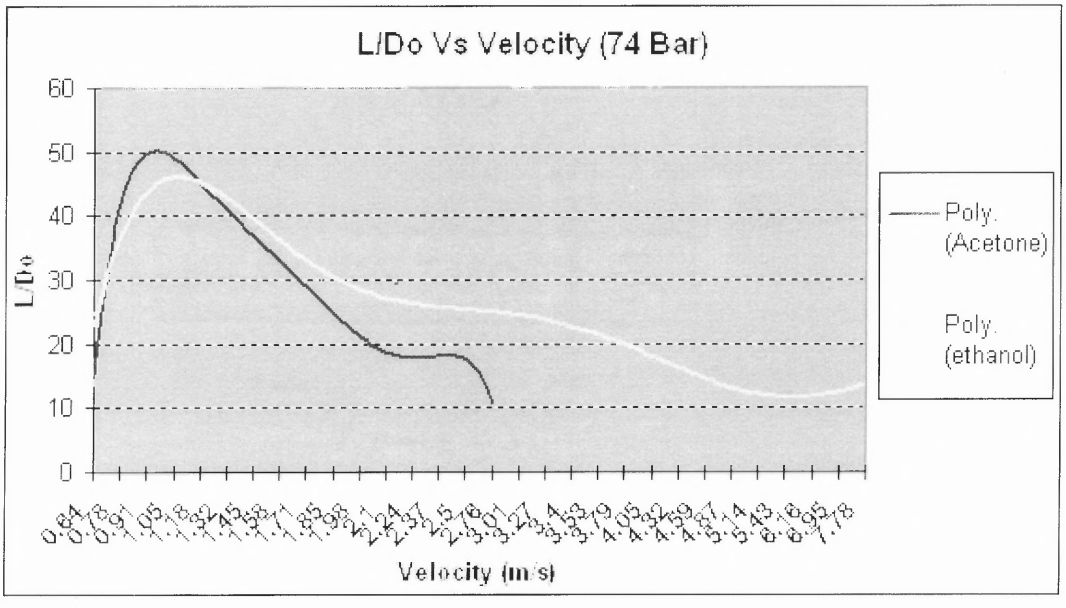

Figure D.3 Pressure = 74 Bar, Temperature = 35C, Velocity of injected ethanol and acetone varies from 0.78 m/s to 7.78 m/s.

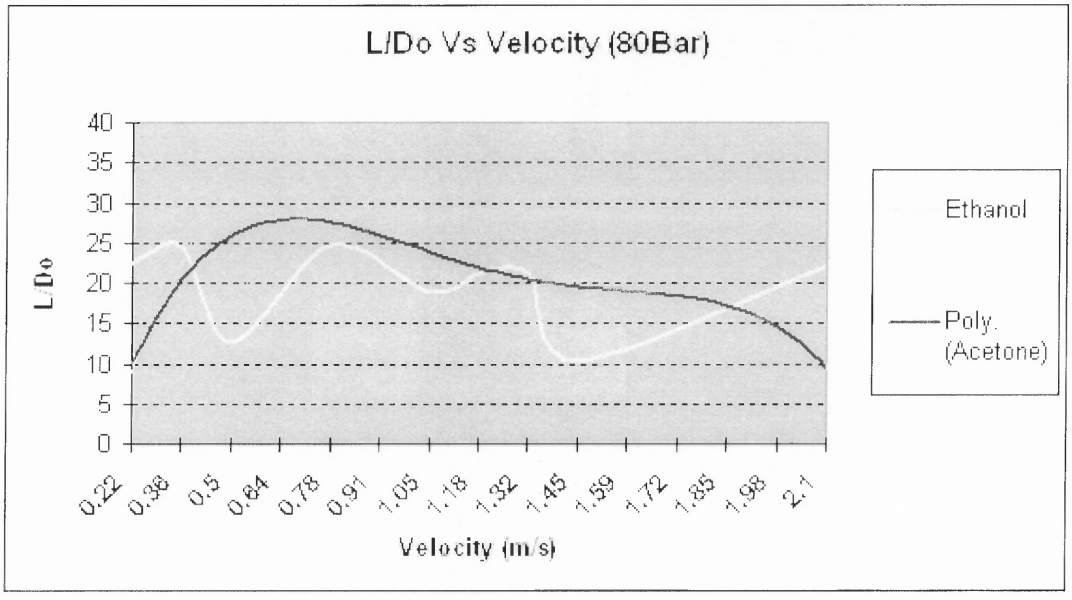

Figure D.4 Pressure = 80 Bar, Temperature = 35C, Velocity of injected ethanol and acetone varies from 0.22 m/s to 2.10 m/s.

E. Particle formation using SAS method

The experiments are done for synthesis and characterization of particle formation using SAS (supercritical as antisolvent) method. Below is the list of experiments done and the results obtained from the experiments.

Condition 2

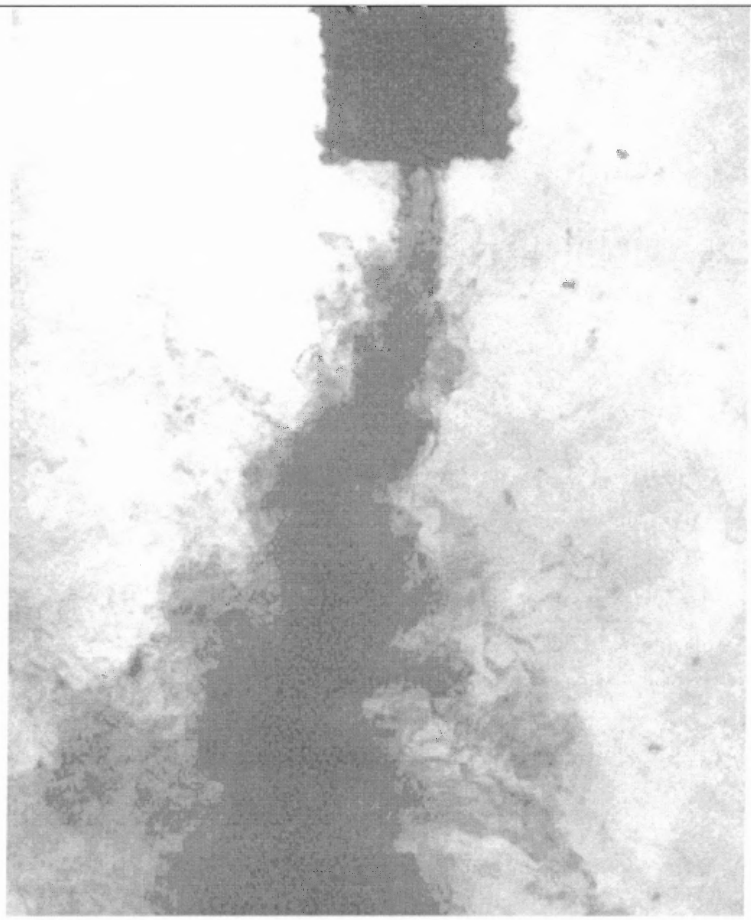

Figure E.1 Injection of solution into view cell P = 120 Bar, T = 35 C, V_{sol} = 0.4 ml/min, v = 1.18 m/s, D_{nozzle} = 127 μm, V_{CO2} = 60, (CO_2 pulsations are not induced).

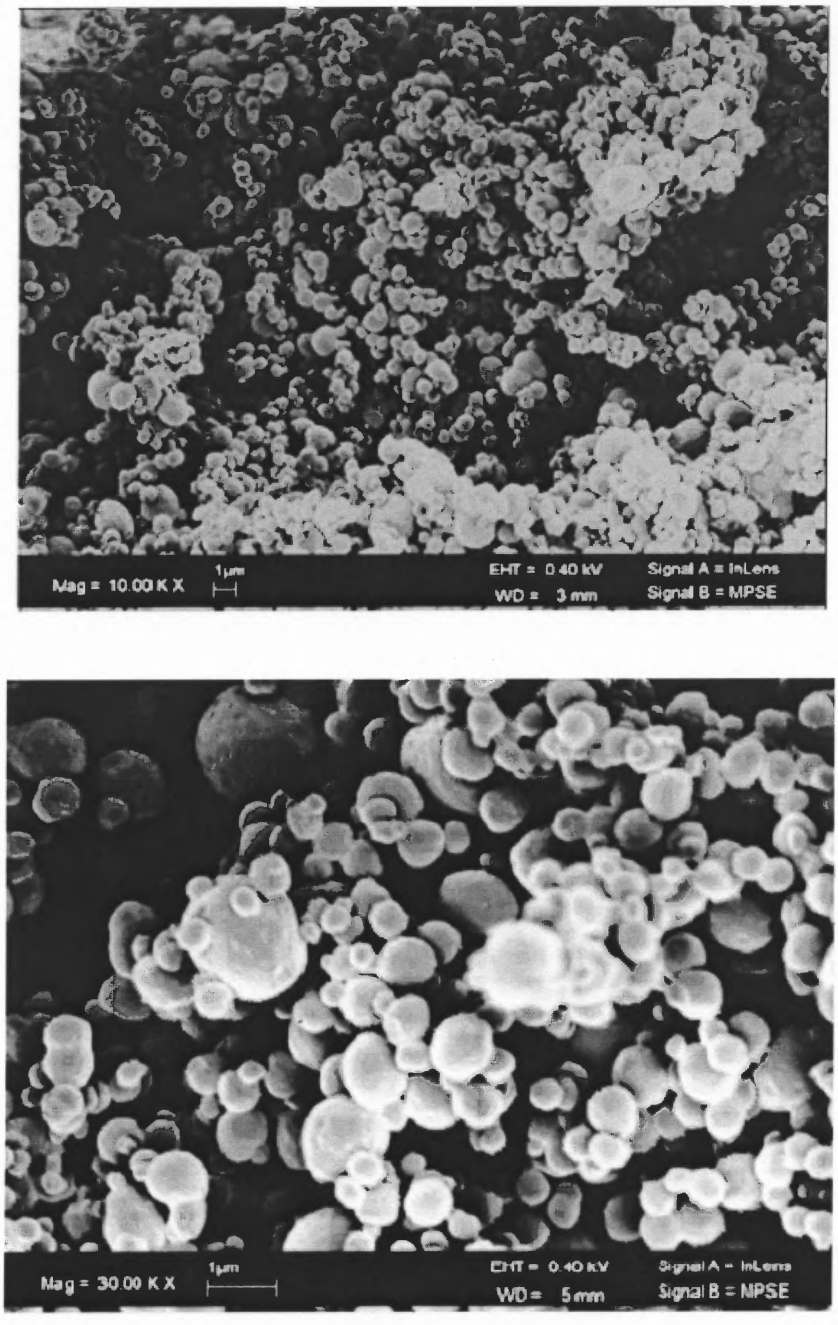

Figure E.2 SEM images of particles formed, P = 120 Bar, T = 35 C, V_{sol} = 0.4 ml/min, v = 1.18 m/s, D_{nozzle} = 127 μm, V_{CO2} = 60, (CO_2 pulsations are not induced).

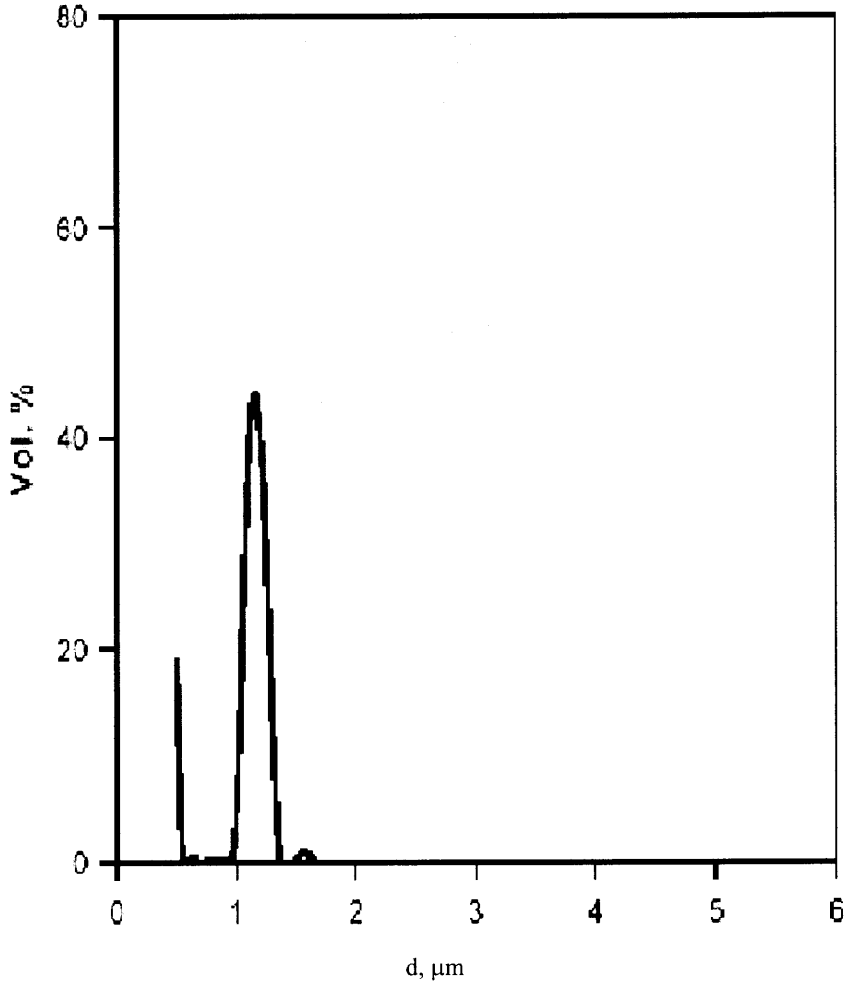

Figure E.3 Particle size distribution (LS 200 microscope) P = 120 Bar, T = 35 C, V_{sol} = 0.4 ml/min, v = 1.18 m/s, D_{nozzle} = 127 μm, V_{CO2} = 60, (CO_2 pulsations are not induced).

Condition 3

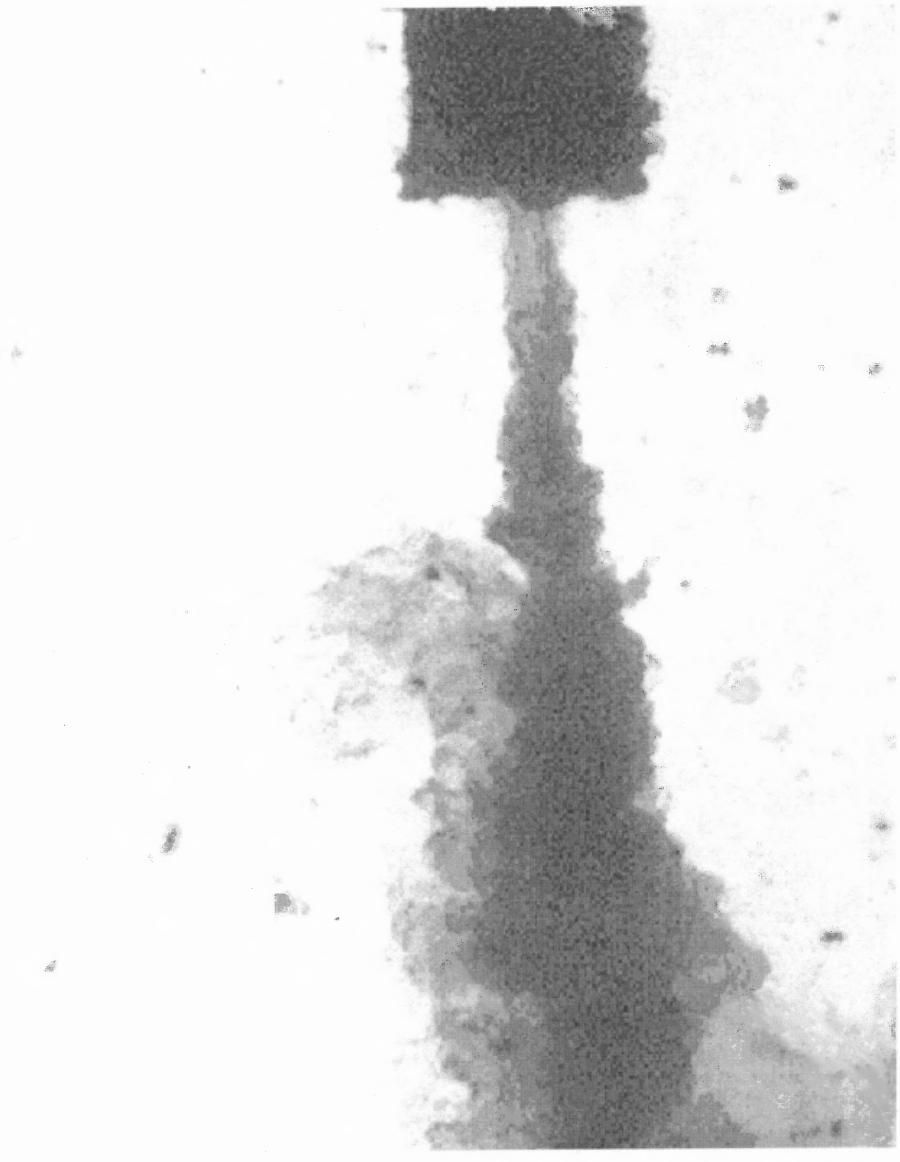

Figure E.4 Injection of solution into the view cell, P = 100 Bar, T = 35 C, V_{sol} = 0.4 ml/min, v = 1.18 m/s, D_{nozzle} = 127 μm, V_{CO2} = 60, CO_2 is injected with pulsations using 20 rpm pump.

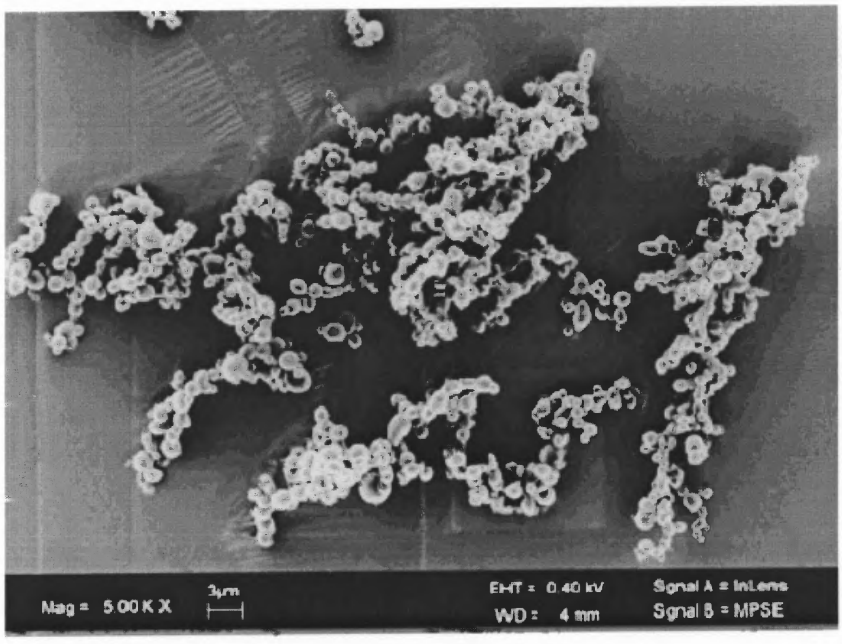

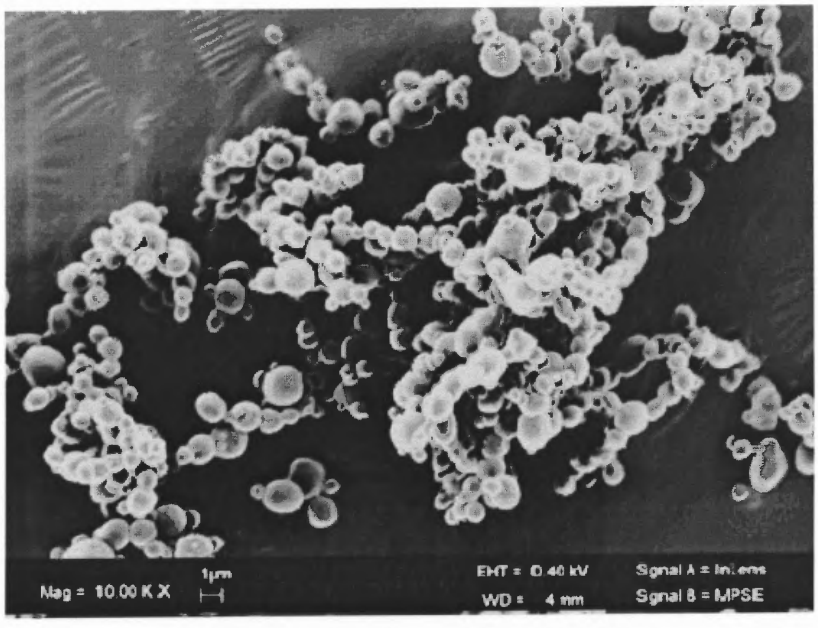

Figure E.5 SEM images of particles formed, P = 100 Bar, T = 35 C, V_{sol} = 0.4 ml/min, v = 1.18 m/s, D_{nozzle} = 127 µm, V_{CO2} = 60, CO_2 is injected with pulsations using 20 rpm pump.

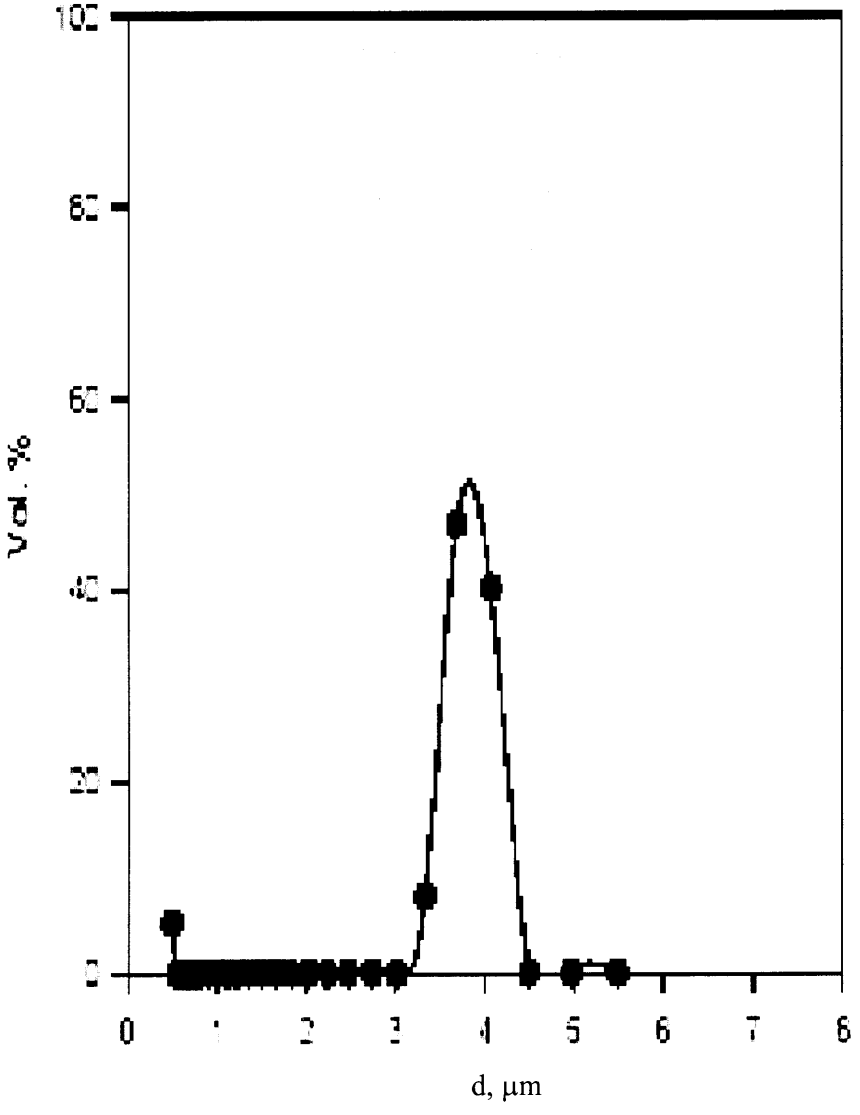

Figure E.6 Particle size distribution (LS 200 microscope).

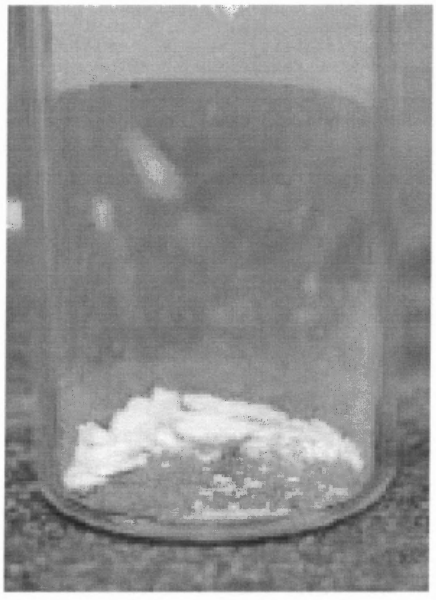

Figure E.7 Particles collected from experiment done without injection of CO_2 pulsations.

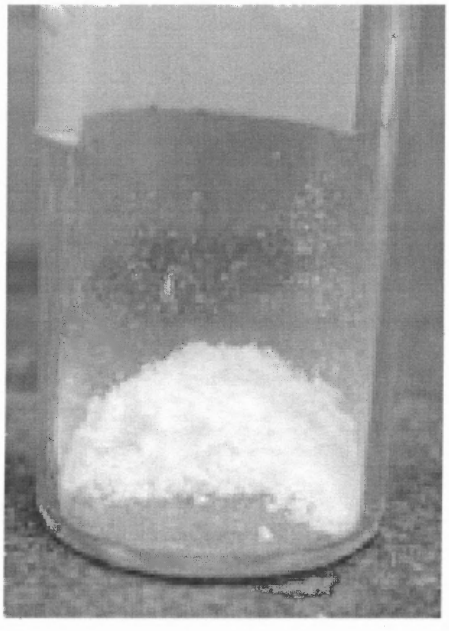

Figure E.8 Particles collected from experiment done with injection of CO_2 pulsations.

Condition 4

Figure E.9 Injection of solution into the view cell, P = 100 Bar, T = 35 C, V_{sol} = 0.4 ml/min, v = 1.18 m/s, D_{nozzle} = 254 μm, V_{CO2} = 60, CO_2 is injected with pulsations using 20 rpm pump.

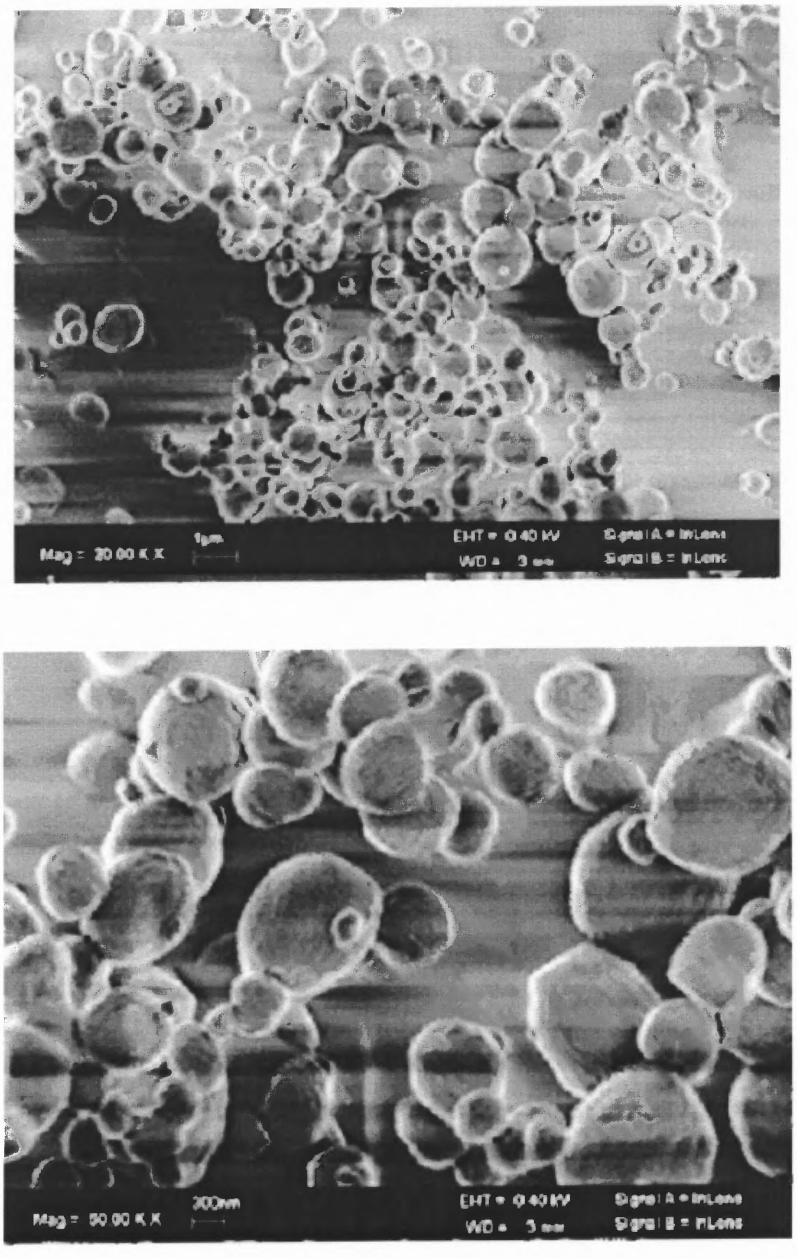

Figure E.10 SEM images of particles formed P = 100 Bar, T = 35 C, V_{sol} = 0.4 ml/min, v = 1.18 m/s, D_{nozzle} = 254 μm, V_{CO2} = 60, CO_2 is injected with pulsations using 20 rpm pump.

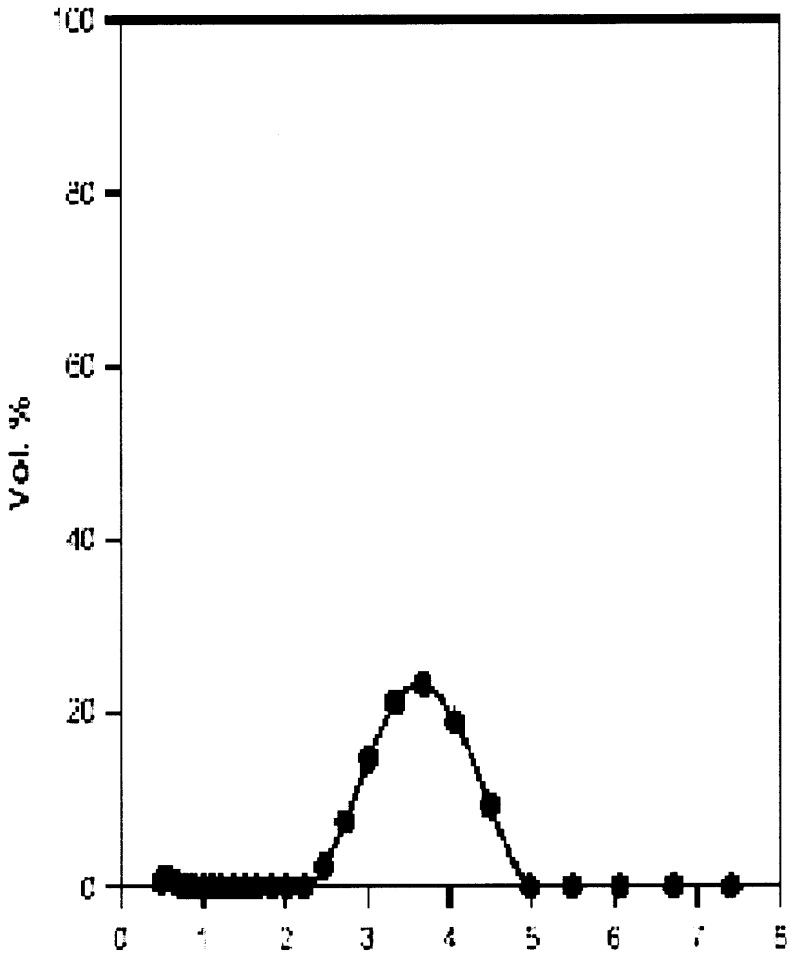

Figure E.11 Particle size distribution (LS 200 microscope) P = 100 Bar, T = 35 C, Vsol = 0.4 ml/min, v = 1.18 m/s, D_{nozzle} = 254 μm, VCO2 = 60, CO_2 is injected with pulsations using 20 rpm pump.

REFERENCES

1. J. Herrmann, R. Bodmeier, Biodegradable, somatostatin acetate containing microspheres prepared by various aqueous and non-aqueous solvent evaporation methods, Eur. J. Pharm. Biopharm. 45 (1998) 75-82.

2. P. Subra, Powders elaboration in supercritical media: comparison with conventional routes, Powder Technology 103 (1999) 2-9.

3. Erdogan Kiran, Pablo Debenedetti., Supercritical Fluids–fundamentals and application, Kluwer Academic Publishers.

4. http://cires.colorado.edu/env_prog/chemrawn/abstracts/Perrut.html [March 24, 2003].

5. M. Sihvonen, Advances in supercritical carbon dioxide technologies, Trends in Food Science & Technology 10 (1999) 217-222.

6. E. Reverchon, P. Subra, Supercritical antisolvent micronization of some biopolymers, Journal of Supercritical Fluids 18 (2000) 239-245.

7. Thomas Kissel, Biodegradable semi-crystalline comb polyesters influence the microsphere production by means of a supercritical fluid extraction technique (ASES), Journal of Controlled Release 63 (2000) 53-68.

8. F. Reche, Simultaneous supercritical fluid derivatization and extraction of formaldehyde by the Hantzsch reaction, Journal of Chromatography A 896 (2000) 51-59.

9. http://www.chem.leeds.ac.uk/People/CMR/props.html [July 01, 2003].

10. Tony Clifford, Fundamentals of supercritical fluids, Oxford University Press (1998).

11. C. Thomasin, H. Nam-Tran, H.P. Merkle, B. Gander, Drug microencapsulation by PLA/PLGA coacervation in the lights of thermodynamics. 1. Overview and theoretical considera-tions, J. Pharm. Sci 87 (1998) 259-268.

12. C. Thomasin, H.P. Merkle, B. Gander, Drug microencapsulating by PLA/PLGA coacervation in the lights of thermodynamics. 2. Parameters determining microsphere formation, J. Pharm. Sci 87 (1998) 269-275.

13. K. Masters, in: 2nd ed, Spray Drying, Leonard Hill Books, London, 1976.

14. J. Herrmann, R. Bodmeier, Biodegradable, somatostatin acetate containing microspheres prepared by various aqueous and non-aqueous solvent evaporation methods, Eur. J. Pharm. Biopharm. 45 (1998) 75-82.

15. Ting-Jie Wang, The characteristics of coherent structures in the rapid expansion flow of the supercritical carbon dioxide, Journal of Supercritical Fluids 24 (2002) 231-237.

16. Michel Perrut, Particle design using supercritical fluids: Literature and patent survey, Journal of Supercritical Fluids 20 (2001) 179-219.

17. B.Yu. Shekunov, Analysis of the supersaturation and precipitation process with supercritical CO_2, Journal of Supercritical Fluids 21 (2001) 257-271.

18. Ram B. Gupta, Production of griseofulvin nanoparticles using supercritical CO2 antisolvent with enhanced mass transfer, International Journal of Pharmaceutics 228 (2001) 19-31.

19. Erdogan Kiran and Joan Brennecke, Supercritical Fluid Engineering Science – Fundamentals and Application, American Chemical Society.

20. Saeed Moshashaee, Supercritical fluid processing of proteins I: Lysozyme precipitation from organic solution, European Journal of Pharmaceutical Sciences 11 (2000) 239-245.

21. E. Reverchon, Production of antibiotic micro- and nano-particles by supercritical antisolvent precipitation, Powder Technology 106 (1999) 23-29.

22. Ernesto Reverchon, Rifampicin microparticles production by supercritical antisolvent precipitation, International Journal of Pharmaceutics 243 (2002) 83-91.

23. H. Kro¨ber, Materials processing with supercritical Antisolvent precipitation: process parameters and morphology of tartaric acid, Journal of Supercritical Fluids 22 (2002) 229-235.

24. D. Dixon, J Appl Polym Sci 50 (1993) 1929-1942.

25. D. Dixon , AIChE Journal, vol 39, No.1.

26. R.Ghaderi, A new method for preparing biodegradable microparticles and entrapment of hydrocortisone in DL -PLG microparticles using supercritical fluids, European Journal of Pharma Sciences 10 (2000) 1-9.

27. Markku Rantakyla, The effect of initial drop size on particle size in the supercritical antisolvent precipitation (SAS) technique, Journal of Supercritical Fluids 24 (2002) 251-263.

28. T. Randolf, S. Yeung, Biotechnol. Prog. (1993) 429-435.

29. B. Yu. Shekunov, Particle formation by mixing with supercritical antisolvent at high Reynolds numbers, Chemical Engineering Science 56 (2001) 2421-2433.

30. Sang-Do Yeo, Recrystallization of sulfathiazole and chlorpropamide using the supercritical fluid antisolvent process, J. of Supercritical Fluids 25 (2003) 143-154.

31. E. Badens, Soy lecithin micronization by precipitation with a compressed fluid antisolvent - influence of process parameters, Journal of Supercritical Fluids 19 (2000) 69-77.

32. A. W. Kerst, Flow regimes of free jets and falling films at high ambient pressure, Chemical Engineering Science 55 (2000) 4189-4208.

33. Robin N. Yoder, Extraction of cloransulam-methyl from soil with subcritical water and supercritical CO_2, J. of Chromatography A 897 (2000) 405-413.

34. C. F. Poole, Supercritical-fluid chromatography and supercritical-fluid extraction, Journal of Biochemical and Biophysical Methods 43 (2000) 1-2.

35. Lin SP, Reitz RD, Drop and Spray Formation from a Liquid Jet, Annu. Rev. Fluid Mech 30 (1998) 85-105.

36. J. Bellan, Supercritical (and subcritical) fluid behavior and modeling: drops, streams, shear and mixing layers, jets and sprays, Progress in Energy and Combustion Science 26 (2000) 329-366.

37. Chehroudi, B., Talley, D. and Coy, E.,"Visual Characteristics and Initial Growth Rates Of Round Cryogenic Jets at Subcritical And Supercritical Pressures", Physics of Fluids 14 (2002) 850-61.

38. Shekunov, B. Yu., J. Baldyga and P. York "Particle formation by mixing with supercritical antisolvent at high Reynolds numbers", Chemical Engineering Science 56 (2001) 2421-2433.

39. Lengsfeld C.S., Delplanque J.P, Barocas V.H., Randolph T.W., J. Phys. Chem, 104 (2000) 2725.

40. E. G. Baburaj, Synthesis of nanocrystalline materials — an overview, Materials Science and Engineering A 301 (2001) 44-53.